

COMPUTATIONAL STUDIES OF THE DERIVATIVES OF FULLERENES AND CARBON NANOTUBES

Ph.D. THESIS

by

VINIT



DEPARTMENT OF CHEMISTRY
INDIAN INSTITUTE OF TECHNOLOGY ROORKEE
ROORKEE – 247667, INDIA
SEPTEMBER, 2019

COMPUTATIONAL STUDIES OF THE DERIVATIVES OF FULLERENES AND CARBON NANOTUBES

A THESIS

*Submitted in partial fulfilment of the
requirements for the award of the degree*

of

DOCTOR OF PHILOSOPHY

in

CHEMISTRY

by

VINIT



**DEPARTMENT OF CHEMISTRY
INDIAN INSTITUTE OF TECHNOLOGY ROORKEE
ROORKEE – 247667, INDIA
SEPTEMBER, 2019**

**© INDIAN INSTITUTE OF TECHNOLOGY ROORKEE, ROORKEE- 2019
ALL RIGHTS RESERVED**





INDIAN INSTITUTE OF TECHNOLOGY ROORKEE

CANDIDATE'S DECLARATION

I hereby certify that the work presented in the thesis entitled **COMPUTATIONAL STUDIES OF THE DERIVATIVES OF FULLERENES AND CARBON NANOTUBES** is my own work carried out during a period from July, 2014 to September, 2019 under the supervision of Prof. Ramachandran C. N., Associate Professor, Department of Chemistry, Indian Institute of Technology Roorkee, Roorkee.

The matter presented in the thesis has not been submitted for the award of any other degree of this or any other Institute.

Dated: December 27, 2019

(Vinit)

SUPERVISOR'S DECLARATION

This is to certify that the above mentioned work is carried out under my supervision.

Dated: December 27, 2019

**(Ramachandran C. N.)
Supervisor**

The Ph. D. Viva-Voice Examination of Vinit, Research Scholar, has been held on **December 27, 2019**.

Chairperson, SRC

External Examiner

This is to certify that the student has made all the corrections in the thesis

Supervisor

Head of Department

Dated: December 27, 2019

Abstract

Carbon exists in different allotropic forms such as graphite, diamond, fullerenes and carbon nanotubes. With the discovery of fullerenes and carbon nanotubes, a new branch of science called nanoscience was emerged. Fullerenes and carbon nanotubes are molecules which can encapsulate various species due to the vacant space available inside. Endohedral complexes of fullerenes and carbon nanotubes have taken wide attention of the scientific community during last few decades due to their wide applications in various fields. These complexes are mainly stabilized by the dispersive interactions between the guest and the host species. The endohedral complexes of fullerenes and carbon nanotubes can be diamagnetic or paramagnetic depending on the nature of the guest. Earlier studies on endohedral complexes of fullerenes and carbon nanotubes provided the details on the structure, stability and properties of some of the complexes in which paramagnetic atoms are trapped inside the cavity of fullerenes. One of the most remarkable findings of those studies is that in $N@C_{60}$, the encapsulated nitrogen atom retained its atomic spin. However, information on spin-spin coupling, spin polarization and spin density transfer in endohedral fullerene dimers, endohedral heterofullerenes and endohedral heterofullerene dimers are lacking. Therefore, it is interesting to know how the spins of atomic nitrogen present inside adjacent cages of dimers interact and how the heteroatom of cage affects the interactions between guest species. An attempt is also made to understand the spin-spin coupling, spin polarization and spin density transfer in the complexes of carbon nanotubes and its BN analogue.

The present thesis consists of seven chapters. In chapter 1, introduction, synthesis and applications of fullerenes and their derivatives are discussed. The structure, stability and properties of various endohedral complexes of fullerenes and heterofullerenes are reviewed. The host-guest interactions in the above complexes as well as the spin-spin coupling between their components are discussed. A brief review on the properties of various derivatives of carbon and boron nitride nanotubes is given.

Chapter 2 briefly reviews the computational methods used in the present work. Various computational methods such as Hartree-Fock, post Hartree-Fock and density functional theoretical methods are briefly explained. It also overviews basis sets, time-dependent density functional methods and spin broken symmetry approach. The chapter also provides details of spin polarization parameter.

In chapter 3, the results of the density functional theoretical calculations on the structure, stability and properties of nitrogen atom encapsulated fullerene derivatives obtained at different levels are discussed. For this purpose, $N@C_{60}$, $N@C_{59}N$ and their respective dimers are considered which are important in the context of spin-spin interactions between the guest and the host as well as that between guest species. For the most stable spin states of each of the above complexes, spin density transfer and spin-spin coupling between different components are investigated. The study also focuses on spin polarization and spin degeneracy of the complexes. The analysis of spin density showed that the encapsulated nitrogen retained its atomic state in $N@C_{60}$ and $N@C_{59}N$. Depending on the multiplicity of $N@C_{59}N$, the unpaired electrons of the encapsulated nitrogen are coupled with those of the cage antiferromagnetically or ferromagnetically. The study also showed that the complex $(N@C_{60})_2$ can exist in two isoenergetic spin states, namely, $^7[(N@C_{60})_2]$ and $^1[(N@C_{60})_2]$. In the former, the encapsulated nitrogens are ferromagnetically coupled, whereas they are coupled anti-ferromagnetically in the latter. A similar coupling between the guest species occurs in the nitrogen analogues $^7[(N@C_{59}N)_2]$ and $^1[(N@C_{59}N)_2]$ which indicates that the nitrogen atom on the surface does not assist any spin interactions between the components of the complexes. On encapsulating nitrogen atom inside fullerene derivatives, the energy gap between the highest occupied molecular orbital (HOMO) and lowest unoccupied molecular orbital (LUMO) ($\Delta E_{\text{HOMO-LUMO}}$) of the latter did not change. It was also revealed that the encapsulation of nitrogen atom inside C_{60} , $C_{59}N$ and their respective dimers is thermodynamically feasible. The thermodynamic feasibility of the formation of $(N@C_{60})_2$ and $(N@C_{59}N)_2$ from their respective monomer units is also discussed.

Considering the fact that boron atom is also reactive and paramagnetic, boron atom encapsulated complexes of C_{60} , $C_{59}B$, and $C_{59}N$ at B3LYP/6-311G* and B3LYP-GD2/6-311G* are investigated in chapter 4. In $B@C_{60}$, the guest atom is located at the centre of host cage. The study showed that the complexes $B@C_{59}B$ and $B@C_{59}N$ are stable in their singlet and triplet states. The electronic properties such as electron affinity (VEA), ionization energy (VIE), and $\Delta E_{\text{HOMO-LUMO}}$ of the complexes are calculated. On encapsulating boron, $\Delta E_{\text{HOMO-LUMO}}$ of C_{60} , $C_{59}B$, and $C_{59}N$ is either decreased or increased depending upon the spin states of the resultant complexes. The transfer of spin density and spin-spin coupling between the guest and the host are examined. The study revealed that ferromagnetic core@shell spin coupling occurs between the host and the guest species of the complexes $B@C_{59}B$ and $B@C_{59}N$ in their triplet state without the transfer of spin density. The spin polarization in the complexes $B@C_{60}$, $B@C_{59}B$ and $B@C_{59}N$ are also discussed. The thermodynamics of encapsulation of boron atom

in C_{60} , $C_{59}B$ and $C_{59}N$ is examined based on the values of change in Gibbs free energy and change in enthalpy. It suggested that the encapsulation of boron atom is thermodynamically feasible.

In chapter 5, the dimer of endohedral fullerene derivatives $(B@C_{59}B)_2$, $(B@C_{59}N)_2$, $(N@C_{59}B)_2$, $(B@C_{59}N-N@C_{59}B)$ and $(B@C_{60})_2$ are investigated using dispersion corrected density functional theory. Several spin states of these complexes are considered and their stable spin states are reported. For $^1[(B@C_{59}B)_2]$ and $^1[(B@C_{59}N-N@C_{59}B)]$, the encapsulated atoms are located near the inner surface of the host cages, in contrast to other spin states where they are positioned at the centre of the cages. In complexes $^1[(B@C_{59}N)_2]$, $^3[(B@C_{59}N)_2]$, $^7[(N@C_{59}B)_2]$, $^1[(B@C_{60})_2]$ and $^3[(B@C_{60})_2]$ the guest atoms are found to be at the centre of the host cages. The spin polarization and the transfer of spin density between the components of the complexes for different stable spin states are analyzed. Based on the spin states of the complexes, the spin-spin interaction is found to be either ferromagnetic or anti-ferromagnetic. Unlike other complexes, in $^1[(B@C_{59}B)_2]$ and $^1[(B@C_{59}N-N@C_{59}B)]$, the spin density is transferred from the guest to the host followed by anti-ferromagnetic coupling between the monomers. The complexes are found to be fully spin polarized, partially spin polarized or spin degenerate depending upon their spin states. The thermodynamic feasibility of formation of the complexes is also examined. The vertical electron affinity, vertical ionization energy and $\Delta E_{\text{HOMO-LUMO}}$ as well as the dipole moment of the above systems are determined. The singlet state of the heterodimer $(B@C_{59}N-N@C_{59}B)$ showed high polarity due to the slight rotation along the dihedral angle ϕ_{NCCB} .

To know the effect of confinement due to different nanotubes, the nitrogen encapsulated complexes of carbon nanotube (CNT), boron nitride nanotubes (BNNT) and their respective dimers are investigated in chapter 6. The study showed that the complexes $^4[\text{N@CNT}]$ and $^4[\text{N@BNNT}]$ are stable due to the van der Waals interactions between the guest and the host species. In these complexes, the guest atoms are located at the center of the host nanotube. Similar to $^4[\text{N@C}_{60}]$, nitrogen atom retains its atomic spin inside CNT and BNNT. The complexes $(\text{N@CNT})_2$ and $(\text{N@BNNT})_2$ are stable in their isoenergetic singlet and septet states. In stable states of $(\text{N@CNT})_2$ and $(\text{N@BNNT})_2$, the guest atoms are shifted towards each other from the center of respective host nanotubes. The effect of the position of nitrogen atom on the stability is also discussed. The analysis of spin density for $(\text{N@CNT})_2$ revealed that the spins of guest nitrogen atoms are antiferromagnetically and ferromagnetically coupled in its singlet and septet states, respectively. Similar results are obtained for $(\text{N@BNNT})_2$. The study also indicated spin polarization in $^4[\text{N@CNT}]$ and $^4[\text{N@BNNT}]$. The singlet states of

$(\text{N@CNT})_2$ and $(\text{N@BNNT})_2$ are spin degenerate whereas their septet states are spin polarized. On encapsulating nitrogen atom, electronic properties such as VEA, VIE and $\Delta E_{\text{HOMO-LUMO}}$ of the host nanotubes remained the same although VEA of BNNT and $(\text{BNNT})_2$ are significantly reduced. The effect of diameter of nanotubes on the spin-spin coupling between the encapsulated nitrogen atoms inside adjacent nanotubes is also examined. It is revealed that the cavity size of the nanotube does not affect the spin-spin coupling between nitrogen atoms present in adjacent CNTs. The spin polarization is also not much affected by decreasing the cavity size of CNTs.

The conclusions and future scope is discussed in chapter 7.



Acknowledgements

It is my great pleasure to take this opportunity to express my sincere gratitude and respect to my supervisor **Prof. C. N. Ramachandran** for his guidance, constant encouragement, unselfish inspiration and amicable cooperation during the course of my work. I owe special gratitude to him for introducing me to the field of computational chemistry. It is my privilege to be a part of his enthusiastic research group. I express my deepest respect to him not only for his guidance throughout my Ph. D. career, but also for his motivation and inspiration towards my future endeavours.

I would also like to thank my research committee members, **Prof. P. Jeevanandam** (Chairman), **Prof. Pallavi Debnath** (Internal Expert) and **Prof. Praveen C. Srivastava** (External Expert) for carrying out regular SRC meetings and providing valuable suggestions from time to time to accomplish my research work smoothly.

I am highly grateful to **Prof. K. R. Justin Thomas (Head)** and **Prof. M. R. Maurya (Former Head)**, Department of Chemistry, Indian Institute of Technology Roorkee, for providing me the essential infrastructural facilities to carry out research investigations. I am also thankful to **Mr. S. P. Singh, Mr. Ankur Sharma, Mr. Madan Pal, Mr. K.C. Tiwari** and other staff members of the Department of Chemistry for being me in every occasion.

I am also obliged to **Dr. P. Smitha** for her constant love, encouragement and affection.

I gratefully acknowledge my lab-mates **Dr. Surinder Pal Kaur, Dr. Sujith K. S., Ankita Joshi, Mohan Tiwari, Peaush Gangwar, Angat Dhiman, Paras, Shivam Rawat, Kapil, V. Shilpi, Sakshi Ganotra, Bhawna Singh Tomar, Manisha Singh, Suman Lata, Rajdeep, Laukesh Sharma, Rajat Pundhir** and **Vishal Chhikara** for maintaining working atmosphere in lab. I really have no words to thank **Dr. Surinder Pal Kaur, Dr. Sujith K. S.** and **Mohan Tiwari** for all interesting and funny conversations we had. They were always been there for me during my good and bad times. Their company helped me to keep doing work and to keep my cool behaviour alive.

I am really thankful to my other friends **Abhayankar Maurya, Sachin Dev** and **Avinash Prajapat** with whom I shared the best time of my life. The page will finish, ink of pen will finish, to thank **Abhayankar Maurya**, maximum I can say about him that “**no friend can be like him for me**” in this entire world.

Life at IITR could not be imagined without friends. I extend my warm thanks to my friends **Nabi Ahamad, Lalit Gangwar, Piyush Tehri, Jatin Mahajan, Shailendra K. Maurya, Gaurav Nim, Amar P. Pandey, Anil Kumar, Dr. Vishnu Singh, Yogseh Kumar,** We all enjoyed a wonderful time in bhawan as well as in campus. I don't have worth words to thank **Nabi Ahamad, Lalit Gangwar, Jatin Mahajan, Shailendra K. Maurya Gaurav Nim,** and **Amar P. Pandey** for their selfless support and help. Special thanks and huge appreciation goes to **Dr. Naveen Kumar** for his guidance, support and encouragement. I feel it was the breakthrough in my career when he met me. He is the person because of him I could achieve many things in my career.

I am thankful to Indian Institute of Technology Roorkee (**IITR**) for providing infrastructure for research work. The University Grants Commission (**UGC**), Government of India is also acknowledged for providing me the fellowship.

Words fail to express my gratefulness to my dearest **Late Tau Ji (Uncle)** and **parents** for their love, affection, constant inspiration and support in all phases of my life. I put on record my sincere love and gratitude to my beloved father and mother for their unflagging love and unconditional support throughout my life. I am grateful to them for being there when I needed them most. My special gratitude is due to my younger sisters **Princi** and **Neelu** for their loving support and encouragement and being a pillar of strength for me and for all the sweet memories. I sincerely acknowledge my cousins **Kushal Pal, Ambrish Kumar, Deepak Kumar, Ankit Kumar, Ankur Kumar** and **Vikul Kumar** for their undefined support and encouragement. The all my other family members are also deeply thankful. My wife **Priya** who has been extremely supportive of me and has made countless sacrifices to help me to achieve this. There are no words in my knowledge to thank her.

Finally, I bow down to **ALMIGHTY GOD** for giving me health and energy to complete this work successfully.

Vinit
IIT Roorkee
September, 2019

List of Abbreviations

Carbon nanotube	CNT
Single-walled carbon nanotube	SWCNT
Boron nitride nanotube	BNNT
Nanowire	NW
Nanotube	NT
Highest occupied molecular orbital	HOMO
Lowest unoccupied molecular orbital	LUMO
Change in Gibbs free energy	ΔG
Change in enthalpy	ΔH
Hartree-Fock	HF
Self-consistent field	SCF
Configuration interaction	CI
Many body perturbation theory	MBPT
Coupled cluster	CC
Density functional theory	DFT
Hohenberg-Kohn	HK
Local density approximation	LDA
Local spin density approximation	LSDA
Generalized gradient approximation	GGA
Slater types orbital	STO
Gaussian type orbital	GTO
Time-dependent density functional theory	TDDFT
Spin polarization parameter	ζ
Stabilization energy	E_{stab}
Basis set superposition error	BSSE
Change in Gibbs free energy associated with encapsulation	$\Delta G_{\text{encapsulation}}$
Change in Gibbs free energy associated with dimerization of monomer units	$\Delta G_{\text{dimerization}}$
Change in enthalpy associated with encapsulation	$\Delta H_{\text{encapsulation}}$
Change in enthalpy energy associated with dimerization of monomer units	$\Delta H_{\text{dimerization}}$
Energy gap between HOMO and LUMO	$\Delta E_{\text{HOMO-LUMO}}$
Vertical electron affinity	VEA
Vertical ionization energy	VIE
Relative energy	R.E.
Hyperfine coupling constant	hfcc



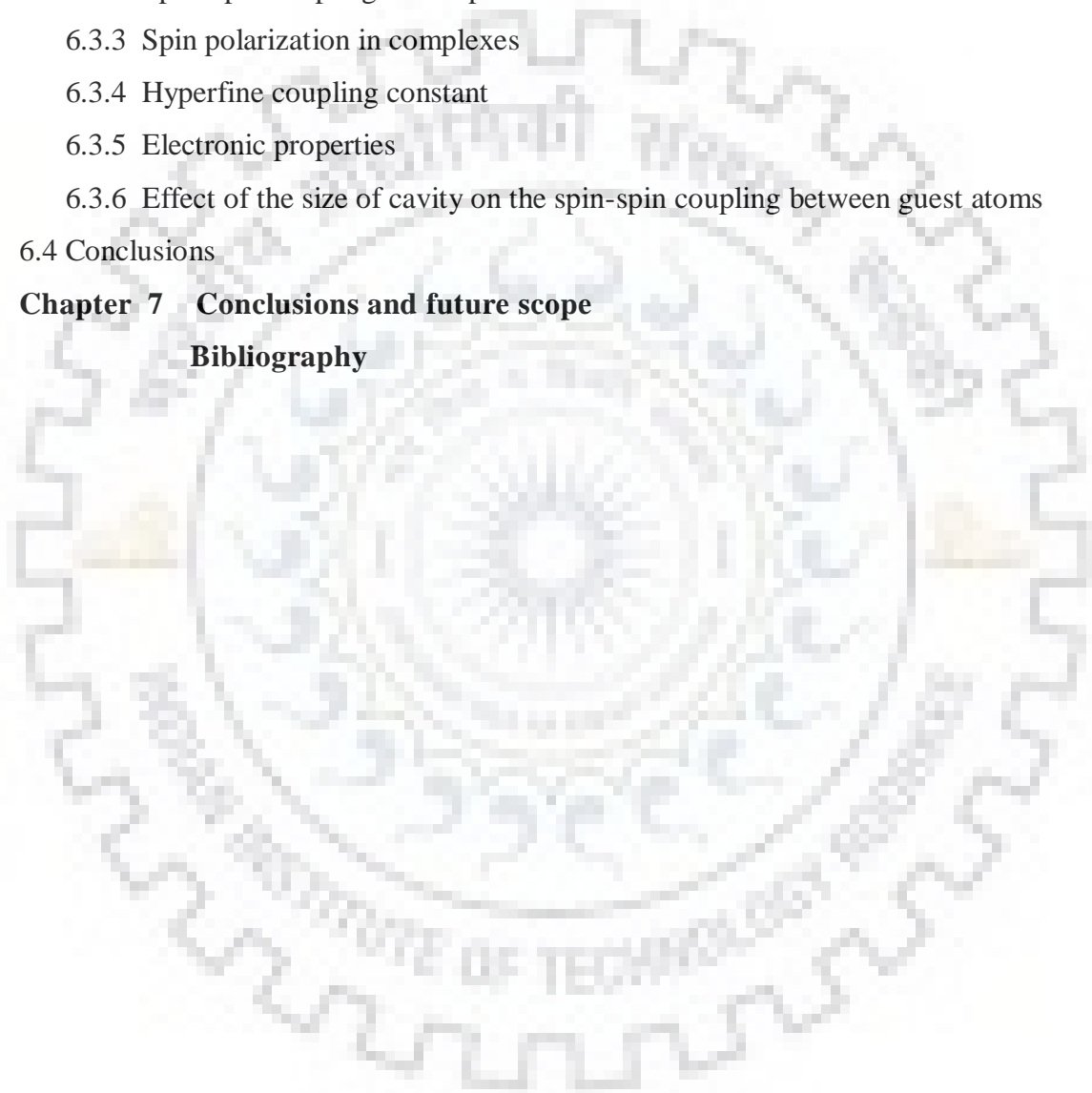


Table of Contents

Candidate's Declaration	
Abstract	i
Acknowledgements	v
List of Abbreviations	vii
Table of Contents	viii
List of Tables	xi
List of Figures	xiii
List of Publications	xvi
List of Conferences / Workshops	xvii
Chapter 1 Introduction	1
1.1 Fullerenes	1
1.1.1 Derivatives of fullerene	1
1.2 Studies on fullerenes and endohedral fullerenes	3
1.3 Studies on heterofullerenes and endohedral heterofullerenes	5
1.4 Carbon Nanotubes (CNTs)	6
1.5 Boron nitride nanotubes (BNNTs)	6
1.6 Endohedral and exohedral complexes of carbon nanotubes	7
1.7 Studies on endohedral carbon nanotubes	7
1.8 Objective of the thesis	12
1.9 Outline of the thesis	13
Chapter 2 Computational Methods	16
2.1 <i>Ab initio</i> methods	16
2.1.1 The Schrödinger equation	17
2.1.2 Hartree-Fock method	18
2.1.3 Post Hartree-Fock methods	19
2.2 Density functional theory (DFT)	20
2.2.1 Thomas-Fermi-Dirac approximation	20
2.2.2 The Kohn-Sham equations	22
2.2.3 Approximations of the exchange-correlation functional	23
2.3 Basis sets	26
2.3.1 Classification of basis sets	27
2.4 Time-dependent density functional theory (TDDFT)	29
2.5 Spin broken symmetry approach	29

2.6 Spin density and spin polarization parameter	30
Chapter 3 Structure, stability and properties of the nitrogen encapsulated fullerene derivatives	31
3.1 Introduction	31
3.2 Computational methods	31
3.3 Results and discussion	33
3.3.1 Structure and stability of the complexes	33
3.3.2 Spin–Spin coupling between guest and host as well as guest atoms of adjacent Cages	36
3.3.3 Energy gap between HOMO and LUMO	40
3.3.4 Thermodynamic feasibility of the formation of the complexes	45
3.4 Conclusions	48
Chapter 4 Structure, stability and properties of the boron encapsulated fullerene derivatives	49
4.1 Introduction	49
4.2 Computational methods	50
4.3 Results and discussion	51
4.3.1 Structure, stability and host–guest interaction	51
4.3.2 Electronic properties	56
4.3.3 Spin–Spin coupling between guest and host	61
4.3.4 Hyperfine coupling constant (hfcc)	61
4.3.5 Thermodynamics of encapsulation of boron in fullerene derivatives	64
4.4 Conclusions	66
Chapter 5 Structure, stability and properties of the dimers of B@C₅₉N and N@C₅₉B	67
5.1 Introduction	67
5.2 Computational methods	68
5.3 Results and discussion	72
5.3.1 Structure and stability of the complexes	72
5.3.2 Spin polarization and transfer of spin density	75
5.3.3 Thermodynamic feasibility of the formation of the complexes	82
5.3.4 Electronic properties	82
5.4 Conclusions	86

Chapter 6 Structure, stability and properties of the nitrogen encapsulated carbon and boron nitride nanotubes	87
6.1 Introduction	87
6.2 Computational methods	88
6.3 Results and discussion	88
6.3.1 Structure and stability of the complexes	88
6.3.2 Spin-Spin coupling in complexes	92
6.3.3 Spin polarization in complexes	95
6.3.4 Hyperfine coupling constant	100
6.3.5 Electronic properties	101
6.3.6 Effect of the size of cavity on the spin-spin coupling between guest atoms	105
6.4 Conclusions	108
Chapter 7 Conclusions and future scope	109
Bibliography	112



LIST OF TABLES

Table No.	Title	Page No.
3.1	Stabilization energy (kcal/mol) of various endohedral complexes for their different spin states. The BSSE corrected values for the most stable spin states are given in parentheses.	35
3.2	The spin density values (in e/au^3) of various nitrogen atoms and the spin polarization parameter (ζ) for the stable state of the complexes.	38
3.3	Calculated HOMO–LUMO energy gap (eV) for various complexes in their most stable spin states.	43
3.4	The change in Gibbs free energy (ΔG) and change in enthalpy (ΔH) for the formation of the complexes relevant to the encapsulation of guest atoms inside the fullerene derivatives. For the dimers, the value of ΔG and ΔH associated with the dimerization monomers units are provided in parenthesis.	46
3.5	The relative energy (R.E.) of various complexes with respect to their trans conformers and the spin density of encapsulated nitrogen atoms.	47
4.1	Stabilization energy (kcal/mol) of various endohedral fullerene complexes in their different spin states. The basis set superposition error (BSSE) corrected values are given in parentheses.	52
4.2	Values of vertical electron affinity (VEA), vertical ionization energy (VIE), and the energy gap between HOMO and LUMO ($\Delta E_{HOMO-LUMO}$) of complexes in their different spin states obtained at the B3LYP/6-311G* Level. The values obtained at B3LYP-GD2/6-311G* level are given in parentheses.	58
4.3	The spin density values (in e/au^3) and hyperfine coupling constant values (hfcc) (in Gauss) on the heteroatom of cage and encapsulated boron atom of various complexes along with the values of spin polarization parameter (ζ) of the complexes.	62
4.4	The change in Gibbs free energy (ΔG) and change in enthalpy (ΔH) due to the boron atom encapsulation in fullerene derivatives.	65
5.1	The stabilization energy and various properties of $C_{59}B$ and its nitrogen encapsulated complex. The value of stabilization energy with BSSE corrections are given in parenthesis.	71
5.2	Relative energies (kcal/mol) of cis and trans form of $(C_{59}N)_2$, $(C_{59}B)_2$ and $(C_{59}B-C_{59}N)$.	72

5.3	Stabilization energies (ΔE_{stab}) of various endohedral heterofullerenes for their different spin states obtained at the B3LYP-GD2/6-311G* level. The basis set superposition error (BSSE) corrected values of stabilization energies are given in parenthesis.	73
5.4	The spin density of various heteroatoms and the spin polarization parameter (ζ) for the stable endohedral complexes.	76
5.5	The relevant molecular orbitals showing the spin density distribution for an isodensity value of 0.02 of stable spin states of various endohedral heterofullerenes. The energies of molecular orbitals are given in Hartree.	79
5.6	The change in Gibbs free energy (ΔG) and change in enthalpy (ΔH) for the formation of the complexes by encapsulating guest atoms in the host cage of the heterofullerene dimer as well as by the dimerization of their respective monomers.	84
5.7	The values of vertical electron affinity (VEA), vertical ionization energy (VIE), energy gap between HOMO and LUMO ($\Delta E_{\text{HOMO-LUMO}}$) and dipole moment (μ) for various heterofullerenes and their complexes.	85
6.1	The stabilization energies of the nitrogen atom encapsulated complexes of nanotubes in their different spin states at B3LYP-GD2/6-311G** level. The values of BSSE corrected stabilization energies are given in parenthesis for the stable states of the complexes.	91
6.2	The stabilization energy of various complexes associated with the encapsulation of nitrogen atom at B3LYP-GD2/6-311G** level. For (CNT) ₂ and rotated-(CNT) ₂ , their relative energy with respect to each other is given.	93
6.3	The spin density on encapsulated nitrogen atoms and the spin polarization parameter (ζ) for the stable endohedral nanotubes.	96
6.4	The calculated values of hyperfine coupling constant (hfcc) of encapsulated nitrogen atom in various endohedral nanotubes	100
6.5	The values of vertical electron affinity (VEA), vertical ionization energy (VIE), energy gap between HOMO and LUMO ($\Delta E_{\text{HOMO-LUMO}}$) of various nanotubes and their nitrogen atom encapsulated complexes.	102
6.6	The calculated stabilization energies of the nitrogen atom encapsulated complexes of (5,5)-CNT in their different spin states at B3LYP-GD2/6-311G** level. The values of BSSE corrected stabilization energies for the stable spin states of the complexes are given in parenthesis.	107

LIST OF FIGURES

Figure No.	Title	Page No.
1.1	Structure of (a) endohedral fullerene, (b) exohedral fullerene, and (c) heterofullerene.	2
1.2	Different types of carbon nanotubes based on the way of rolling graphene sheet.	8
1.3	Structure of boron nitride nanotube (BNNT).	9
1.4	Structure of (a) endohedral carbon nanotube and (b) exohedral carbon nanotube.	9
3.1	Optimized geometries of C_{60} , $C_{59}N$, their nitrogen encapsulated complexes, and their respective dimers.	34
3.2	Spin density difference plots for various complexes in their most stable spin states with an isodensity value of 0.0004. The blue color represents the excess of α spin density, and the orange color represents the excess of β spin density.	39
3.3	Isodensity surface plots of α -spin highest occupied and lowest unoccupied molecular orbitals of the complexes with an isodensity value of 0.02. For triplet state of ${}^3[N@C_{59}N]$, the β -spin orbitals are shown.	41
3.4	Isodensity surface plots of highest occupied and lowest unoccupied β -spin molecular orbitals of the complexes with an isodensity value of 0.02. For triplet state of ${}^3[N@C_{59}N]$, α -spin orbitals are shown.	42
3.5	The α - and β -spin HOMO and LUMO energy levels of ${}^2[C_{59}N]$, ${}^3[N@C_{59}N]$ and ${}^5[N@C_{59}N]$.	44
4.1	Optimized geometries of the complexes in their different spin states.	53
4.2	Figure illustrating the internuclear distances for some of the selected atoms of $C_{59}B$, $C_{59}N$ and their complexes. The diameter of the cage with respect to the heteroatom, its nearest carbon and along the perpendicular direction is also shown in the right bottom of each panel.	54
4.3	Isodensity surface plots of α -spin highest occupied and lowest unoccupied molecular orbitals of the complexes in their different spin states with an isodensity value of 0.02.	59

4.4	The β -spin isodensity surface of highest occupied and lowest unoccupied molecular orbitals of the paramagnetic species with an isodensity value of 0.02.	60
4.5	Spin density difference plots of various complexes in their different spin states with isodensity value of 0.0004. The blue color represents the excess of α -spin density, and the orange color represents the excess of β -spin density.	63
5.1	The optimized geometries of N@C ₅₉ B in its various spin states.	70
5.2	The spin density distribution plot of triplet and quintet states of N@C ₅₉ B with an isodensity value of 0.0004.	70
5.3	Optimized geometries of various stable spin states of different endohedral heterofullerenes. The grey, violet and green colored spheres represent carbon, boron and nitrogen atoms, respectively. The multiplicity of the complexes is given in superscript.	74
5.4	Spin density difference plots for the various endohedral heterofullerenes in their stable spin states for an isodensity value of 0.0004. The blue color represents an excess of α -spin density, and the orange color represents an excess of β -spin density. The multiplicity of the complexes is given in superscript.	77
6.1	Optimized geometries of CNT, BNNT, (CNT) ₂ , (BNNT) ₂ and their respective nitrogen atom encapsulated complexes. The grey, violet and green colored spheres represent carbon, boron and nitrogen atoms, respectively. The multiplicity for each of the complexes is given in superscript.	90
6.2	The geometries and relative energies of parallel and slipped parallel form of respective dimers of benzene and borazine at B3LYP-GD2/6-311G** level.	94
6.3	Spin density difference plots for endohedral nanotubes in their stable spin states for an isodensity value of 0.0004.	96
6.4	The relevant molecular orbitals showing spin density distribution for the stable spin states of various endohedral nanotubes with an isodensity value of 0.02. The energies of orbitals are given in Hartree.	97
6.5	Isodensity surface plots of highest occupied and lowest unoccupied molecular orbitals of the complexes in their stable spin states with an isodensity value of 0.02.	103

- 6.6** Optimized geometries of (5,5)-CNT, N@(5,5)-CNT and their respective dimers. The grey, violet and green colored spheres represent carbon, boron and nitrogen atoms, respectively. The multiplicity of the complexes is given in superscript. 106
- 6.7** The spin density difference plots of $^4[\text{N}@(5,5)\text{-CNT}]$, $^1[(\text{N}@(5,5)\text{-CNT})_2]$ and $^7[(\text{N}@(5,5)\text{-CNT})_2]$ for an isodensity value of 0.0004. The spin density values (e/au³) on guest nitrogen atoms along with the spin polarization parameter (ζ) are also given. 107



List of Publications

Publications from the thesis

1. **Vinit**, K.S. Sujith, C. N. Ramachandran, Spin-Spin interaction in nitrogen atom encapsulated C₆₀, C₅₉N, and their respective dimers, *J. Phys. Chem. A*, **2016**, 120, 6990-6997.
2. **Vinit**, C. N. Ramachandran, Structure, stability, and properties of boron encapsulated complexes of C₆₀, C₅₉B and C₅₉N, *J. Phys. Chem. A*, **2017**, 121, 1708-1714.
3. **Vinit**, C. N. Ramachandran, Spin density transfer from guest to host in endohedral heterofullerene dimers, *Phys. Chem. Chem. Phys.* **2019**, **21**, 7605-7612.
4. **Vinit**, C. N. Ramachandran, Confinement of atomic nitrogen in carbon and boron nitride nanotubes (*to be submitted*).

Other Publications

1. Mohan Tiwari, **Vinit**, C. N. Ramachandran, Catalytic reduction of SO₂ by CO using carbon intercalated gold clusters, *Chem. Phys. Lett.* **2019**, 726, 111-116.

List of Conferences/Workshops

1. Organized and given an oral presentation entitled **“Spin-Spin coupling and spin polarization in fullerene derivatives”** in **“3rd North West Meeting on Spectroscopy, Structure and Dynamics, 2019 (SSD-2019)”** held from April 05th-07th, 2019 organized by Department of Chemistry at IIT Roorkee, Roorkee.
2. Attended and presented a poster entitled **“Spin-Spin Interactions in Endohedral B,N-Heterofullerenes”** in **“ACS on Campus”** organized by Department of Chemistry at IIT Roorkee, Roorkee during February 7th, 2018.
3. Attended and successfully completed the *GIAN course* on **“Computationally Aided Materials Designing for Materials Genome”** held at IIT Indore, Indore during January 04th-08th, 2018.
4. Organized and participated in **Contemporary Facets in Organic Synthesis (CFOS 2017)**, held from December 22th-24th, 2017 organized by Department of Chemistry at IIT Roorkee, Roorkee, India.
5. Attended and presented a poster entitled **“Spin-Spin Interaction in Endohedral Heterofullerenes”** in the **“1st North West Meeting on Spectroscopy, Structure and Dynamics, 2017 (SSD-2017)”** held from March 18th-19th, 2017, organized by Birla Institute of Technology and Science, Pilani, Rajasthan, India.
6. Attended and presented a poster entitled **“Electron Spin-Spin Interaction in Endohedral Complexes of Fullerenes and Heterofullerenes”** in the **“15th Indian Theoretical Chemistry Symposium”** held from December 14th-17th, 2016, organized by University of Hyderabad, Hyderabad, India.
7. Volunteered and participated in **International Conference on Advanced Materials 2016 (ICAM-2016)**, held from March 4th-7th, 2016 organized by Department of Chemistry at IIT Roorkee, Roorkee, India.
8. Attended and presented a poster entitled **“Density functional studies of nitrogen encapsulated endohedral complexes of C₆₀, C₅₉N and their respective dimers”** in the **“18th CRSI National Symposium in Chemistry”** held from February 5th-7th, 2016, organized jointly by Institute of Nano Science and Technology and Panjab University.
9. Attended and presented a poster entitled **“Interaction of the Guest Species Beyond the Cage: The case of N@C₆₀”** in **Asian Academic Seminar 2015**, held from March, 6th-10th, 2015 organized jointly by JSPS Japan, IISER Kolkata and IACS Kolkata, India.



Chapter-1

Introduction

Carbon exists in its different allotropic forms such as graphite, diamond, fullerenes and carbon nanotubes [1]. Among these, the serendipitous discoveries of fullerenes and carbon nanotubes at the end of last century paved the way for a new branch of science called nanoscience [2, 3]. The fullerenes and carbon nanotubes find various applications due to their different properties. A brief discussion about fullerenes, carbon nanotubes and their derivatives are given below.

1.1 Fullerenes

The fullerenes were discovered when the graphite was vaporized in presence of helium atmosphere during the studies on the polycyclic hydrocarbons relevant to interstellar chemistry [2]. For the discovery of fullerenes, Nobel prize in chemistry was awarded jointly to Kroto, Curl and Smalley in 1996. In contrast to graphite, made up of only hexagons, the framework of fullerene includes both hexagons and pentagons [1, 2]. It is known that pentagons lead to spherical or ellipsoidal structures. One of the most abundant fullerenes is C_{60} in which 12 pentagons and 20 hexagons are arranged in the form of a soccer-ball. There are two types of bonds present in C_{60} which differ in their bond lengths (1.40 Å and 1.46 Å). The molecular point group of C_{60} fullerene is icosahedral (Ih). Based on the similarity between the shape of C_{60} with the football as well as the Montreal biosphere by Buckminster Fuller, C_{60} fullerene is also known as buckyball or Buckminster fullerene. In 1990, Krätschmer, Lamb, Fostiropoulos and Huffman produced C_{60} fullerene in milligram amounts using the resistive heat on graphite [4]. In nature, fullerenes are found in hydrocarbon flames, soots and minerals [5-7].

1.1.1 Derivatives of fullerene

Buckminster fullerene has a cavity of diameter 7.09 Å and forms different types of derivatives viz. endohedral fullerenes, exohedral fullerenes and heterofullerenes as represented in figure 1.1. The derivatives in which atoms, ions, or small molecules occupy the inner cavity of fullerenes are known as endohedral fullerenes and are denoted by $G@C_n$, where G represents the guest species and n is the number of carbon atoms of the fullerene cage. Heath *et al.* synthesized the endohedral fullerene $La@C_{60}$ using the laser ablation technique when graphite was ablated in a solution of $LaCl_3$ [8]. The synthesis of $La@C_{60}$ opened a new direction in the studies of fullerene and later several guest species including various types of atoms and small molecules (di-atomic, tri-atomic and tetra-atomic etc.) were encapsulated in the cavity of fullerenes [9-18].

The other derivatives of fullerene in which species linked to the outer surface of fullerene cage are known as exohedral fullerenes (figure 1.1 b). The first two exohedral fullerene synthesized were $C_{60}Pt(PPh_3)_2$ and $C_{60}Pd(PPh_3)_2$ [19-22]. Later, various exohedral fullerenes have been synthesized with different metals such as Ti, Nb, Re, Fe, Ru and Ni as guest species [23-28]. Since then, several reports are available on different exohedral fullerenes [29-35]. Among these, the theoretical studies on the structure and stability of various $C_{60}F_n$ ($n = 2, 4, 6, \dots, 52$) take a special attention as the studies showed exohedral derivatization of fullerenes by fluorine enhanced the polarity and hence its solubility in polar solvents [33, 34]. The variation in electronic properties of C_{60} with the exohedral functionalization has also been reported. [35].

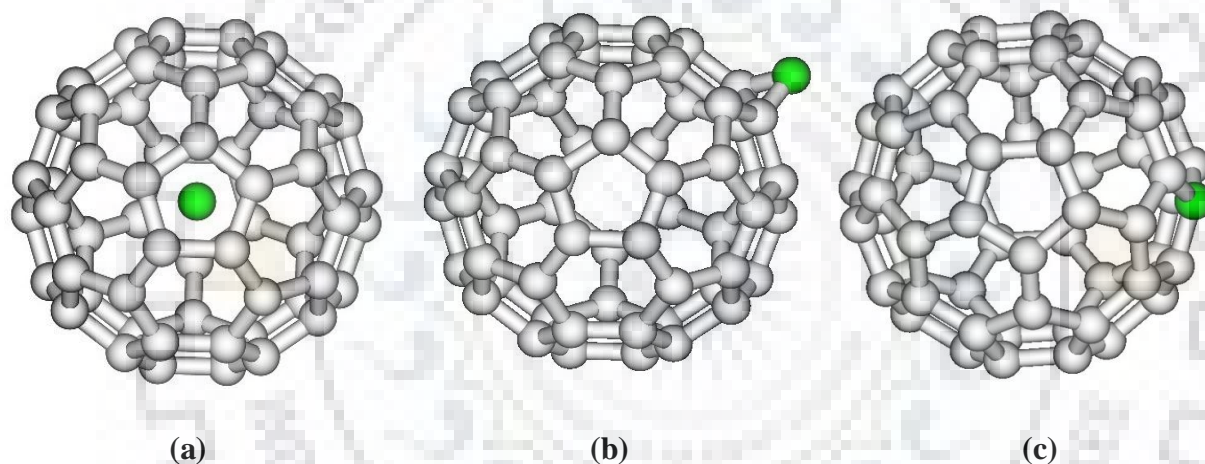


Figure 1.1. Structure of (a) endohedral fullerene, (b) exohedral fullerene, and (c) heterofullerene.

Another important class of fullerene derivative is heterofullerene where at least one carbon atom of the cage is replaced by heteroatom such as boron, nitrogen and phosphorous (figure 1.1 c) [36-39]. Heterofullerenes are considered as an interesting material, because of their structure, chemical functionality and electronic properties. The vaporization of graphite in the atmosphere of pyrrole and boron-nitride leads to the formation of azafullerenes and borofullerenes, respectively [40-41]. The synthesis of azafullerene cation $C_{59}N^+$ was reported from a cluster of N-MEM (N-methoxyethoxy methyl) ketolactam by the atom bombardment technique [42]. The subsequent formation of $(C_{59}N)_2$ dimer by *in situ* reduction of $C_{59}N^+$ cation was also reported.

Batirev and his co-workers investigated the electronic structure of $(C_{59}B)_2$ using quantum chemical calculations [43].

The fullerenes and their derivatives are useful in various fields due their exceptional properties. The fullerenes can be used in photovoltaics due to their *n*-type semiconducting properties [44-45]. They have also been proposed as antiviral agent, photosensitizer, antioxidant, drug delivery carriers, hydrogen storage and dehydrogenation materials [46-50]. Fullerenes have also been found to be useful to create the assemblies of the superparamagnetic species [51-52]. Similar to fullerenes, endohedral fullerenes find potential applications in MRI [53-55] and X-ray [56] diagnosis. They are also used as radiotracers [57-58], antitumor agent [59-60], superconductor [61] and ferroelectric material [62-63]. Endohedral fullerenes have also been proposed as a candidate for quantum computing [64-66]. It has also been reported that reactions become spontaneous inside a fullerene cavity [67]. Recently, Mehdi *et al.* showed the catalytic applications of heteroatom (B, N, Si, P and S) doped fullerenes towards the oxidation of CO, conversion of NO to N_2O and reduction of N_2O to N_2 [68-70].

1.2 Studies on fullerenes and endohedral fullerenes

The endohedral fullerenes have become a demanding material since last few decades due to their unique electronic, optical and magnetic properties [9-10]. As mentioned before, taking graphite as a starting material Kroto *et al.* synthesized the first endohedral fullerene $La@C_{60}$ in 1985 using the laser ablation method [8]. Followed by the synthesis of $La@C_{60}$, several other endohedral fullerenes of different size were reported which encapsulate various guest species including noble gases, reactive atoms, metal atoms, and small molecules [9-18, 71-81]. Several experimental and theoretical investigations about the encapsulation of various reactive species inside C_{60} fullerenes have been reported thereafter [82-91].

The formation of fullerene dimers and their complexes also gained the attention of scientific community especially those working in the field of fullerenes. Rao *et al.* observed the formation of $(C_{60})_2$ via cycloaddition reaction by exposing C_{60} to uv-visible light [92]. The above cycloaddition reaction was confirmed by several other experimental and theoretical techniques [93-102]. Followed by the synthesis of $(C_{60})_2$, Farrington *et al.* reported the formation of the derivatives of $(N@C_{60})_2$ via a 1, 3 dipolar cycloaddition reaction [103].

The encapsulation of paramagnetic species inside fullerene can alter the magnetic properties of the latter which has become a topic of interest since last few decades. The endohedral fullerenes with paramagnetic guest species have been investigated theoretically [104-113]. For example; Park *et al.* studied the encapsulation of paramagnetic atoms such as nitrogen, phosphorus, oxygen and sulphur inside C_{60} [104]. Their results suggested that the dispersion interactions between components lead to the stability of complexes. Their studies also revealed that the guest species retained their spin states. Further, Lu *et al.* investigated the encapsulation of nitrogen, oxygen and fluorine atoms in the cavity of C_{60} and revealed that the complexes are stable due to dispersion interaction between guest and host cage [105]. The study also showed that the atomic spin states of the guest atoms are retained inside C_{60} . The theoretical studies of polonium encapsulated C_{60} indicated triplet state of the complex as stable in which polonium occupies the centre of C_{60} retaining its electronic configuration [106]. Asif *et al.* examined the effect of encapsulation of B_2 , O_2 and Ge_2 inside C_{60} on the stability of their respective complexes in their singlet and triplet states [107]. Their investigations revealed that the spins of guest species are unaltered inside C_{60} . On the other hand, studies of endohedral complexes of C_{60} with guest species calcium, scandium and yttrium showed that the electrons of outer most s-orbitals of guest species are transferred to C_{60} cage [108]. The density functional studies of $Gd@C_{60}$ showed that the complex is stable in its septet state in which there is electron transfer from guest to host [109]. The study also reported the antiferromagnetic spin coupling between Gd and C_{60} . The structural, electronic and magnetic properties of defective uranofullerene $U_2@C_{61}$ have been investigated using the density functional methods [110, 111]. To induce the defect in $U_2@C_{60}$, an extra carbon atom was added to different sites of the outer surface of C_{60} cage. The presence of an unpaired electron on the surface of $U_2@C_{61}$ leads to a significant change in the magnetic properties compared to that of $U_2@C_{60}$. The studies also showed the complex as stable in quintet state with antiferromagnetic coupling between the components U_2 and C_{61} . Nakagawa and co-workers studied the isolation, structure and electromagnetic properties endohedral complexes of exohedral fullerenes $La@C_{60}(CF_3)_{3,5}$ and $Gd@C_{60}(CF_3)_{3,5}$ [112]. Their results showed that the energy gap between HOMO and LUMO of $La@C_{60}$ and $Gd@C_{60}$ widened on addition of CF_3 units over the surface of cage. It was also revealed that the spins of guest and host of $Gd@C_{60}(CF_3)_3$ are antiferromagnetically coupled. Using theoretical and experimental methods, Qian *et al.* investigated on the electronic structure and magnetic properties of $Gd_3N@C_{80}$ and showed that the complex has high magnetic moment of $21.0 \mu_B$ [113]. It was also revealed that the spin density is localized only on the guest species of $Gd_3N@C_{80}$.

1.3 Studies on heterofullerenes and endohedral heterofullerenes

As mentioned earlier, the substitution of at least one carbon of fullerene cage by the heteroatom (B, N, and P etc.) leads to the formation of heterofullerenes [114]. Several theoretical and experimental studies have been reported on the heterofullerenes with the heteroatoms from boron and nitrogen family. [42-49, 114-120]. When graphite was vaporized in the atmosphere of pyrrole and boron-nitride, it resulted in the formation of azafullerenes and borofullerenes, respectively [46-47]. Followed by the synthesis of azafullerene and borofullerene, the theoretical studies on the heterofullerenes such as $C_{59}B$, $C_{59}N$, $C_{59}Al$, $C_{59}Ga$, $C_{59}In$, $C_{59}Ge$, and $C_{59}As$ were reported [43-44, 49, 115-120]. The investigations of the electronic structure and properties of $C_{59}B$ and $C_{59}N$ using the tight-binding approximation method indicated that the former is electron deficient and latter is electron rich [116]. Andreoni *et al.* also reported similar results using the Car-Parrinello method [117]. The studies of heterofullerenes with heteroatoms from the boron family indicated that the HOMO-LUMO energy gap is decreased compared to that of C_{60} [118]. The density functional studies on the heterofullerenes $C_{59}X$ (where X is heteroatom from the boron, nitrogen and carbon family) revealed that the properties of heterofullerenes are significantly different from those of C_{60} fullerenes [119]. The boron and nitrogen atom substituted fullerenes of different combination have been studied using the time-dependent density functional theory (TDDFT) and it was revealed that the absorption properties of fullerene can be tuned with appropriate substitution [120]. The hyperfine coupling constant (hfcc) of the heteroatom in heterofullerene has been investigated using the electron spin resonance spectroscopy [121-122]. The value of hfcc for ^{14}N in azafullerene is 3.60 at a g-value of 2.0004 [121]. Later, the values of hfcc of nitrogen atom in azafullerenes $C_{19}N$, $C_{59}N$, $C_{69}N$, and $C_{75}N$ were reported by Schrier *et al.* using density functional methods [122]. Several articles and reviews about the synthesis and various properties of heterofullerenes and their dimers are available in literature [123-134].

Various endohedral heterofullerenes have been investigated using the theoretical and experimental methods [135-140]. The theoretical studies of the encapsulation of hydrogen atom in $C_{59}B$ and $C_{59}P$ have been performed which revealed that the hydrogen atom is bonded to inner surface of the heterofullerenes $C_{59}B$ and $C_{59}P$ [135]. Recently, using molecular surgery method Murata and his co-workers synthesized $H_2@C_{59}N$, $H_2O@C_{59}N$ and their respective dimers [136-137]. The 1H NMR spectra of $H_2O@C_{59}N$ showed that the relaxation time of guest water molecule is significantly decreased compared to that of free molecule due to the effect of paramagnetic $C_{59}N$ host cage. Furthermore, NMR spectra of the dimer indicated that guest water molecules present in adjacent cages do not interact with each other. In another study by

the same group, the synthesis of $\text{H}_2@\text{C}_{59}\text{N}^+$ and $\text{H}_2\text{O}@\text{C}_{59}\text{N}^+$ has been done using molecular surgery method [138]. This study revealed strong intramolecular electrostatic interaction between C_{59}N^+ and H_2O in contrast to its isoelectronic systems $\text{H}_2\text{O}@\text{C}_{60}$. The electron affinity (EA) of $\text{H}_2\text{O}@\text{C}_{59}\text{N}$ has been determined using the high-resolution photoelectron imaging spectroscopy and found that EA of the complex is 0.0092 eV lower than that of free host cage [139]. *Ab initio* and density functional studies on Gd_2 and Dy_2 encapsulated C_{79}N reported strong magnetic exchange coupling between guest atoms [140].

1.4 Carbon Nanotubes (CNTs)

The cylindrical structures formed by the rolling of graphene sheets are known as carbon nanotubes. In 1991, the carbon nanotubes were firstly synthesized by the Ijima using an arc discharge method [3]. The different forms of carbon nanotubes such as long, short, single-walled, multi-walled, open, and closed are available nowadays. Due to electron delocalization, CNTs show amazing electronic properties. Carbon nanotubes have high tensile strength, Young's modulus and excellent mechanical strength [141-142].

The single-walled carbon nanotubes (SWCNTs) can be classified based on a pair of indices (n, m) called the chiral vector. Depending on the values of n and m, SWCNTs are classified into three types. These include (i) armchair (n=m), (ii) zigzag (m=0) and chiral (n≠m≠0) and are shown in figure 1.2. The carbon nanotubes show metallic and semiconducting properties based on their structure [143-145]. The armchair carbon nanotube is metallic as its conduction band is near to the valence band. Hence electrons can easily enter to the conduction band. On the other hand, zigzag and chiral carbon nanotubes are semiconducting due to relatively high energy difference between conduction and valence bands.

1.5 Boron nitride nanotubes (BNNTs)

The structural analogous of CNTs by replacing C_2 units by BN units are known as BNNTs (Figure 1.3). Although, CNTs and BNNTs are structurally similar, they differ in their chemical and physical properties [146-148]. Unlike CNTs, the electronic properties of BNNTs are independent of chirality. In 1995, Chopra *et al.* synthesised BNNTs by applying arc discharge on h-BN sheet [149]. Using this technique, BNNTs of 1-3 nm diameters and 200 nm lengths were obtained. Later, other well-known techniques such as laser ablation and chemical vapour deposition were also used for the synthesis of BNNTs [150-151].

CNTs and BNNTs find applications in various fields due to their peculiar properties such as electrical, chemical, mechanical, optical, and thermal [146-148, 152-159]. The nanotubes have unique structures by which they possess high surface area, good stiffness and resilience. The carbon nanotubes can be used in the field of drug delivery, tissue engineering, artificial implants, energy storage, hydrogen storage etc. [146-148, 152-159]. CNTs can also be used as electrochemical supercapacitor, field-emitting devices, transistors, nanopropes, artificial implants, preservatives, energy storage and hydrogen storage material, sensors, composite material, and templates.

1.6 Endohedral and exohedral complexes of carbon nanotubes

Similar to fullerenes, carbon nanotubes can also accommodate various atoms, ions and molecules inside the cavities. Such type of complexes are known as endohedral carbon nanotubes and is denoted as G@CNT, where G represents the guest species (figure 1.4 a). Various endohedral complexes of CNT with different guest species have been reported [160-168].

The carbon nanotubes associate in the form of bundles in solvents. The exohedral functionalization of carbon nanotubes prevent the formation of such bundles to some extent and disperse CNTs in solutions. This type of complexes of CNTs is known as exohedral carbon nanotube (figure 1.4 b). The exohedral functionalization of carbon nanotubes have been achieved using organic or inorganic molecules, organic-inorganic hybrid molecules, metal nanoparticles, proteins, enzymes and polymers, [169-170].

1.7 Studies on endohedral carbon nanotubes

In a confined environment, the properties of atoms and molecules can be changed drastically. As mentioned above, various species can be confined inside the carbon nanotube due to their hollow structure. The encapsulation of various molecules and clusters inside carbon nanotubes has been investigated using various experimental and theoretical techniques [143, 161, 164, 173-178]. Li and coworkers theoretically studied the encapsulation of α -, β -, and γ -Ga nanowires (NW) in carbon nanotubes and showed that β -, and γ -Ga nanowire encapsulated complexes of CNT are more stable than the complex of α -Ga nanowire [179]. The stability of endohedral complexes of β -, and γ -Ga nanowires with CNT mainly arises due to the strong

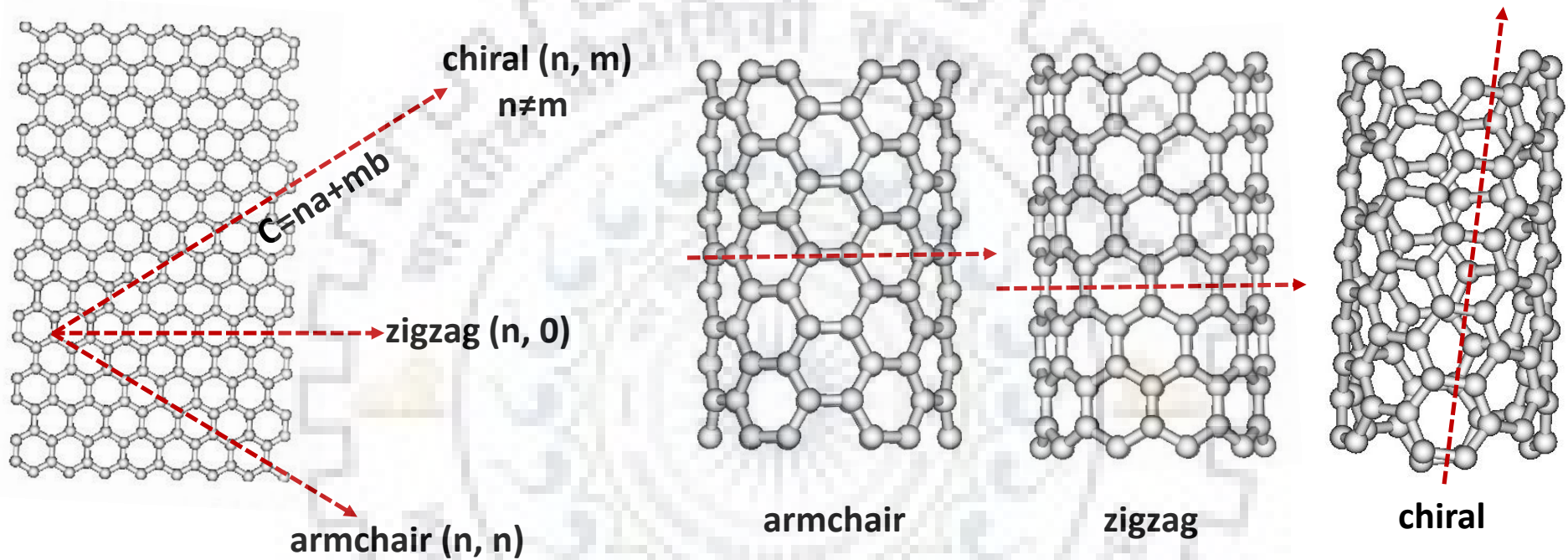


Figure 1.2. Different types of carbon nanotubes based on the way of rolling graphene sheet.

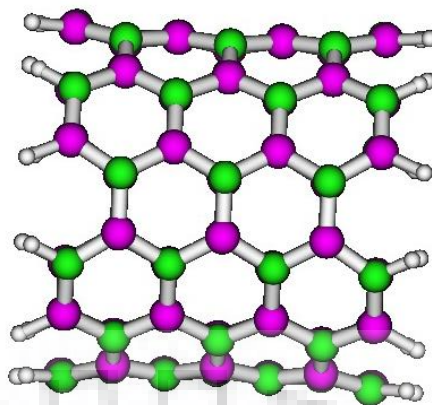


Figure 1.3. Structure of boron nitride nanotube (BNNT).

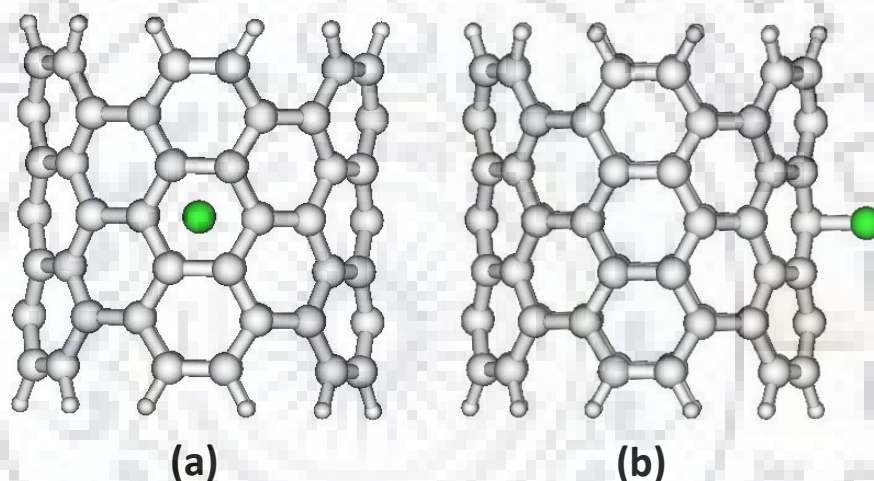


Figure 1.4. Structure of (a) endohedral carbon nanotube and (b) exohedral carbon nanotube

interaction of Ga nanowire with inner wall of CNT. The density functional theory has also been applied on Gd and Gd-carbide nanowire encapsulated carbon nanotube to investigate their structural, electronic and magnetic properties [180]. The study showed that the interaction between Gd atoms and inner walls of CNT in GdNW@CNT is strong compared to that of Gd-Gd bond resulting in the stretching of the bond. However, in the endohedral complex of Gd-carbide with CNT, the interaction between Gd atoms and inner wall of CNT is weaker than that between Gd and C atoms of Gd-carbide. Zhou and coworkers investigated the structural, electronic and transport properties of Gd/Eu chain encapsulated complexes of carbon nanotube using density functional methods [181]. Their study showed that Gd and Eu chains occupy off center positions inside the carbon nanotube. The results also reported the spin polarization at

the Fermi level when Gd-chain is encapsulated in (8,8)-CNT. Paduani investigated the MnNW encapsulated carbon nanotube using density functional methods to infer their structure, stability and electronic properties [182]. His results indicated that the electron spin of Mn atoms of MnNW coupled ferromagnetically inside carbon nanotubes. The electronic, optical and mechanical properties of diamond nanowire encapsulated CNT (CNW@CNT) have been examined using first principle calculations [183]. It was revealed that the complex (CNW@CNT) is stable due to weak van der Waals forces between the units. Using density functional methods, the stability and electronic properties of endohedral complexes of sulfur nanowire with CNT (SNW@CNT) have been investigated [184]. The study revealed that sulphur nanowire and carbon nanotube interacts *via* van der Waals forces leading to the stability of the complex. The encapsulation of sulphur nanowire in carbon nanotubes can alter the electronic properties of the latter. Recently, Huang and co-workers theoretically examined the structure and electronic properties of nitrogen chain (N_8) encapsulated (n, 0)-CNT (n = 6, 7, 8...12) and found that $N_8@$ (9, 0)-CNT is more stable compared to other complexes [185]. The study also revealed that the electronic properties of CNT were changed on encapsulating N_8 -chain inside.

Apart from the encapsulation of various nanowires and chains inside carbon nanotubes, various organic molecules have also been encapsulated in carbon nanotube [186-195]. These types of complexes are stable due to the attractive host-guest interactions. Using density functional theory, Kuwahara *et al.* investigated about the polyenes $C_{10}H_2$, $C_{10}H$, C_{10} , C_6H_2 , C_4H_2 and C_6H_{14} encapsulated (10, 0) CNT and showed that the resultant complexes are stabilized by 1.48, 2.04, 2.18, 1.05, 0.55, and 1.48 eV, respectively [186]. However, such stabilization was not observed when the above species were encapsulated inside a (10, 10) CNT. Khorsand *et al.* applied density functional theory to investigate the structural, energetics and properties of penicillamine encapsulated zigzag and armchair CNTs [187]. The study indicated that the van der Waals interactions along with the charge transfer from guest molecule to carbon nanotube stabilize the complex. Yumura *et al.* studied the encapsulation of π -conjugated oligomer (methyl terminated terfurans) inside the carbon nanotube [188]. It indicated that the arrangement of guest species inside carbon nanotube depends on the extent of host-guest interaction. The encapsulation of the drug doxorubicin (DOX) inside CNT has been examined theoretically by Wang *et al.* [189]. Their studies reported that the encapsulation becomes exothermic when the diameter of CNT is ~ 11.0 Å. Due to the host-guest interaction a bathochromic shift has been observed in the absorption spectra of β -carotene that confined

inside a carbon nanotube [190]. Orellana and co-workers investigated the terthiophene (T3) encapsulated complexes of zigzag carbon nanotube using density functional theory [191]. The band structure of the complex T3@CNT showed that the guest molecule retained its electronic properties. Debbichi *et al.* studied the complex anthracene@CNT using density functional theory and revealed that the electronic properties of the complex depend on the location of guest molecule [192]. Chernov and his co-workers studied the optical properties of graphene nanoribbon (GNR) encapsulated CNT and found that the complexes show photoluminescence in the visible and infrared regions of the spectrum [193]. Using the dispersion corrected density functional theoretical methods, Tripathy *et al.* investigated the effect of confinement on the proton transfer in Zundel cation using both carbon and boron nitride nanotube [194-195]. More details about the encapsulation of several other organic molecules inside CNT are available in a review by Y. J. Dappe [162].

The encapsulation of various atoms, molecules and clusters inside carbon nanotube has also been investigated experimentally and theoretically. This includes *ab initio* studies on the encapsulation of lithium and sodium atoms inside carbon nanotubes [196]. The results suggested that the guest atoms do not interact with each other when their concentration is up to 2.3 atomic percent [196]. In another study, the magnetic nanoparticles of iron were encapsulated in single walled carbon nanotube to investigate the magnetic properties of the complex [197]. The study showed that the iron nanoparticles encapsulated complexes of carbon nanotube exhibit ferromagnetic and superparamagnetic properties at room and low temperatures, respectively. Giménez-López *et al.* experimentally reported the encapsulation of archetypical single molecule magnet $\text{Mn}_{12}\text{O}_{12}(\text{O}_2\text{CCH}_3)_{16}(\text{H}_2\text{O})_4$ inside carbon nanotube and reported that the guest molecule retained its magnetic properties [198]. This study also suggested that the complex is a hybrid nano structure which combines the single molecule magnetic properties of guest and functional properties of host carbon nanotube. The density functional studies of rare gas dimers (He_2 , Ne_2 , Ar_2 and Kr_2) encapsulated (5, 5) and (6, 6) carbon nanotube revealed that the complexes are stable when guest species aligned parallel to the tube axis [199]. This study also showed that the bond distance between the atoms of rare gas dimer is decreased when they are located perpendicular to the carbon nanotube. In addition, Balasubramani *et al.* reported the energetics and host-guest interactions in the rare gas atom encapsulated carbon nanotube complexes using both analytical and density functional methods [200]. Their results suggested that the encapsulation of guest atoms is feasible in various carbon nanotubes depending on the size of guest as well as that of cavity of carbon nanotube.

1.8 Objective of the thesis

Over the last few decades, the endohedral complexes of fullerene and carbon nanotubes have gained wide attention. Among these, the encapsulation of atomic nitrogen in C_{60} can be considered as one of the most important studies where nitrogen atom retained its spin state. In this context, it is important to know that how the spins of guest species in two adjacent cages interact and how does heteroatom of the cage assist the interaction between the guest species. Similar questions are relevant for the boron atom encapsulated derivatives of fullerenes as boron is also reactive and paramagnetic. Different atoms inside the cavity and on the cage may affect the spin-spin coupling and hence attention is also given to the heterodimers formed by various combinations of $B@C_{59}N$ and $N@C_{59}B$. Although, some studies have been reported on the structure, stability and properties of endohedral fullerenes and heterofullerenes [8-18, 69-90, 104-120, 135-139], the spin-spin coupling, spin polarization and spin density transfer in endohedral fullerene dimers, endohedral heterofullerenes and endohedral heterofullerene dimers were not considered in earlier investigations.

One of the most important objectives of the thesis is to investigate the structure, stability and properties of nitrogen atom encapsulated fullerene derivatives. The complexes considered in the present study are $(N@C_{60})$, $(N@C_{59}N)$ and their respective dimers which are most important in the context of spin interactions between host-guest and guest-guest as mentioned above. The aim of present investigation is to understand the spin-spin coupling and spin density transfer between the components of above complexes. The study also plans to investigate on spin polarization and spin degeneracy in the complexes. The thesis aims to examine the effect of encapsulation of nitrogen atom inside fullerene cage on the energy gap between HOMO-LUMO of the latter. It is also important to study the thermodynamic feasibility of the formation of the complexes and hence the present thesis also focus on the calculation of change in Gibbs free energy (ΔG) and change in enthalpy (ΔH) associated with the encapsulation of nitrogen atom in various fullerene derivatives as well as the calculation of the above parameters associated with the dimerization of monomer units.

As mentioned earlier, boron is also reactive and paramagnetic atom. Therefore, it is of significance interest to investigate the structure, stability and properties of the boron atom encapsulated fullerene derivatives. In this regard, the idea is to study the complexes $B@C_{60}$, $B@C_{59}B$ and $B@C_{59}N$. The present investigations aims at understanding the spin-spin coupling and spin density transfer between guest and host of the above complexes. Another goal of the

present study is to examine the spin polarization and spin degeneracy in the complexes. The present study aims on examining the effect of encapsulation of boron atom inside host cages on the electronic properties of the latter. As above complexes are experimentally not available, which necessitates the investigation of thermodynamics of boron encapsulation inside various fullerene derivatives.

Another objective of the present thesis is to study the structure, stability and properties of dimers of nitrogen and boron atom encapsulated fullerene derivatives. For this purpose, the complexes $(B@C_{59}N)_2$, $(B@C_{59}N-N@C_{59}B)$ and $(N@C_{59}B)_2$ are considered. An attempt is also made to compare the above complexes to those of $(B@C_{59}B)_2$ and $(B@C_{60})_2$. The present study aims to investigate the spin-spin coupling and spin density transfer between host-guest and guest-guest of the complexes. To make the study more versatile, the present thesis also focuses on the studies on the spin polarization, spin degeneracy and electronic properties of the complexes. The study also aims to report about the thermodynamic feasibility of the formation of complexes based on the change in Gibbs free energy (ΔG) and enthalpy (ΔH) associated with different ways.

Similar to fullerenes, the carbon nanotubes can also host nitrogen atoms. Therefore, it would be interesting to study the structure, stability and properties of nitrogen atom encapsulated carbon nanotube, boron nanotube and their respective dimers. The present study aims at understanding the spin-spin coupling between the components of the endohedral nanotubes. In addition, the plan is also made to the report the nature of spin polarization in the complexes. To make the study more comprehensive, attempts have also made to investigate the effect of nitrogen encapsulation on various electronic properties such as electronic affinity, ionization energies and HOMO-LUMO energy gap of free host cages.

1.9 Outline of the thesis

The present thesis consists of seven chapters. Chapter 1 gives an introduction on fullerenes and their derivatives. The synthesis and applications of fullerenes and their derivatives are also reviewed. The discussion on the structure, stability and various properties of endohedral fullerenes as well as endohedral heterofullerenes followed by host-guest interactions and spin-spin coupling between their components are discussed. The structure, synthesis and applications of carbon and boron nitride nanotubes are briefly explained. The endohedral and exohedral derivatives of nanotubes are discussed. Studies about the encapsulation of various

species inside the carbon nanotube are presented. The effect of encapsulation of various molecules inside carbon nanotube on various properties of the latter are discussed.

To explore the structure, stability and various properties of endohedral derivatives of fullerenes, heterofullerenes, carbon nanotubes and boron nitride nanotubes, the density functional theoretical methods are applied. Thus, in chapter 2, an overview of various computational methods including the Hartree-Fock, post Hartree-Fock, density functional theoretical methods, basis sets, time-dependent density functional methods and spin broken symmetry approach are briefly explained. The details of the spin polarization parameter are also provided.

In chapter 3, the results obtained from the studies on the nitrogen atom encapsulated fullerene derivatives are presented. The host-guest and guest-guest spin coupling in stable states of the above complexes are discussed. The spin density transfer and spin polarization in the complexes are also analyzed. The effect of encapsulation of guest species on the energy gap between HOMO-LUMO of the host cage is also examined. The thermodynamic feasibility of the formation of the above complexes is discussed.

The findings of the study of the boron atom trapped fullerenes derivatives are reported in chapter 4. The stabilization energy and the host-guest interactions in the above complexes are presented. The spin-spin interactions and the transfer of spin density between trapped boron atom and the host fullerene in the complexes are also discussed in this chapter. The spin polarization in the above complexes is discussed. The influence of the encapsulation of boron atom in various host cavities on the properties of latter is also examined. The thermodynamics of the encapsulation of boron is also investigated.

In chapter 5, the outcomes of the investigations on the dimers of nitrogen as well as boron atom encapsulated fullerene derivatives are presented. The ground state of each of the above systems is reported. For stable states of the complexes, the spin-spin interactions between components species, spin polarization and spin density transfer are analyzed and presented. Based on the values of ΔG and ΔH , the thermodynamic feasibility of formation of endohedral heterofullerene dimers *via* different ways are reported. The electronic properties of the above dimers are also discussed.

In chapter 6, the results obtained from the studies of nitrogen atom encapsulated carbon nanotube, boron nitride nanotube and their respective dimers are presented. Various possible spin states of the dimers are considered for this purpose. The spin-spin coupling between guest and host as well as that between two guests of the above complexes for their stable spin states

are presented. The spin polarization and spin degeneracy are also discussed for the stable systems. The effect of encapsulation of nitrogen atom on various electronic properties such as electronic affinity, ionization energies and HOMO-LUMO energy gap of nanotubes are also examined in this chapter. The effect of the diameter of nanotubes on spin-spin coupling between components of the endohedral complexes is also determined. A comparison between the results of nitrogen atom encapsulation in the dimer of nanotube with those of fullerene is also provided.

In chapter 7, the summary of thesis and future scope are discussed.







Chapter-2

Computational Methods

Over the last few decades, computational chemistry has emerged as an independent field in chemical science due to rapid developments of the computer hardware and software as well as the implementation of theoretical methods [201-202]. The structure, stability and properties of chemical species, which are either expensive or difficult to get, can be accurately predicted by computational methods. Using the computational techniques one can elucidate the structure, stability and properties of various chemical species [104-111].

Broadly, there are two types of differ in the underlying theoretical methods. In one of the methods, the classical laws of motion are used to predict the molecular computational methods which structure and properties. In this method (e.g. classical molecular dynamics simulations), the interactions of electrons are not explicitly considered and hence is not adequate to describe most of the properties of the systems. In another method, the quantum chemical laws are used to describe the atoms and molecules and are more accurate to predict the properties of the chemical systems.

In the quantum mechanical method, the electronic energy of a system is obtained by solving the Schrödinger equation corresponding to its wave function. However, the Schrödinger equation cannot be solved analytically for systems with more than one electron. The chemical species which consists of several nuclei and large number of electrons rules out the possibility of an analytic solution and necessitate the need for approximate solution to Schrödinger equation. These approximations methods include variation and perturbation techniques. Two main theoretical approaches used widely nowadays are *ab initio* and density functional methods. A brief discussion of these methods is given below.

2.1 *Ab initio* methods

Ab initio is a Latin word which means “from the beginning”. *Ab initio* methods solve the Schrödinger equation only by using the values of fundamental physical constant, to determine the electronic energy and various properties of the chemical systems [203]. Considering the importance of *ab initio* techniques in the investigation of the various properties of chemical species, the theoretical approach employed in various *ab initio* methods are briefly discussed below.

2.1.1 The Schrödinger equation

According to the postulates of quantum mechanics, the characteristics of a chemical species can be represented by a mathematical function called wave function (ψ) [202, 203-207]. The quantum mechanical methods characterize an electronic system by solving either the time dependent or time independent Schrödinger equation. The time dependent Schrödinger equation is given as

$$\hat{H}\psi(x, t) = -i\hbar \frac{\partial\psi(x, t)}{\partial t} \quad (2.1)$$

and time-independent form of Schrödinger equation can be written as

$$\hat{H}\psi(x) = E\psi(x) \quad (2.2)$$

where, \hat{H} and ψ represent the Hamiltonian operator and the molecular wave function, respectively. The Hamiltonian operator \hat{H} can be expressed as

$$\hat{H} = \hat{T}_n + \hat{T}_e + \hat{V}_{ee} + \hat{V}_{nn} + \hat{V}_{ne} \quad (2.3)$$

where, \hat{T}_n is the kinetic energy of nuclei; \hat{T}_e is the kinetic energy of the electrons; \hat{V}_{nn} , \hat{V}_{ee} and \hat{V}_{ne} are the operator for potential energies due to the interactions between the nucleus-nucleus, electron-electron and nucleus-electron, respectively.

As mentioned above, the analytical solution to Schrödinger equation is possible only for single electron systems. For systems consisting of many electrons, several approximations are incorporated to simplify their Hamiltonian operator. One of the most important approximations is Börn-Oppenheimer approximation which separates the motion of the nuclei and that of the electrons [208]. In this approximation, the nuclei are considered as fixed points as they are significantly heavier compared to the electrons. Considering the fact that the positions of nuclei are fixed, the resultant electronic Hamiltonian becomes

$$\hat{H} = -\frac{1}{2} \sum_{i=1}^N \nabla_i^2 - \sum_{i=1}^N \sum_{A=1}^M \frac{Z_A}{r_{iA}} + \sum_{i=1}^N \sum_{j>i}^N \frac{1}{r_{ij}} \quad (2.4)$$

where, the first term in equation 2.4 denotes the operator for the kinetic energy of electrons, the second term denotes the operator for the nucleus-electron attractions and third term represents the operator for the potential energy of interactions between electrons. More details on the Börn-Oppenheimer approximation are available in various standard text books of Quantum Chemistry [206-210].

2.1.2 Hartree-Fock method

A simple method to solve Schrödinger equation for many body systems is Hartree-Fock Method (HF). In this method, it is considered that the electron is moving in an average field generated by other electrons of the species. The wave function is known as the Hartree product and is expressed as

$$\psi(r_1, r_2, \dots, r_N) = \Phi_1(r_1)\Phi_1(r_2) \dots \Phi_1(r_N) \quad (2.5)$$

where, $\Phi_1(r_1), \Phi_1(r_2), \dots, \Phi_1(r_N)$ represent the wave function for r_1, r_2, \dots and r_N electrons, respectively. The above wave function is not antisymmetric, which is expected for a wave function describing electrons. In this regard, the Hartree-Fock wave functions are built from the wave functions of atomic orbitals in the form of a determinant known as Slater determinant which is expressed as

$$\Psi = \frac{1}{\sqrt{N!}} \begin{vmatrix} \chi_1(X_1) & \chi_2(X_1) & \dots & \chi_N(X_1) \\ \chi_1(X_2) & \chi_2(X_2) & \dots & \chi_N(X_2) \\ \vdots & \vdots & \ddots & \vdots \\ \chi_1(X_N) & \chi_2(X_N) & \dots & \chi_N(X_N) \end{vmatrix} \quad (2.6)$$

where $\frac{1}{\sqrt{N!}}$ represents the normalization factor. In the above Slater determinant, $\chi_N(X_N)$ represents N electrons occupy in N spin orbitals.

According to variation theorem, the expectation value of energy for a given trial wave function of any system is larger or equal to the true ground state energy. Thus, the lowest energy wave function can be considered as the best approximation to the true ground state energy wave function.

HF equation can be solved by variation method by minimizing the Hartree-Fock energy

$$\hat{F}(x_1)\chi_i(x_1) = \epsilon_i\chi_i(x_1) \quad (2.7)$$

where, $\hat{F}(x_1)$ is called Fock operator and is expressed as

$$\hat{F}(x_1) = \hat{H}_{x_1} + \sum_{x_2}^{n/2} (2\hat{J}_{x_1x_2} - \hat{K}_{x_1x_2}) \quad (2.8)$$

where \hat{H}_{x_1} represents the Hamiltonian operator for electron x_1 which consists of kinetic energy operator of electron and the potential energy operator describing the interaction between electron and nuclei. The repulsion between electrons is accounted by coulomb operator $\hat{J}_{x_1x_2}$, the exchange energy between electrons is obtained by exchange operator $\hat{K}_{x_1x_2}$.

The coulomb operator $\hat{J}_{x_1x_2}$ and exchange operator $\hat{K}_{x_1x_2}$ are expressed as

$$\hat{J}_{x_1x_2}f(x_1) = f(x_1) \int |\phi_j(x_2)|^2 \frac{1}{r_{x_1x_2}} d\mathbf{r} \quad (2.9)$$

$$\hat{K}_{x_1x_2}f(x_1) = \phi_j(x_1) \int \frac{\phi_j^*(x_2)f(x_2)}{r_{x_1x_2}} d\mathbf{r} \quad (2.10)$$

where $f(x_1)$ represents an arbitrary function for electron x_1 .

In HF method, the average field by an electron depends on the spin orbitals of other electrons and hence HF equation is a non linear equation. Thus, the above equation can be solved by iterative procedure known as self-consistent field (SCF) method.

In SCF method, the initial spin orbitals (ϕ_i) are guessed from which the average field sensed by each electron is calculated. Further, eigen value is obtained by solving the equation 2.7 for a new set of spin orbitals. The new fields can be obtained using these new sets of spin orbitals. The above iteration is repeated until convergence is achieved. The energy of a spin orbital is given by

$$\epsilon_i = \langle \phi_i | \hat{F} | \phi_i \rangle \quad (2.11)$$

The energy of a system of N electrons is expressed as

$$E_0 = 2 \sum_i^{n/2} \epsilon_i - \sum_i^{n/2} \sum_j^{n/2} 2 \langle \phi_i | \hat{J}_j | \phi_i \rangle - \langle \phi_i | \hat{K}_j | \phi_i \rangle + V_{NN} \quad (2.12)$$

where, $n/2$ is the number of occupied spatial orbital and V_{NN} is the internuclear repulsion energy. The major shortcoming of this method is that it does not account the correlation energy between electrons. Hence, the ground state energy calculated using Hartree-Fock method is larger than that of true energy. Thus, several post Hartree-Fock methods have been developed which are capable to account the electronic correlation energy.

2.1.3 Post Hartree-Fock methods

As discussed above, the Hartree-Fock method does not consider the electron correlation energy between electrons where each of the electron moves in the average field generated by remaining $n-1$ electrons [204]. To overcome these problems, the post Hartree-Fock methods were introduced. The electron correlation energy can be incorporated by considering a multi-determinant wave function instead of single determinant wave function. In post Hartree-Fock methods, the number of determinants in wave function depends on the size of basis set which means that bigger the size of basis set, more the number of determinants in the wave function. Further, to calculate the electron correlation energy the infinite size of basis set is required

which is not possible for larger chemical systems. To calculate the electronic correlation energy, several post Hartree Fock methods such as configuration interaction (CI), many body perturbation theory (MBPT) and coupled cluster (CC) methods are developed. These methods are computationally very expensive especially for the large molecules as considered in the present study and hence they are not used.

2.2 Density functional theory (DFT)

To investigate the properties of the systems containing large number of atoms, the density functional methods can be considered as a replacement to traditional *ab initio* methods to some extent. Over the last few decades, this technique has gained immense popularity. In density functional methods, the energy of a multi electron is computed using the electron density $\rho(\mathbf{r})$, where, the electron density $\rho(\mathbf{r})$ is a function of only three variables x, y, z [209-210]. Density functional methods are computationally less expensive than that of post Hartree-Fock methods due to the replacement of $3N$ degree of freedom by three spatial coordinates x, y, z of N -body system. DFT is based on some approximations which are discussed below.

2.2.1 Thomas-Fermi-Dirac approximation

This model is independently developed by Thomas and Fermi in which the wave function is replaced by electron density $\rho(\mathbf{r})$ [211-212]. According to this model, the energy of a many body system in an external potential $V_{ext}(\mathbf{r})$ is a function of electron density $\rho(\mathbf{r})$ and is written as

$$E_{TF}[\rho(\mathbf{r})] = A_1 \int \rho(\mathbf{r})^{5/3} d^3r + \int \rho(\mathbf{r}) V_{ext}(\mathbf{r}) d^3r + \frac{1}{2} \iint \frac{\rho(\mathbf{r})\rho(\mathbf{r}')}{|\mathbf{r}-\mathbf{r}'|} d^3r d^3r' \quad (2.13)$$

where, the first term is for kinetic energy of non-interacting electrons, second is for coulomb interaction energy between nuclei and electrons. The last term denotes the repulsive energy between the electrons. The exchange and correlation energy between electrons cannot be calculated using Thomas-Fermi model. To overcome the above problem, a local exchange term was added in equation 2.13 by Dirac in 1930 [213]. The resultant expression is written as

$$E_{TFD}[\rho(\mathbf{r})] = A_1 \int \rho(\mathbf{r})^{5/3} d^3r + \int \rho(\mathbf{r}) V_{ext}(\mathbf{r}) d^3r + \frac{1}{2} \iint \frac{\rho(\mathbf{r})\rho(\mathbf{r}')}{|\mathbf{r}-\mathbf{r}'|} d^3r d^3r' + A_2 \int \rho(\mathbf{r})^{4/3} d^3r \quad (2.14)$$

The equation 2.14 is called Thomas-Fermi-Dirac equation. To solve this equation at stationary points, the Lagrange parameters can be used

$$\delta\{E_{TDF}[\rho(\mathbf{r})] - \mu(\int \rho(\mathbf{r})d^3r - N)\} = 0 \quad (2.15)$$

where, μ is the Lagrange parameter which is known as chemical potential or Fermi energy at 0 K. On solving equation 2.15, Thomas-Fermi-Dirac equation becomes

$$\frac{5}{3}A_1\rho(\mathbf{r})^{2/3} + V_{ext}(\mathbf{r}) + \frac{1}{2}\int \frac{\rho(\mathbf{r}')}{|\mathbf{r}-\mathbf{r}'|} d^3r' + \frac{4}{3}A_2\rho(\mathbf{r})^{1/3} - \mu = 0 \quad (2.16)$$

The above equation gives the ground state density of a chemical system. The limitation of Thomas-Fermi Dirac approximation is that it does not consider the bonding between atoms.

The Hohenberg-Kohn (HK) theorems

DFT is mainly based on two theorems which are stated by Hohenberg and Kohn in 1964 [214] and are given below:

Theorem I

The first theorem states, “the external potential $V_{ext}(\mathbf{r})$ is directly related to the electron density $\rho(\mathbf{r})$, and hence the the total energy is a unique functional of electron density $\rho(\mathbf{r})$ ”.

According to the above theorem, the chemical system can be described by the ground state electron density. The energy $E[\rho]$ of a chemical system can be written in terms of the ground state electron density $\rho(\mathbf{r})$ and external potential $V_{ext}(\mathbf{r})$

$$E[\rho] = F[\rho] + \int \rho(\mathbf{r})v^{ext}(\mathbf{r})d\mathbf{r} \quad (2.17)$$

$$\text{and} \quad F[\rho] = T[\rho] + V_{ee}[\rho] \quad (2.18)$$

where, $T[\rho]$ and $V_{ee}[\rho]$ represent the functional form of kinetic and electron-electron interaction energy.

Theorem II

The second theorem states, “the electron density that minimizes the ground state energy of overall functional is the exact ground state density corresponding to the solution of the Schrödinger equation”.

Second theorem of Hohenberg and Kohn states that the energy of a chemical species can be determined using variational method. As stated above, the minimization of energy of a chemical species can be done using electron density $\rho(\mathbf{r})$, hence a trial electron density can be used. The total energy of a system corresponding to the trial electron density for a given external potential follows the inequality as given

$$E[\rho'] \geq E[\rho_0] \quad (2.19)$$

where, ρ' and ρ_0 are the trial and ground state electron density, respectively.

As described above, based on the Hohenberg and Kohn theorems the energy of a system can be determined using the ground state electron density. However, the true ground state energy of a system cannot be calculated using above two theorems due to the unknown functional $F[\rho]$. As a solution to the above problem, Kohn-Sham method was introduced by Kohn and Sham in 1965 [215].

2.2.2 The Kohn-Sham equations

The practical application of Hohenberg and Kohn theorem in computational chemistry was possible due to the model developed by Kohn-Sham [215]. The main drawback of the Hohenberg and Kohn model was the poor illustration of kinetic energy. To overcome this, Kohn and Sham considered a system of non-interacting particles which possess exactly the same ground state electron density to the system of interacting particles. In this approach, Kohn-Sham considered that the N non-interacting electrons are moving in a single particle potential $\hat{V}_{KS}(r)$ and the resulting Hamiltonian can be written as

$$\hat{H}_{KS} = -\frac{1}{2}\nabla^2 + \hat{V}_{KS}(\mathbf{r}) \quad (2.20)$$

The solution of one-electron Schrödinger equations is as follows

$$\left(-\frac{1}{2}\nabla^2 + V_{KS}(\mathbf{r})\right)\psi_i(\mathbf{r}) = \epsilon_i\psi_i(\mathbf{r}) \quad (2.21)$$

where, the eigenvalue of each of the N orbitals is denoted by ϵ_i . For the non-interacting electrons, the kinetic energy $T_S[\rho(\mathbf{r})]$ is expressed as

$$T_S[\rho(\mathbf{r})] = -\frac{1}{2}\sum_{i=1}^N \int \psi_i^*(\mathbf{r})\nabla^2 \psi_i(\mathbf{r})d\mathbf{r} \quad (2.22)$$

Kohn and Sham introduced a functional $E[\rho(\mathbf{r})]$ to incorporate the difference between non-interacting and interacting kinetic energies

$$E[\rho(\mathbf{r})] = T_S[\rho(\mathbf{r})] + J[n(\mathbf{r})] + E_{XC}[\rho(\mathbf{r})] + E_{ne}[\rho(\mathbf{r})] \quad (2.23)$$

$$= T_S[\rho(\mathbf{r})] + \frac{1}{2} \iint \frac{\rho(\mathbf{r}_1)\rho(\mathbf{r}_2)}{r_{12}} d\mathbf{r}_1 d\mathbf{r}_2 + E_{XC}[\rho(\mathbf{r})] + \int V_{Ne}\rho(\mathbf{r})d\mathbf{r} \quad (2.24)$$

$$= -\frac{1}{2} \sum_i^N \langle \varphi_i | \nabla^2 | \varphi_i \rangle + \frac{1}{2} \sum_i^N \sum_j^N \iint |\varphi_i(\mathbf{r}_1)|^2 |\varphi_j(\mathbf{r}_2)|^2 d\mathbf{r}_1 d\mathbf{r}_2 + E_{XC}[\rho(\mathbf{r})] - \sum_i^N \int \sum_A^M \frac{Z_A}{r_{1A}} |\varphi_i(\mathbf{r}_1)|^2 d\mathbf{r}_1 \quad (2.25)$$

The Kohn-Sham method has a main drawback that it does not take into account of exchange correlation energy functional $E_{XC}[\rho(\mathbf{r})]$ properly. To get a more accurate form of the density functional theory, it is necessary to obtain the exact exchange correlation energy functional, $E_{XC}[\rho(\mathbf{r})]$ or potential $V_{XC}[\rho(\mathbf{r})]$. The exchange correlation energy functional was incorporated in the density functional theory for which several approximations of the exchange energy functional are developed and are explained below.

2.2.3 Approximations of the exchange-correlation functional

To obtain the exact exchange correlation energy functional, various approximations are introduced which are discussed below. These approximations are extremely helpful for computing various properties of chemical systems. The main advantage of these approximations is that they take significantly less computational time.

2.2.3.1 Local density approximation (LDA)

To calculate the exchange correlation energy of a system, LDA is the simplest approach in DFT [206]. In LDA, electron density is considered in the form of local uniform electron gas. The exchange correlation energy functional is dependent on the local uniform electron gas and given as

$$E_{XC}^{LDA}[\rho(\mathbf{r})] = \int \rho(\mathbf{r}) \epsilon_{XC}(\rho(\mathbf{r})) d\mathbf{r} \quad (2.26)$$

$$E_{XC}^{LDA}[\rho(\mathbf{r})] = \int \rho(\mathbf{r}) [\epsilon_X(\rho(\mathbf{r})) + \epsilon_C(\rho(\mathbf{r}))] d\mathbf{r} \quad (2.27)$$

where, the exchange and correlation energies for the homogeneous local electron gas $\rho(\mathbf{r})$ are represented by the term ϵ_X and ϵ_C , respectively.

In an open shell system α and β electron densities of a system are not equal. In such cases, LDA is replaced by the local spin density approximation (LSDA). The expression for the LSDA is represented as

$$E_{XC}^{LSDA}[\rho^\alpha(\mathbf{r}), \rho^\beta(\mathbf{r})] = \int \rho(\mathbf{r}) \epsilon_{XC}(\rho^\alpha(\mathbf{r}), \rho^\beta(\mathbf{r})) d\mathbf{r} \quad (2.28)$$

$$E_{XC}^{LSDA}[\rho^\alpha(\mathbf{r}), \rho^\beta(\mathbf{r})] = \int \rho(\mathbf{r}) \left[\epsilon_X(\rho^\alpha(\mathbf{r}), \rho^\beta(\mathbf{r})) + \epsilon_C(\rho^\alpha(\mathbf{r}), \rho^\beta(\mathbf{r})) \right] d\mathbf{r} \quad (2.29)$$

The most common examples of LDA functional are Perdew-Zunger 81 (PZ81), Perdew-Wang 92(PW92) and Vosko-Wilk-Nusair (VWN) [216-218]. The local density approximation is reported to be less accurate in results for the quantitative analysis of the chemical species. The main outcome of the LDA and LSDA approximations is that they are useful in deriving more advanced approximations *viz.* generalized gradient approximation (GGA) and meta-generalized gradient approximations.

2.2.3.2 Generalized gradient approximation (GGA)

The results obtained for various chemical systems using LDA and LSDA functionals were similar to those for Hartree-Fock methods [202]. To improve the accuracy of the results obtained using these approximations, the non-uniform electron gas was proposed. For the deviation in the electron density with the positions of electrons, the first derivative of the electron density ($\nabla\rho(\mathbf{r})$) is incorporated in the LSDA functional. The functional form of generalized gradient approximation (GGA) is expressed as

$$E_{XC}^{GGA}[\rho] = \int \rho(\mathbf{r}) \epsilon_{XC}^{GGA}[\rho(\mathbf{r})] d\mathbf{r} + \int F_{XC}[\rho(\mathbf{r}), \nabla\rho(\mathbf{r})] d\mathbf{r} \quad (2.30)$$

where, F_{XC} represents the correction term. Several GGA functionals have been reported such as Perdew-Wang (PW91), Becke (B or B88), Lee-Yang-Par (LYP), Perdew (P86) and Perdew-Burke-Ernzerhof (PBE) for calculating exchange and correlation contribution [219-223].

2.2.3.3 Hybrid-GGA functional

To make further improvement over the GGA-functional, the Hartree Fock exchange term was incorporated in the functional. In quantum chemistry, the most widely used hybrid functional is B3LYP (Becke, three-parameter, Lee-Yang-Parr). The hybrid functional B3LYP is a combination of three parameters such as HF exchange, density functional exchange and correlation exchange [224-225]. The expression for B3LYP is given as

$$E_{XC}^{B3LYP} = E_{XC}^{LDA} + a_0(E_{XC}^{HF} - E_{XC}^{LDA}) + a_x(E_X^{GGA} - E_X^{LDA}) + a_c(E_C^{GGA} - E_C^{LDA}) \quad (2.31)$$

where $a_0 = 0.20$, $a_x = 0.72$ and $a_c = 0.81$ are the parameters obtained from the experimental atomization energies [206, 224]. The E_{XC}^{LDA} represents the VWN exchange correlation given by Vosko-Wilk-Nusair, E_X^{GGA} represents the B88 exchange given by Becke, and E_C^{GGA} represents the LYP correlation proposed by Lee-Yang-Parr. Other examples of the hybrid functional are PBE0 [226] and HSE [227].

2.2.3.4 Meta GGA functional

The GGA functional depends on the electron density $\rho(\mathbf{r})$ and its first derivative ($\nabla\rho(\mathbf{r})$). To improve GGA functionals, the higher derivatives of $\rho(\mathbf{r})$ are also included in the functional. These form of the functional are called meta-GGA functional [228-229] and their mathematical form is expressed as

$$E_{XC}^{MGGA}[\rho] = \int \rho(\mathbf{r}) \epsilon_{XC}^{GGA}[\rho(\mathbf{r})] d\mathbf{r} + \int F_{XC}[\rho(\mathbf{r}), \nabla\rho(\mathbf{r})] d\mathbf{r} + \int G_{XC}[\rho(\mathbf{r}), \nabla^2\rho(\mathbf{r})] d\mathbf{r} \quad (2.32)$$

where, F_{XC} and G_{XC} represent the correction terms. This class of functional is known to be suitable for studying charge transfer, kinetics and thermochemical properties of chemical species. Several functionals such as Minnesota 05 [230], Minnesota 06 [228], Minnesota 08 [229], Minnesota 11 [232-233], and Minnesota 12 [234] reported by Donald Truhlar are of this category and are known as Minnesota functionals. The amount of exchange energy functional is different in each Minnesota functional. Minnesota functionals were reported to be suitable for the studies of transition metal complexes [235-236].

2.2.3.5 Long range corrected functional

The major deficiency of the above mentioned functionals is that they do not take into account the London dispersion and van der Waals forces between non-bonded atoms [237-238]. However, such interactions play very important role in the studies of biomolecules, host-guest complexes and adsorption of the molecule over the surfaces. Keeping this in mind, Stefan Grimme incorporated the empirical-long range $C_n R^{-n}$ corrections to the GGA functionals [239]. The energy for a dispersion corrected functional can be written as

$$E_{DFT-D} = E_{KS-DFT} + E_{disp} \quad (2.33)$$

where, E_{KS-DFT} represents the Kohn-Sham density functional energy and E_{disp} is an empirical dispersion corrected energy [240-241] given as

$$E_{disp} = - \sum_{n=6,8,10\dots} \sum_{i=1}^{N-1} \sum_{j=i+1}^N S_n \frac{C_n^{ij}}{R_{ij}^n} f_{dmp}(R_{ij}) \quad (2.34)$$

where, N is number of atoms, the dispersion coefficient of the ij pair of an atom is denoted by C_n^{ij} , the global scaling factor is described by S_n , and R_{ij} represents the atomic distance between two atoms. The f_{dmp} is a damping function which avoids the short range interaction between atoms and are expressed as

$$f_{dmp}(R_{ij}) = \frac{1}{1 + e^{-d\left(\frac{R_{ij}}{R_r} - 1\right)}} \quad (2.35)$$

where, R_r denotes the sum of van der Waals radii of atoms. The dispersion interaction was introduced by Grimme in B3LYP hybrid functional in the form of GD2 and GD3 [240-245]. Several other dispersion corrected functionals such as B97-D3 [242], ω B97-XD [243-244], etc. are also developed. The functional B3LYP-GD2 reproduced the experimental results for C_{60} fullerene and is chosen for the present thesis work [245-248].

2.3 Basis sets

In order to perform quantum chemical calculations, the wave function of the system has to be specified. The wave function is characterized by a basis set of known functions. The linear combination of mathematical functions which mimics the atomic orbital of an atom is known as basis set. In computational chemistry, the atomic orbitals were described by the Slater Type Orbitals (STOs) in which the wave function decreased exponentially with respect to the distance of the orbitals from the nuclei [249]. Later, to make the integration faster the Gaussian Type Orbitals were introduced [250]. The STOs can be written in polar coordinates form and given as

$$\chi_{nlm}^{\zeta}(r, \theta, \phi) = N r^{n-1} e^{-\zeta r} Y_l^m(\theta, \phi) \quad (2.36)$$

Moreover, the polar and Cartesian coordinates form of GTOs is given as

$$\chi_{nlm}^{\zeta}(r, \theta, \phi) = N r^{2n-2-l} e^{-\alpha r^2} Y_l^m(\theta, \phi) \quad (2.37)$$

$$\chi_{nlm}^{\zeta}(r, \theta, \phi) = N x^{l_x} y^{l_y} z^{l_z} e^{-\alpha r^2} \quad (2.38)$$

where, N represents the normalization constant and $l = l_x + l_y + l_z$ describes the type of orbital (if $l = 1$ then orbital is p).

In order to get the accuracy near to that from STO, the linear combination of GTO's can be used. Further, the contracted Gaussian type orbitals (CGTOs) are expressed as linear combination of gaussian primitives and can be written as

$$\chi_v = \sum_{\mu=1}^M d_{\mu v} g_v(\alpha_v) \quad (2.39)$$

where, $d_{\mu v}$ represents the contraction coefficient and g_v represents the primitive Gaussians.

2.3.1 Classification of basis sets

2.3.1.1 Minimal basis sets

The minimal basis set is the smallest basis set where a minimum number of basis functions are used to describe atomic systems. For example, to define a hydrogen and helium atom a single s-function is used. To describe the first row elements of the periodic table, two set of s-functions (1s and 2s) and a set of p-functions ($2p_x$, $2p_y$, $2p_z$) are used. The second row elements of the periodic table can be characterized by three s-functions (1s, 2s, and 3s) and two p-functions (2p and 3p).

2.3.1.2 Double-zeta and Split-valence basis sets

An improvement over the minimal basis sets is double-zeta basis set which is obtained by replacing each STO with two STOs that differ in their ζ values. For example, two s-functions (1s and 1s') are used for hydrogen; four s-functions (1s, 1s', 2s and 2s') and two p-functions (2p and 3p) are used for the first row elements, respectively.

Use of double zeta basis set for each orbital of an atom is computationally expensive. To make it computationally less expensive, split-valence basis sets were introduced, where only one STO for core orbitals and more than one STO for valence orbitals are used. Based on the STOs used for valence orbitals, split-valence basis sets are named as double zeta, triple zeta, quadruple zeta and quintuple zeta.

2.3.1.3 Polarization and diffuse functions

The shape of atomic orbitals is distorted when they participate in chemical bonding due to the shift in electron densities. This phenomenon is called polarization. Thus, it is necessary to add polarization factors to achieve more accurate representation of atomic orbitals in a molecule. To allow polarization factors, STOs of higher angular momentum than the real angular momentum of valence shell are added in the basis functions. The most common example of polarization functions is Double-Zeta plus polarization basis set (DZP), where, three p-functions for hydrogen atom and five d-functions for first or second row elements of periodic table are added for polarization factor.

On the other hand, to describe ions and weak bonding in molecules, diffuse functions are added in the basis function. To add the diffuse functions in basis sets, one s-function and one p-function for non-hydrogen atoms and one s-function for hydrogen atom are added.

2.3.1.4 Pople basis sets

John Pople and his co-workers introduced a notation to represent the split-valence basis set in the form of $n-ijG$ or $n-ijkG$, where the primitive gaussian for core electrons and valence electrons are denoted by n and ij or ijk , respectively. For example, in 6-311G basis set, the six primitive gaussian type orbitals (PGTOs) are used to elucidate the core shell orbitals and three functions represent the valence shell electrons which are further described by three, one and one PGTOs, respectively [251].

To represent polarization and diffuse functions, the notation ‘*’ and ‘+’, respectively, are used. For example, in 6-311G**, the first asterisk denotes the addition of five d functions on the atoms other than hydrogen atoms and the second asterisk is used for the addition of the three p-functions on hydrogen atom. In 6-311++G basis set, the first “+” is used to describe the addition of diffuse function over atoms other than hydrogen and the second “+” is used to describe the addition of diffuse function over hydrogen atom. In the present work, 6-311G* basis set is used as it is found to be appropriate for the study of complexes of fullerenes for results of reliable accuracy.

2.3.1.5 Correlation-consistent basis sets

In 1989, Dunning and his co-workers defined a new class of basis set known as correlation-consistent basis sets [252]. This class of basis set is used to study the weakly bonded chemical species and are represented by cc-pVXZ where, ‘cc’ represents the correlation-consistent, ‘p’ describes the polarization functions added on all atoms and ‘VXZ’ denotes valence, cardinal number X and zeta, respectively. Further, cardinal number can be of different order such as X=D (double), T (triple) and Q (quadruple). This class of basis sets is further improved by adding diffuse function and denoted as aug-cc-pVXZ where, ‘aug’ indicates augmented.

2.4 Time-dependent density functional theory (TDDFT)

As mentioned above, theorem I of Hohenberg-Kohn density functional theory is appropriate for ground state of the system. To study the excited states of chemical species, Runge and Gross extended DFT to its time dependent analogue [253]. For this purpose, the time-dependent (TD) potential was incorporated in DFT [254-255]. According to Runge and Gross theorem, the time-dependent probability density $\rho(\mathbf{r}, t)$ of finding an electron of spin \mathbf{S} at position \mathbf{r} can be given as

$$\rho(\mathbf{r}, t) = N \sum_{S_1, S_2, \dots, S_N} \int \int d^3 \mathbf{r}_2 \dots \int d^3 \mathbf{r}_N |\psi(\mathbf{r}_1, \mathbf{r}_2 \dots \mathbf{r}_N, S_1, S_2 \dots S_N, t)|^2 \quad (2.40)$$

where, N is the number of electrons in system. The general form of Hamiltonian operator by Runge and Gross can be expressed as

$$\hat{H}(t) = \hat{T} + \hat{V}_{ext}(t) + \hat{V}_{ee} \quad (2.41)$$

where \hat{T} is kinetic energy operator, $\hat{V}_{ext}(t)$ is external potential operator at time t , and \hat{V}_{ee} is the operator for electron-electron interaction. TDDFT is useful to explain the optical response of chemical species which cannot be explained solely using density functional theory. The details are widely discussed in standard text book [255]. In the present thesis, TDDFT method is employed to obtain the absorption spectra of the complexes of fullerene.

2.5 Spin broken symmetry approach

In computational chemistry, the unrestricted density functional approach is good enough to investigate the structure and energy for open shell systems [256]. However, it does not describe the lower spin states of biradical properly as it defines the lower spin states by a single determinant. The solution of higher spin states can be easily described by the single determinant. To achieve the correct solution for the lower spin states the broken symmetry approach can be used as suggested by Noodleman [257-259]. This approach is also known as spin projection technique. The broken symmetry solution is a mixture of the high and low spin states. Thus, to achieve the accurate solution for the low spin states of biradical systems the broken symmetry approach is used in the present thesis which is described below.

To estimate the energy of the antiferromagnetic singlet state of the biradical complexes of n fragments, the broken symmetry calculations using the wave function of the high spin state of the complexes were performed. For this purpose, the stability of wavefunction for the optimized geometry of the biradical complex in its highest stable spin state, where both biradical centers having same spin has to be verified. This is followed by guess for the antiferromagnetic singlet using above initial wavefunction and further optimization of the antiferromagnetically coupled singlet state.

2.6 Spin density and spin polarization parameter

The spin density transfer and spin polarization in chemical species can be analyzed using their spin density values and spin polarization parameter [209, 260]. The difference between α and β spins of each atom is called spin density on that atom. The spin polarization properties of the chemical species can be assessed with the help of spin polarization parameter as given below

$$\zeta = \frac{\rho(\alpha) - \rho(\beta)}{\rho(\alpha) + \rho(\beta)}; \text{ if } 0 < \zeta < 1 \text{ (partially spin polarized)} \quad (2.42)$$

if $\zeta = 1$ (fully spin polarized)

if $\zeta = 0$ (spin degenerate)

where, $\rho(\alpha)$ and $\rho(\beta)$ represents the density of α and β electrons, respectively. Thus, in the present thesis, the spin density transfer and the spin polarization properties of various complexes of the fullerene and carbon nanotubes are determined using the values of spin density and spin polarization parameter.





Chapter-3

Structure, stability and properties of the nitrogen encapsulated fullerene derivatives

3.1 Introduction

The synthesis and various applications of fullerenes and their derivatives were discussed in chapter 1. The earlier studies on the dimers of fullerenes as well as azafullerenes were also discussed. As was mentioned before, the encapsulation of reactive species inside C_{60} was a major development due to the stability of the resulting complex. These include the encapsulation of highly reactive atomic nitrogen inside C_{60} , in which nitrogen atom retained its atomic spin in the complex suggesting it as suitable for quantum computing [11].

As discussed in chapter 1, several theoretical studies have been reported on the encapsulation of paramagnetic species inside the cavity of C_{60} . In all these studies, spin-spin coupling and spin density transfer between guest and host are limited to the cage made of carbon atoms. The studies of nitrogen atom encapsulated azafullerenes are not reported earlier. Since nitrogen retains its spin in $N@C_{60}$, it is important to know how the presence of a nitrogen atom inside the adjacent cage affects the spin of encapsulated nitrogen. Further, it should also be investigated that how the spin-spin interaction in $N@C_{59}N$ and its dimer affected due to the nitrogen atom of the cage.

Keeping this in mind, the present chapter aims to study the structure, stability and properties of $N@C_{60}$, $N@C_{59}N$ and their respective dimers in detail. The spin density transfer and the spin-spin coupling between guest and host as well as those between guests in adjacent cages of the above complexes are investigated for their different stable spin states. The spin polarization parameter (ζ) for the stable states of the complexes is also calculated using the spin density values. The effect of the encapsulation of guest species in the host cages on the energy gap between HOMO and LUMO of the latter is also examined. The thermodynamic feasibility of formation of complexes is studied based on the values of change in Gibbs free energy (ΔG) and change in enthalpy (ΔH) of the complexes.

3.2 Computational methods

All calculations reported in this study were carried out using Gaussian 09 program [261]. Geometry optimization was performed for C_{60} , $N@C_{60}$, $C_{59}N$, $N@C_{59}N$, and their respective dimers. The hybrid density functional B3LYP with and without the Grimme's empirical dispersion correction (i.e., B3LYP-GD2) in conjunction with 6-311G* basis set was used for all the calculations [224, 240]. The energy gap between the highest occupied molecular orbital

(HOMO) and lowest unoccupied molecular orbital (LUMO) for C_{60} obtained by the above methods is 2.7 eV and is in agreement with the value reported experimentally earlier [245-246]. The calculated vertical ionization energy (7.63 eV) and vertical electron affinity (2.44 eV) were also found to be in excellent agreement with the corresponding experimental values of 7.60 and 2.46 eV, respectively [247-248].

For the complexes $N@C_{59}N$, $(N@C_{60})_2$, and $(N@C_{59}N)_2$, various possible spin states of each species were considered. The wave functions corresponding to various spin states of different complexes were verified for their stability and confirmed that they are stable. The stabilization energy of each state was computed, and on the basis of that most stable spin state of each type of the complexes was determined. The frequency analysis confirmed that the optimized geometry of the most stable state of each type of the complexes corresponds to minimum on the respective potential energy surface. The stabilization energy of the complex was calculated as follows:

$$E_{stab} = E_{complex} - E_{components} \quad (3.1)$$

where, $E_{complex}$ and $E_{components}$ are the energy of complex and their components, respectively. The stabilization energy of the most stable complex is further corrected for basis set superposition error (BSSE) [262].

To investigate the spin-spin coupling and spin density transfer between components of stable spin states of the complexes, the spin density difference on the heteroatoms were calculated. To get insight into the spin polarization of the complexes, the spin polarization parameter was calculated as given in chapter 2. The calculated spin density difference and the molecular orbital diagrams of HOMO and LUMO are plotted using the program GaussView 5 [263].

To examine the thermodynamic feasibility of the formation of complexes, the values of change in Gibbs free energy (ΔG) and change in enthalpy (ΔH) associated with the encapsulation of guest species in the cage were determined. For dimers, the above values were also calculated for the dimerization of two endohedral fullerene units. The equations which are used to calculate the above thermodynamic parameters are given as

$$\Delta G_{encapsulation} = G_{complex} - G_{cage} - G_{guests} \quad (3.2)$$

$$\Delta G_{dimerization} = G_{complex} - G_{monomer\ units} \quad (3.3)$$

where $\Delta G_{encapsulation}$ is the change in Gibbs free energy associated with the encapsulation of guest atoms in the host cage. $\Delta G_{dimerization}$ corresponds to the free energy change associated with dimerization of the two monomer endohedral fullerenes. $G_{complex}$, G_{cage} , G_{guests} and $G_{monomer\ units}$ represent the Gibbs free energies of the complex, host cage, guest atoms and monomer endohedral fullerenes, respectively. The change in enthalpy (ΔH) was also computed using the same procedure.

3.3 Results and discussion

3.3.1 Structure and stability of the complexes

The optimized geometries of various systems studied are depicted in figure 3.1. The stabilization energy calculated for the complexes with and without the contribution from dispersion interactions are listed in table 3.1. From the table, it can be seen that the complex $N@C_{60}$ has stabilization energy 1.22 and -9.69 kcal/mol at B3LYP/6-311G* and B3LYP-GD2/6-311G* levels, respectively. In $N@C_{60}$, the guest nitrogen atom is located at the centre of C_{60} as indicated in figure 3.1. The stabilization energies of $(N@C_{60})_2$ in its singlet, triplet, quintet, septet and nonet states are -20.75 , 30.41 , 19.16 , -20.75 and 18.71 kcal/mol at B3LYP-GD2/6-311G* level, respectively. From the above values, it is evident that the complex $(N@C_{60})_2$ is stable in its isoenergetic singlet and septet states whereas other states of the complex are unstable. This holds true for the stabilization energies obtained at B3LYP/6-311G* level. In ${}^7[(N@C_{60})_2]$, the guest nitrogen atoms are located at the center of respective host cages. The values of stabilization energy calculated using B3LYP and B3LYP-GD2 functional indicate that van der Waals interaction is the major interaction that leads to the stability of these complexes.

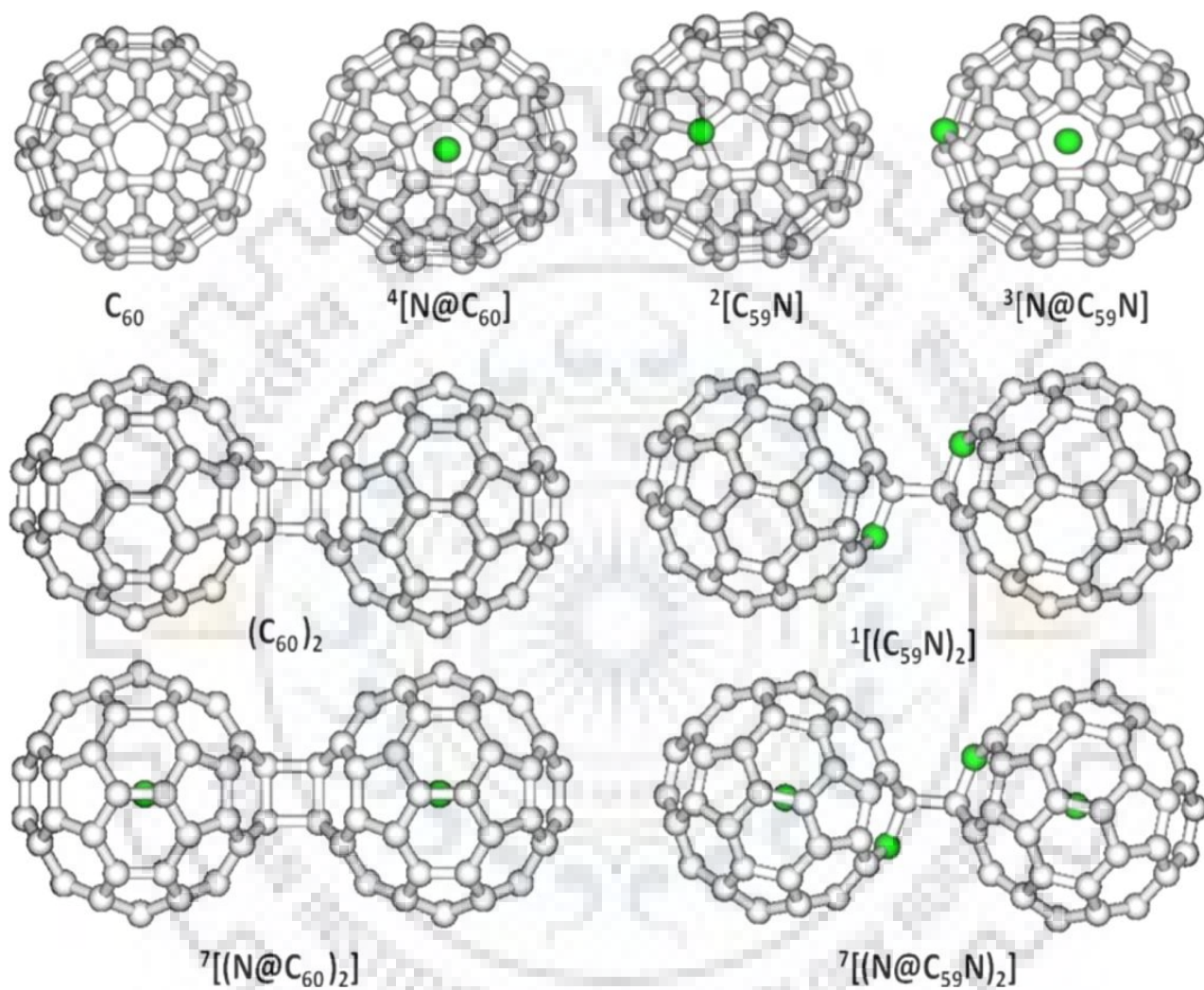


Figure 3.1. Optimized geometries of C_{60} , $C_{59}N$, their nitrogen encapsulated complexes, and their respective dimers.

Table 3.1. Stabilization energy (kcal/mol) of various endohedral complexes for their different spin states. The BSSE corrected values for the most stable spin states are given in parentheses.

Complexes	B3LYP/6-311G*	B3LYP-GD2/6-311G*
$^4[\text{N@C}_{60}]$	1.22 (3.55)	-9.69 (-7.45)
$^1[(\text{N@C}_{60})_2]$	1.64	-20.75
$^3[(\text{N@C}_{60})_2]$	52.93	30.41
$^5[(\text{N@C}_{60})_2]$	41.81	19.16
$^7[(\text{N@C}_{60})_2]$	1.65 (6.37)	-20.75 (-15.86)
$^9[(\text{N@C}_{60})_2]$	41.29	18.71
$^1[\text{N@C}_{59}\text{N}]$	13.81	14.93
$^3[\text{N@C}_{59}\text{N}]$	1.02 (3.08)	-10.22 (-8.03)
$^5[\text{N@C}_{59}\text{N}]$	1.11 (3.22)	-10.13 (-7.92)
$^1[(\text{N@C}_{59}\text{N})_2]$	2.36	-20.28
$^3[(\text{N@C}_{59}\text{N})_2]$	52.14	--- ^a
$^5[(\text{N@C}_{59}\text{N})_2]$	34.85	11.85
$^7[(\text{N@C}_{59}\text{N})_2]$	2.36 (6.47)	-20.28 (-15.91)
$^9[(\text{N@C}_{59}\text{N})_2]$	36.64	13.69

^aConvergence error.

The calculated values of stabilization energy for the singlet, triplet and quintet spin states of $N@C_{59}N$ are 14.93, -10.22 and -10.13 kcal/mol at B3LYP-GD2/6-311G* level, respectively. This indicates that the complex is stable in its nearly isoenergetic triplet and quintet state. The energy of the singlet state of the above complex is significantly higher than that for triplet and quintet states. In both triplet and quintet states of $N@C_{59}N$, the guest nitrogen atom is occupied at the centre of the host cage. The energy difference between triplet and quintet states of $N@C_{59}N$ is negligible compared to thermal energy at room temperature, suggesting that the complex can exist in both triplet and quintet states.

As reflected from the values of stabilization energies of $(N@C_{59}N)_2$ for its various spin states in table 3.1, the complex is stable in its isoenergetic singlet and septet spin states with the stabilization energy value of -20.28 kcal/mol. Similar to $(N@C_{60})_2$, the guest nitrogen atoms are occupied at the respective center of the cages in the stable state of $(N@C_{59}N)_2$. The low value of stabilization energy for the encapsulation of nitrogen atom inside the host cage indicates that guest and host species interact *via* van der Waals forces.

3.3.2 Spin–Spin coupling between guest and host as well as guest atoms of adjacent cages

The calculated values of spin density of the encapsulated nitrogen and the nitrogen of the cage for stable states of the systems are listed in table 3.2. The values of spin polarization parameter (ζ) for the stable states of systems are also given in the table. The spin density difference plots for the complexes are shown in figure 3.2. It can be seen from the table that nitrogen atom encapsulated in C_{60} has a spin density of 2.97 e/au³ suggesting that the electronic configuration of the free state is retained. This suggests that there is no spin density transfer from the encapsulated nitrogen to the host cage. Moreover, the complex $N@C_{60}$ is fully spin polarized as reflected from the values of its spin polarization parameter 1.00. Considering the fact that spin density of nitrogen of ${}^7[(N@C_{60})_2]$ is equal to that of $N@C_{60}$, it can be concluded that there is no transfer of spin density between two guest species or between guest species and host. This is also confirmed from the spin density difference plot of septet state of $(N@C_{60})_2$, where the spin density difference is distributed only on nitrogen atoms, suggesting a ferromagnetic coupling between them. The value spin polarization parameter (ζ) of ${}^7[(N@C_{60})_2]$ is 1.00 which indicates that the complex is fully spin polarized. In the singlet state of $(N@C_{60})_2$, spin of the unpaired electrons of nitrogen atoms in the adjacent cages are anti-ferromagnetically coupled as evident from their spin density values of 2.97 and -2.97 e/au³ as obtained from the broken symmetry

calculations discussed in chapter 2. In contrast to septet state of $(N@C_{60})_2$, the singlet state of the complex is spin degenerate as indicated from zero value of ζ .

The complex $N@C_{59}N$ has two different types of nitrogen atoms, one that is encapsulated inside the cage (N_{encap}) and the other that substitutes one of the carbon atoms (N_{cage}) of the cage. Thus, the spin density associated with both types of nitrogen atoms of the complex in its triplet and quintet states were analyzed. A comparison of spin–spin coupling between encapsulated nitrogen and that of the cage in $N@C_{59}N$ to the respective nitrogen atoms of $(N@C_{59}N)_2$ showed some interesting results. For $C_{59}N$ in its ground state, the spin density is distributed over the entire cage rather than only on nitrogen atom. The latter possess a spin density of only 0.08 e/au^3 suggesting that the unpaired electron is delocalized over all atoms of the cage. The encapsulated nitrogen atom (N_{encap}) has nearly the same value of spin density (2.95 and 2.97 e/au^3) for triplet and quintet states of $N@C_{59}N$. The values of spin density listed in table 3.2 also suggest that there is no spin density transfer from trapped nitrogen to that of the cage for both spin states of the complex. The spin densities of nitrogen of the cage (N_{cage}) for triplet and quintet states of $N@C_{59}N$ are -0.08 and 0.08 e/au^3 , respectively. This indicates that ferromagnetic or anti-ferromagnetic spin–spin coupling occurs between the guest and the host in $N@C_{59}N$ depending upon the spin states of the complex. From the values of spin polarization parameter of triplet ($\zeta=0.50$) and quintet ($\zeta=1.00$) states of $N@C_{59}N$, it can be revealed that the former is partially spin polarized whereas the latter is fully spin polarized.

For the lowest energy septet state $(N@C_{59}N)_2$, the excess α -electron spin density of 2.97 e/au^3 resides only on the encapsulated nitrogens without any transfer to the host cage. Thus, in ${}^7[(N@C_{59}N)_2]$ the unpaired electrons on each guest species are ferromagnetically coupled. In contrast to septet state, in singlet state of $(N@C_{59}N)_2$, anti-ferromagnetic coupling occurs between the spin of encapsulated nitrogens of adjacent cages. The singlet and septet states of the complex $(N@C_{59}N)_2$ are spin degenerated and fully spin polarized as reflected from their ζ value of 0.00 and 1.00 , respectively. It can also be concluded that in $N@C_{59}N$ and in its dimer, the presence of nitrogen on the cage does not assist spin density transfer between guest and host.

Table 3.2. The spin density values (in $e/a.u.^3$) of various nitrogen atoms and the spin polarization parameter (ζ) for the stable state of the complexes.

Complexes	B3LYP/6-311G*		B3LYP-GD2/6-311G*	
	Spin density	Spin polarization parameter (ζ)	Spin density	Spin polarization parameter (ζ)
4N	3.00	1.00	3.00	1.00
$^4[N@C_{60}]$	$N_{encap} = 2.97$	1.00	$N_{encap} = 2.97$	1.00
$^1[(N@C_{60})_2]$	$(N_{encap})_1 = 2.97, (N_{encap})_2 = -2.97$	0.00	$(N_{encap})_1 = 2.97, (N_{encap})_2 = -2.97$	0.00
$^7[(N@C_{60})_2]$	$(N_{encap})_1 = (N_{encap})_2 = 2.97$	1.00	$(N_{encap})_1 = (N_{encap})_2 = 2.97$	1.00
$^2[C_{59}N]$	$N_{cage} = 0.08$	1.00	$N_{cage} = 0.08$	1.00
$^3[N@C_{59}N]$	$N_{encap} = 2.95, N_{cage} = -0.08$	0.50	$N_{encap} = 2.96, N_{cage} = -0.08$	0.50
$^5[N@C_{59}N]$	$N_{encap} = 2.97, N_{cage} = 0.08$	1.00	$N_{encap} = 2.97, N_{cage} = 0.08$	1.00
$^1[(N@C_{59}N)_2]$	$(N_{encap})_1 = 2.97, (N_{encap})_2 = -2.97$ $N_{cage} = 0.00$	0.00	$(N_{encap})_1 = 2.97, (N_{encap})_2 = -2.97$ $N_{cage} = 0.00$	0.00
$^7[(N@C_{59}N)_2]$	$(N_{encap})_1 = (N_{encap})_2 = 2.97$ $N_{cage} = 0.00$	1.00	$(N_{encap})_1 = (N_{encap})_2 = 2.97$ $N_{cage} = 0.00$	1.00

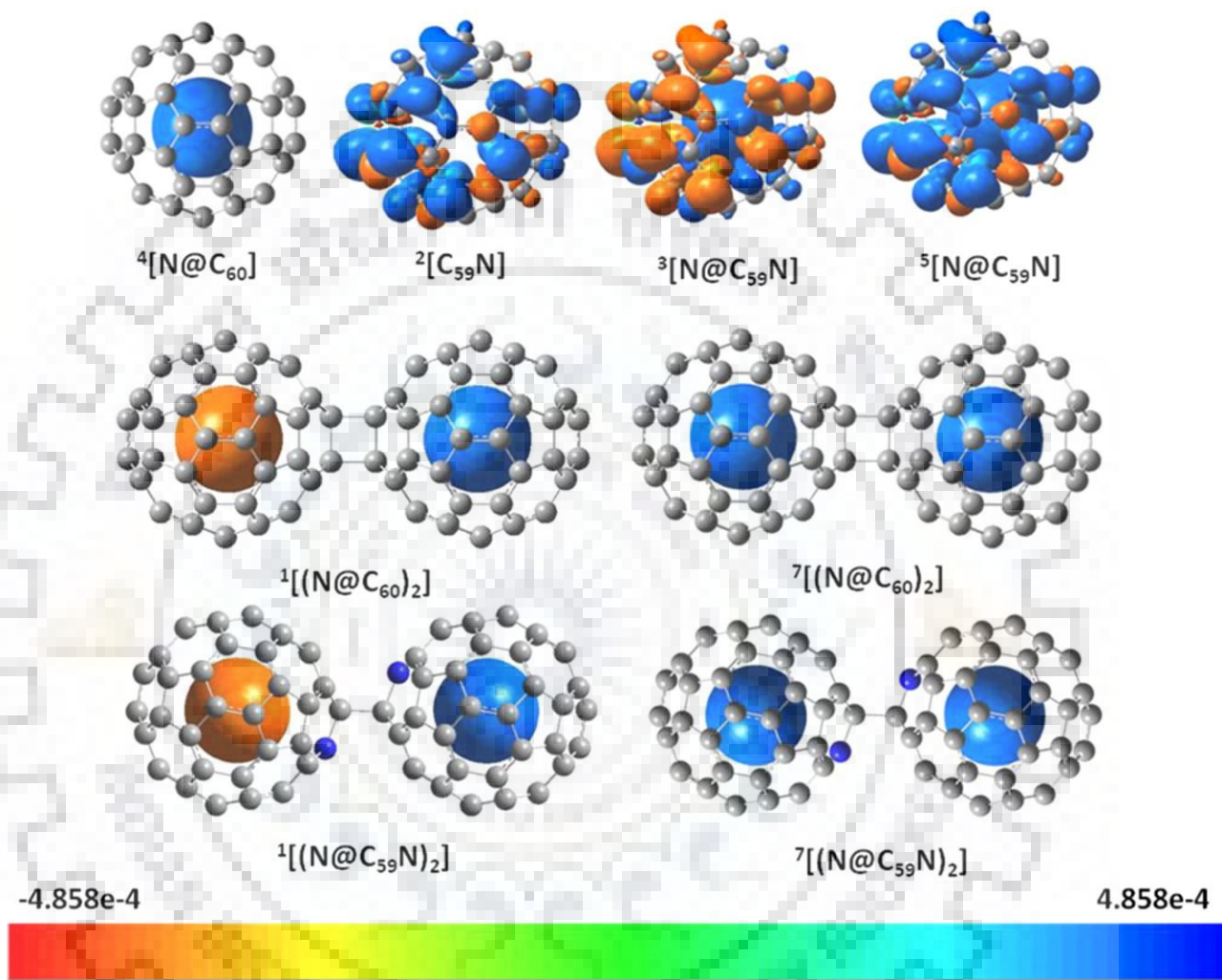


Figure 3.2. Spin density difference plots for various complexes in their most stable spin states with an isodensity value of 0.0004. The blue color represents the excess of α spin density, and the orange color represents the excess of β spin density.

The complex $(\text{N@C}_{59}\text{N})_2$ can be considered to be formed by the dimerization of two $\text{N@C}_{59}\text{N}$ radicals with the pairing of unpaired electrons of each cage. Although the spin density difference plot indicates an excess spin density on the host cage of $\text{N@C}_{59}\text{N}$, no such excess α or β spin density is observed in any of the cages of dimer for its singlet and septet states, confirming the pairing of electrons during dimerization.

3.3.3 Energy gap between HOMO and LUMO

To investigate the effect of encapsulation of nitrogen atom inside various types of cages on the energy gap between HOMO and LUMO of the latter, the energy gap between the above orbitals for various species is calculated and is listed in table 3.3. The diagrams of α -spin frontier molecular orbitals of the systems are depicted in figure 3.3. For the system containing unpaired electrons α -spin in figure 3.3 whereas their corresponding β -spin orbitals are shown in figure 3.4. It can be seen that the energy gap between HOMO and LUMO of C_{60} (2.75 eV) is nearly unaffected by the encapsulation of nitrogen atom inside. From the molecular orbital diagrams of C_{60} and N@C_{60} , it is also clear that the frontier molecular orbitals of N@C_{60} are mainly formed from the atoms of host cage. This is understandable because the molecular orbitals derived from nitrogen are lower in energy because of its higher electronegativity. Similarly, the HOMO–LUMO energy gap (2.48 eV) of host $(\text{C}_{60})_2$ is also unaffected by the encapsulation of nitrogens. Like in N@C_{60} , the frontier orbitals of $(\text{N@C}_{60})_2$ are formed mainly from carbon atoms of the cage as clear from figure 3.3.

The HOMO–LUMO energy gap of C_{59}N is 1.27 eV. It remained the same for the triplet and quintet states of $\text{N@C}_{59}\text{N}$. For $\text{N@C}_{59}\text{N}$, the energy gap is considered for either α - or β -spin orbitals depending on the spin state of the complex. The reason for choosing the α -spin orbital for the quintet state and β -spin orbital for triplet state of $\text{N@C}_{59}\text{N}$ can be explained on the basis of the spin density difference plot and the HOMO–LUMO energy levels given in figure 3.2 and figure 3.5, respectively. The figures clearly illustrate that, unlike $^5[\text{N@C}_{59}\text{N}]$, $^3[\text{N@C}_{59}\text{N}]$ has β -spin density on the host cage. It is also clear from figure 3.3 that the HOMO of all these complexes is centered on the host cage. Thus, for $^3[\text{N@C}_{59}\text{N}]$, the HOMO–LUMO energy gap for β -spin orbital is considered. Figure 3.3 shows that HOMO and LUMO of $^5[\text{N@C}_{59}\text{N}]$ have no contribution from the encapsulated nitrogen, although there is a slight contribution of the encapsulated nitrogen towards HOMO and LUMO of $^3[\text{N@C}_{59}\text{N}]$.

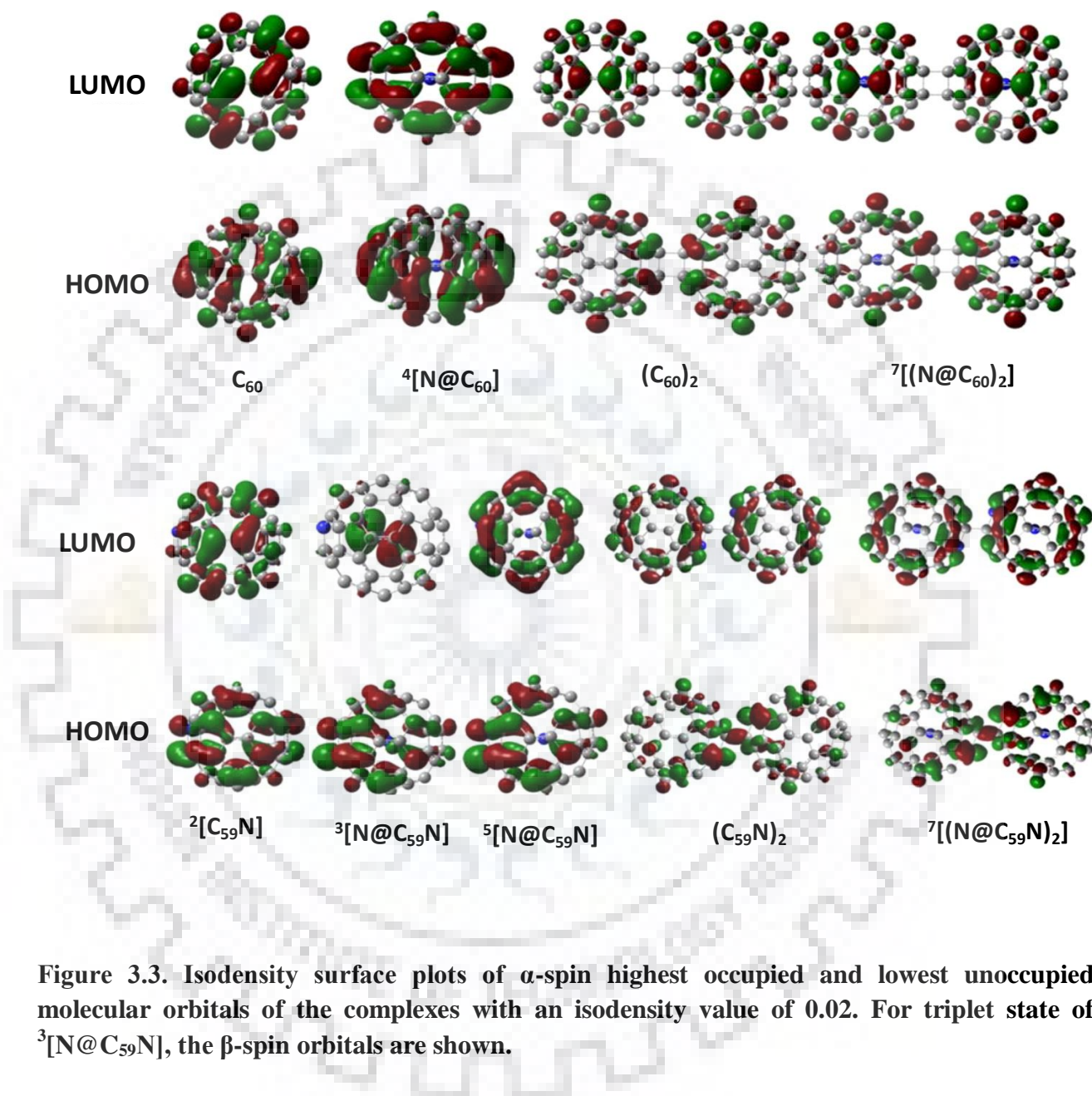


Figure 3.3. Isodensity surface plots of α -spin highest occupied and lowest unoccupied molecular orbitals of the complexes with an isodensity value of 0.02. For triplet state of $^3[N@C_{59}N]$, the β -spin orbitals are shown.

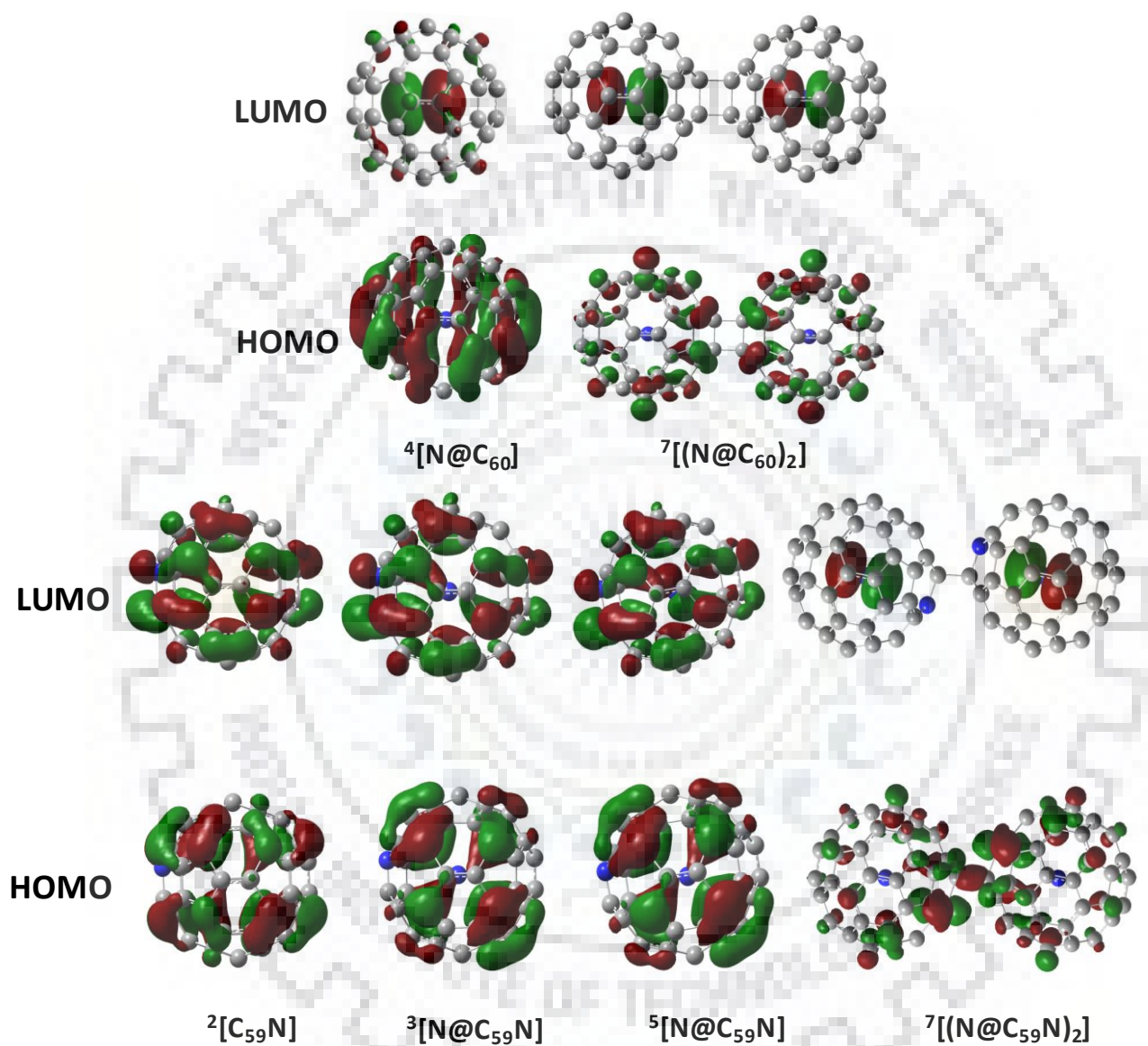


Figure 3.4. Isodensity surface plots of highest occupied and lowest unoccupied β -spin molecular orbitals of the complexes with an isodensity value of 0.02. For triplet state of $^3[\text{N@C}_{59}\text{N}]$, α -spin orbitals are shown.

Table 3.3. Calculated HOMO–LUMO energy gap (eV) for various complexes in their most stable spin states

Complexes	B3LYP/6-311G*	B3LYP-GD2/6-311G*
C_{60}	2.75	2.74
${}^4[N@C_{60}]$	α	2.74
	β	2.66
$(C_{60})_2$	2.48	2.47
${}^7[(N@C_{60})_2]$	α	2.48
	β	2.43
${}^2[C_{59}N]$	α	1.27
	β	2.46
${}^3[N@C_{59}N]$	α	2.45
	β	1.25
${}^5[N@C_{59}N]$	α	1.27
	β	2.44
$(C_{59}N)_2$	2.21	2.20
${}^7[(N@C_{59}N)_2]$	α	2.22
	β	2.12

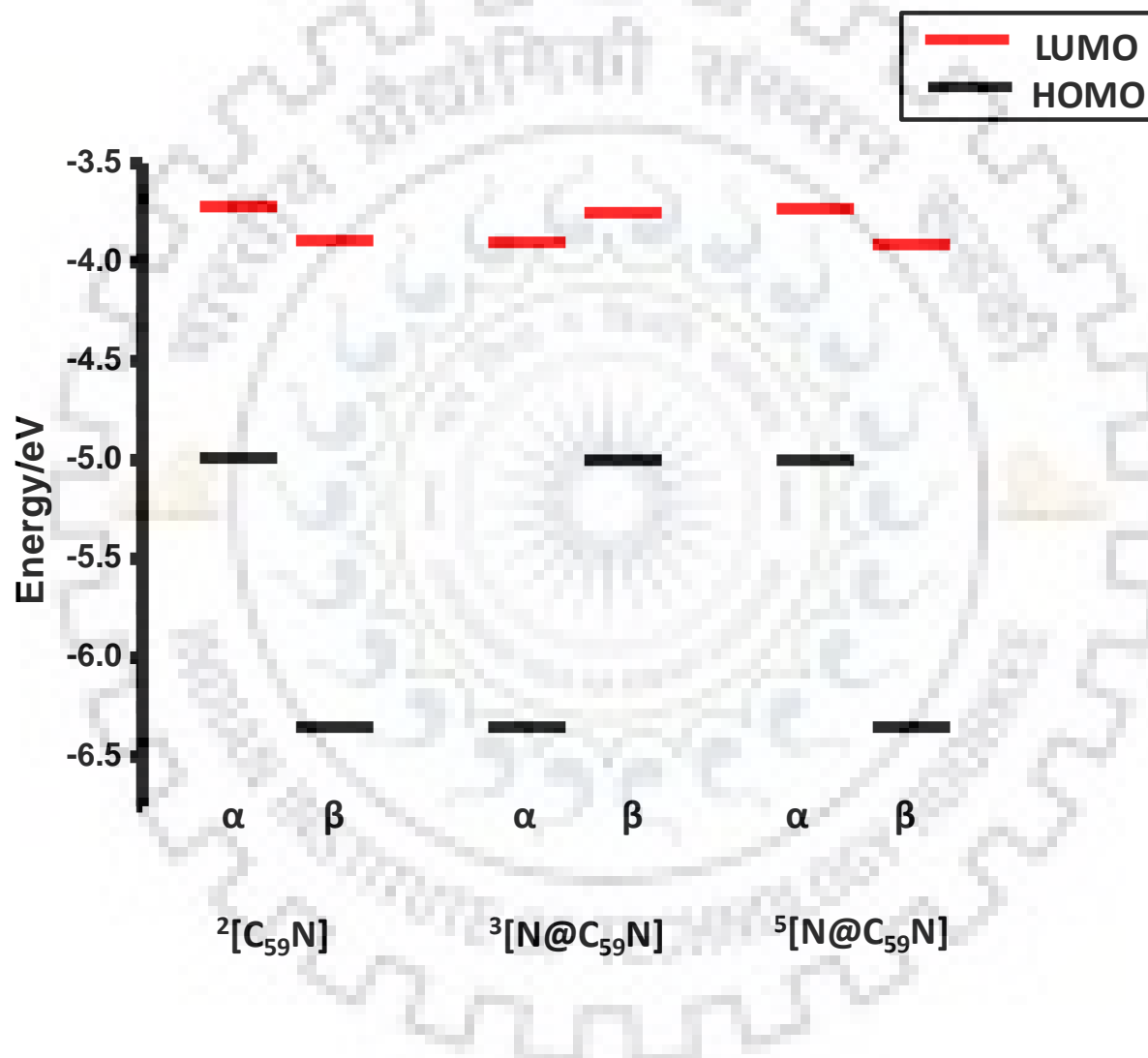


Figure 3.5 The α - and β -spin HOMO and LUMO energy levels of ²[C₅₉N], ³[N@C₅₉N] and ⁵[N@C₅₉N].

The HOMO–LUMO energy gap of $(C_{59}N)_2$ is 2.21 eV, which is unaffected by the encapsulation of nitrogen atoms inside the cage. The respective HOMO and LUMO of $(C_{59}N)_2$ and $(N@C_{59}N)_2$ are quite similar in appearance as evident from figure 3.3. As mentioned for other endohedral complexes, the HOMO and LUMO of $(N@C_{59}N)_2$ are mainly contributed by the carbon and nitrogen atoms of the cage.

The effect of dimerization of C_{60} , $N@C_{60}$, $C_{59}N$, and $N@C_{59}N$ on the HOMO–LUMO energy gap was examined, and it is found that the HOMO–LUMO energy gap for C_{60} and $N@C_{60}$ is decreased by ~ 0.27 eV on forming their respective dimers. For the complexes $C_{59}N$ and $N@C_{59}N$, the dimerization led to an increase in the HOMO–LUMO energy gap by ~ 0.95 eV in agreement with the enhanced stability of the dimer.

3.3.4 Thermodynamic feasibility of the formation of the complexes

In order to know the thermodynamic feasibility of the formation of complexes for their stable states, the change in Gibbs free energy (ΔG) and change in enthalpy (ΔH) corresponding to the encapsulation of nitrogen inside fullerene derivatives were calculated and are listed in table 3.4. For dimer, the values of ΔG and ΔH associated with the dimerization of monomer units are also calculated. For ${}^4[N@C_{60}]$, the values of ΔG and ΔH due to the encapsulation of nitrogen atom inside C_{60} are -3.78 kcal/mol and -9.70 kcal/mol, respectively, at B3LYP-GD2/6-311G* level. This suggests that the encapsulation of nitrogen atom inside C_{60} is thermodynamically feasible. The values of ΔG and ΔH for the triplet state of $N@C_{59}N$ are -4.08 kcal/mol and -9.82 kcal/mol, respectively, at B3LYP-GD2/6-311G* level which indicate that the formation of complex is thermodynamically feasible. Similarly, the formation of $N@C_{59}N$ in its triplet state is also thermodynamically feasible as reflected from the respective values of ΔG and ΔH listed in table 3.4. The complex ${}^7[(N@C_{60})_2]$ can be obtained by the encapsulation of nitrogen atoms inside adjacent cages of $(C_{60})_2$ as indicated from the values of ΔG of -8.77 kcal/mol and ΔH of -19.51 kcal/mol. However, it may be difficult to obtain the same *via* the dimerization of $N@C_{60}$ as clear from the value of ΔG (0.49 kcal/mol). As clear from the values of ΔG and ΔH in table 3.4, the formation of dimer ${}^7[(N@C_{59}N)_2]$ is thermodynamically feasible either by the encapsulation of nitrogen atoms inside the adjacent cages of $(C_{59}N)_2$ or by the dimerization of $N@C_{59}N$ although the formation is more feasible *via* the dimerization of $N@C_{59}N$.

Table 3.4. The change in Gibbs free energy (ΔG) and change in enthalpy (ΔH) for the formation of the complexes relevant to the encapsulation of guest atoms inside the fullerene derivatives. For the dimers, the value of ΔG and ΔH associated with the dimerization monomers units are provided in parenthesis.

Complexes	ΔG (kcal/mol)		ΔH (kcal/mol)	
	B3LYP/6-311G*	B3LYP-GD2/6-311G*	B3LYP/6-311G*	B3LYP-GD2/6-311G*
$^4[(N@C_{60})]$	8.24	-3.78	0.91	-9.70
$^3[(N@C_{59}N)]$	7.46	-4.08	1.09	-9.82
$^5[(N@C_{59}N)]$	7.31	-3.46	1.24	-9.70
$^7[(N@C_{60})_2]$	13.98 (22.00)	-8.77 (0.49)	2.48 (10.19)	-19.51 (-13.24)
$^7[(N@C_{59}N)_2]$	14.45 (-12.95)	-5.39 (-30.71)	2.25 (-27.14)	-20.02 (-47.18)

The encapsulation of nitrogen is considered only for the trans isomer of $(C_{59}N)_2$ as earlier experimental observations report that $(C_{59}N)_2$ exists in its trans form [42, 123]. However, the gauche isomer $(C_{59}N)_2$ is slightly lower energy (~ 0.5 kcal/mol) compared to its trans isomer as reported earlier theoretically [264]. The experimental studies of Hummelen *et al.* reported that the dimer $(C_{59}N)_2$ shows 30 lines in ^{13}C NMR suggesting a reasonably symmetric structure [42]. The studies of Pitchler *et al.* support $(C_{59}N)_2$ trans form [123]. Thus, to examine whether the orientation of the host cage affects the spin–spin interaction between the guest species, the encapsulation of two nitrogen atoms in the cages of the gauche isomer of $(C_{59}N)_2$ for the singlet and the septet states was also investigated. The results of the above calculations are listed in table 3.5. From the values of spin density of nitrogen obtained for the endohedral complexes of gauche and trans isomers, it can be concluded that the orientation of the cage has no significant effect on the interaction between the encapsulated guest species.

Table 3.5. The relative energy (R.E.) of various complexes with respect to their trans conformers and the spin density of encapsulated nitrogen atoms.

System	Conformers	B3LYP/6-311G*		B3LYP-GD2/6-311G*	
		R. E. (kcal/mol)	Spin density (e/au ³)	R. E. (kcal/mol)	Spin density (e/au ³)
$^1[(C_{59}N)_2]$	Trans	0.00	----	0.00	-----
	Gauche	-0.68	----	-0.90	-----
$^1[(N@C_{59}N)_2]$	Trans	0.00	$(N_{encap})_1 = 2.97$ $(N_{encap})_2 = -2.97$	0.00	$(N_{encap})_1 = 2.97$ $(N_{encap})_2 = -2.97$
	Gauche	-1.05	$(N_{encap})_1 = 2.97$ $(N_{encap})_2 = -2.97$	-1.29	$(N_{encap})_1 = 2.97$ $(N_{encap})_2 = -2.97$
$^7[(N@C_{59}N)_2]$	Trans	0.00	$(N_{encap})_1 = 2.97$ $(N_{encap})_2 = 2.97$	0.00	$(N_{encap})_1 = 2.97$ $(N_{encap})_2 = 2.97$
	Gauche	-1.05	$(N_{encap})_1 = 2.97$ $(N_{encap})_2 = 2.97$	-1.29	$(N_{encap})_1 = 2.97$ $(N_{encap})_2 = 2.97$

3.4 Conclusions

In the present chapter, the density functional theoretical studies were performed to investigate the structure, stability, and magnetic properties of nitrogen atom encapsulated complexes of fullerene derivatives. It was found that the triplet and quintet states of $N@C_{59}N$ are nearly isoenergetic suggesting that the complex can exist in either of the spin states. For the most stable spin state of each of the complexes, the spin–spin coupling and the spin density transfer between guest and the host cage as well as those between guest species of adjacent cages were investigated. The spin polarization in the stable states of the complexes was also studied. In the triplet state of $N@C_{59}N$, the spin density of encapsulated nitrogen and that of host cage was found to be anti-ferromagnetically coupled, opposite to the ferromagnetic coupling in its quintet state. Moreover, the values of spin density on the encapsulated nitrogen atom in triplet and quintet state of $N@C_{59}N$ suggested that the guest nitrogen atom retained its atomic spin. The present study also showed that the complexes $(N@C_{60})_2$ and $(N@C_{59}N)_2$ are stable both in their septet and singlet states. Unlike in metallofullerenes, there is no electron transfer between guest and host species in the above complexes and hence guests retained their atomic spin. The spins of the respective guest nitrogen atoms of $(N@C_{60})_2$ and $(N@C_{59}N)_2$ were antiferromagnetically and ferromagnetically coupled in their singlet and septet states, respectively. The study also showed that the complexes are spin degenerate and spin polarized in their lower and higher spin states, respectively.

The effect of the encapsulation of nitrogen atom inside various cages on the energy gap between HOMO and LUMO of the latter were examined. In all cases, the HOMO–LUMO energy gap is unaffected due to the encapsulation of nitrogen. Thus, stability of the complex is entirely due to the dispersion interaction between the encapsulated nitrogen and the host cage. It was also found that the formation of $(C_{59}N)_2$ and $(N@C_{59}N)_2$ from their respective monomers leads to an increase in the HOMO–LUMO energy gap in contrast to that for $(C_{60})_2$ and $(N@C_{60})_2$. The values of the thermodynamic parameters ΔG and ΔH for the complexes indicated that the formation of nitrogen atom encapsulated fullerene derivatives is thermodynamically feasible.

In conclusion, taking nitrogen-encapsulated fullerenes as a prototype of two spin center molecules, the stability, magnetic properties, and nature of interaction between two paramagnetic guest species encapsulated in adjacent cages were studied. The effect of a heteroatom on the surface of the cage in the interaction was also examined using an experimentally viable system.

Chapter-4

Structure, stability and properties of the boron encapsulated fullerene derivatives

4.1 Introduction

The studies on heterofullerenes suggested that the properties of fullerenes can be altered by suitable substitution of carbon atom by heteroatom [114-122]. As mentioned in chapter 1, several experimental and theoretical reports are available on endohedral fullerenes and endohedral heterofullerenes discussing their structure, stability and various properties [71-91, 104-111, 135-140]. In chapter 3 of the present thesis, the electron spin-spin coupling and spin density transfer in the endohedral complexes of C_{60} , $C_{59}N$ and their respective dimers with nitrogen as the endohedral species were discussed. The above study revealed that unlike in $N@C_{60}$, an antiferromagnetic or a ferromagnetic coupling between the guest and the host occurs in $N@C_{59}N$, depending upon the spin state of the complex.

Like nitrogen, boron is also a reactive and paramagnetic atom adjacent to carbon in periodic table and is capable to form endohedral complexes with fullerene derivatives. Thus, it is interesting to know how the spin of encapsulated boron atom interacts with that of paramagnetic host fullerene derivatives or how the encapsulated boron atom affects the properties of the latter. Thus, the structure, stability and properties of boron atom encapsulated complexes of various fullerene derivatives (C_{60} , $C_{59}B$ and $C_{59}N$) are investigated in the present chapter. For this purpose, possible spin states of the complexes are considered. The electronic properties of the stable states of the boron atom encapsulated fullerene derivatives are discussed. The spin-spin interaction and spin density transfer between guest and host of the stable states of the above complexes are studied. Further, the spin polarization in the complexes is also examined. The effect of confinement on the isotropic hyperfine coupling constant (hfcc) of boron atom due to different cages is examined. The thermodynamic feasibility of the boron encapsulation in various fullerenes derivatives is determined.

4.2 Computational Methods

All calculations were performed using Gaussian 09 program [261]. Geometry optimization was performed for C_{60} , $C_{59}N$, $C_{59}B$, and their boron encapsulated derivatives using the hybrid density functional, B3LYP with and without Grimme's empirical dispersion correction (B3LYP-GD2) in conjunction with 6-311G* basis set [224, 240]. The selection of methods B3LYP/6-311G* and B3LYP-GD2/6-311G* used was already justified in chapter 3. The value of hyperfine coupling constant for ^{14}N (3.6 G) of $C_{59}N$ obtained by these methods also agrees well with the experimental value [121].

For the complexes $B@C_{59}B$ and $B@C_{59}N$, various possible spin states were considered. The stabilization energy was calculated as was given in equation 3.1. for various possible spin states of complexes and from which the most stable spin state was determined. The frequency analysis confirmed that the optimized geometry of the most stable state of each type of complexes corresponds to minima on the respective potential energy surface. The broken symmetry calculations were performed to analyze the antiferromagnetic singlet state of the complexes using their high spin state wave function. The wave functions corresponding to various spin states of different complexes were tested for their stability and confirmed that they are stable. In order to know the spin polarization in above complexes, the spin polarization parameter (ζ) was calculated using equation 2.42.

The vertical ionization energy (VIE) and vertical electron affinity (VEA) of the species were calculated from the energy of the neutral, cationic, and anionic species using the optimized geometries of the respective neutral species. The electron spin density associated with the heteroatom of cage and encapsulated boron atom of the complexes was also calculated. The spin density difference distribution and the isodensity surface of HOMO and LUMO were plotted using the program GaussView 5 [263]. The values of hyperfine coupling constant corresponding to the heteroatom of the cage and the guest species therein were calculated. To examine the thermodynamic feasibility of boron encapsulation inside various fullerene derivatives, the change in Gibbs free energy (ΔG) and change in enthalpy (ΔH) associated with the encapsulation of boron inside the cage was calculated as was done in chapter 3 for similar systems. The absorption studies were performed using the TDDFT formalism at the B3LYP/6-311G* level.

4.3 Results and discussion

4.3.1 Structure, stability and host–guest interaction

The optimized geometries of different complexes for their various spin states are depicted in figure 4.1. The calculated values of stabilization energies for various spin states of the complexes are listed in table 4.1. The stabilization energy of -11.52 kcal/mol for $B@C_{60}$ obtained at B3LYP-GD2/6-311G* level compared to that of 6.0 kcal/mol at the B3LYP/6-311G* level suggests that the stabilization of the complex mainly arises due to the dispersion interaction between the guest and the host. In the stable state of the complex, boron atom occupied at the centre of host cage.

The stabilization energy of the complex that formed by the encapsulation of boron atom inside the paramagnetic cage $C_{59}B$ shows that, among the possible two spin states of the complex $B@C_{59}B$, the singlet state is ~ 40.0 kcal/mol more stable than the triplet one. In the complex $^1[B@C_{59}B]$, the encapsulated boron is located near to one of C_5B hexagonal rings of the cage which forms a nearly hexagonal pyramidal geometry. The distances of encapsulated boron to atoms of C_5B hexagonal ring of the cage are in the range of 1.95 – 2.13 Å as shown in figure 4.2. In the triplet state of the complex, the encapsulated boron is located near to the center of the cage. The studies also showed that the complex $B@C_{59}N$ is stable in its singlet and triplet states with the stabilization energy of -24.12 and -12.46 kcal/mol, respectively, which indicates that the former is more stable by 11.66 kcal/mol than the latter. In the complex $^1[B@C_{59}N]$, the encapsulated boron is located adjacent to a C_5 pentagonal ring of the cage that is bonded to nitrogen of the cage, thereby forming an approximate pentagonal pyramidal structure. The distances of encapsulated boron atom to nearby C_5 pentagonal ring of $^1[B@C_{59}N]$ are in the range of 1.84 – 1.96 Å as indicated in figure 4.2. In the triplet state of $B@C_{59}N$, the encapsulated boron is located near the center of the cage.

To investigate the stability of antiferromagnetic singlet state of the complex, broken symmetry calculations were performed for the complexes. The stabilization energy of the antiferromagnetic states of $B@C_{59}B$ and $B@C_{59}N$ are 40.89 kcal/mol and 11.72 kcal/mol higher energy than the corresponding closed shell singlet states. The antiferromagnetic singlet and triplet states were found to be of same energy.

Table 4.1. Stabilization energy (kcal/mol) of various endohedral fullerene complexes in their different spin states. The basis set superposition error (BSSE) corrected values are given in parentheses.

Complexes	Multiplicity	B3LYP/6-311G*	B3LYP-GD2/6-311G*
B@C ₆₀	2	6.00 (7.95)	-11.52 (-9.56)
B@C ₅₉ B	1	-43.20 (-41.20)	-52.68(-50.61)
	3	5.79 (7.63)	-11.57(-9.67)
B@C ₅₉ N	1	-13.72 (-11.21)	-24.12 (-21.48)
	3	5.13 (7.07)	-12.46 (-10.51)

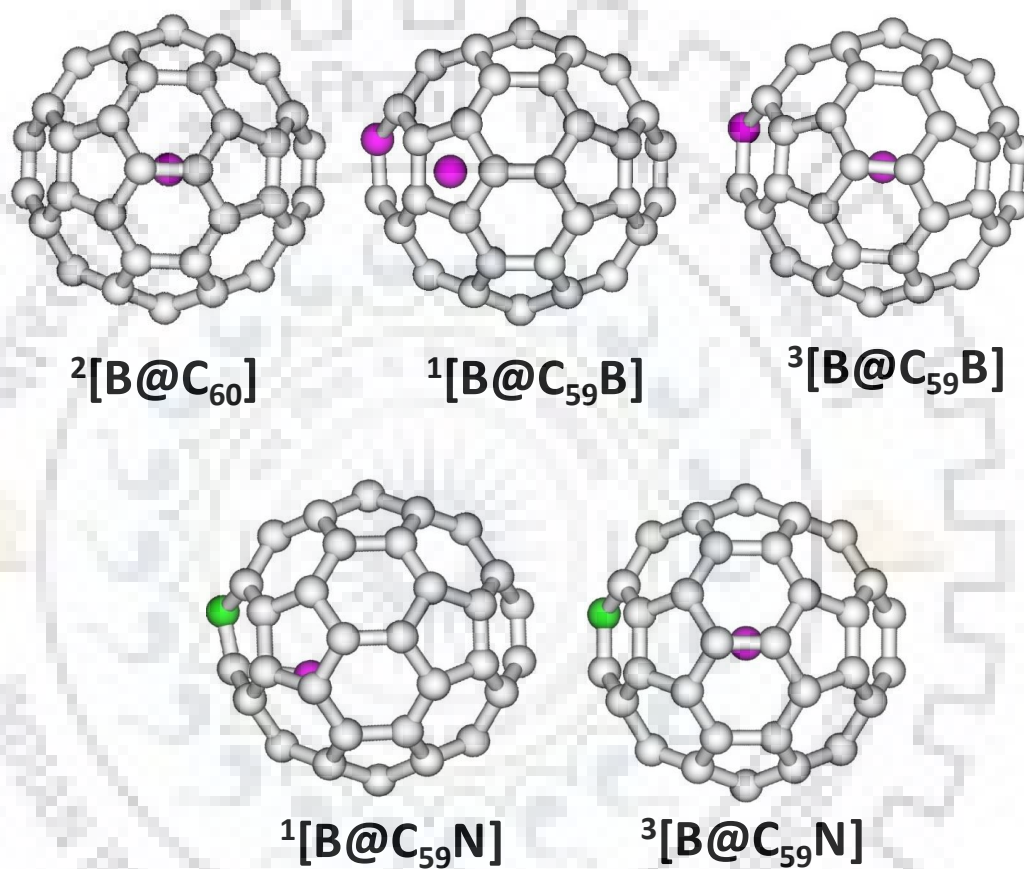


Figure 4.1. Optimized geometries of the complexes in their different spin states.

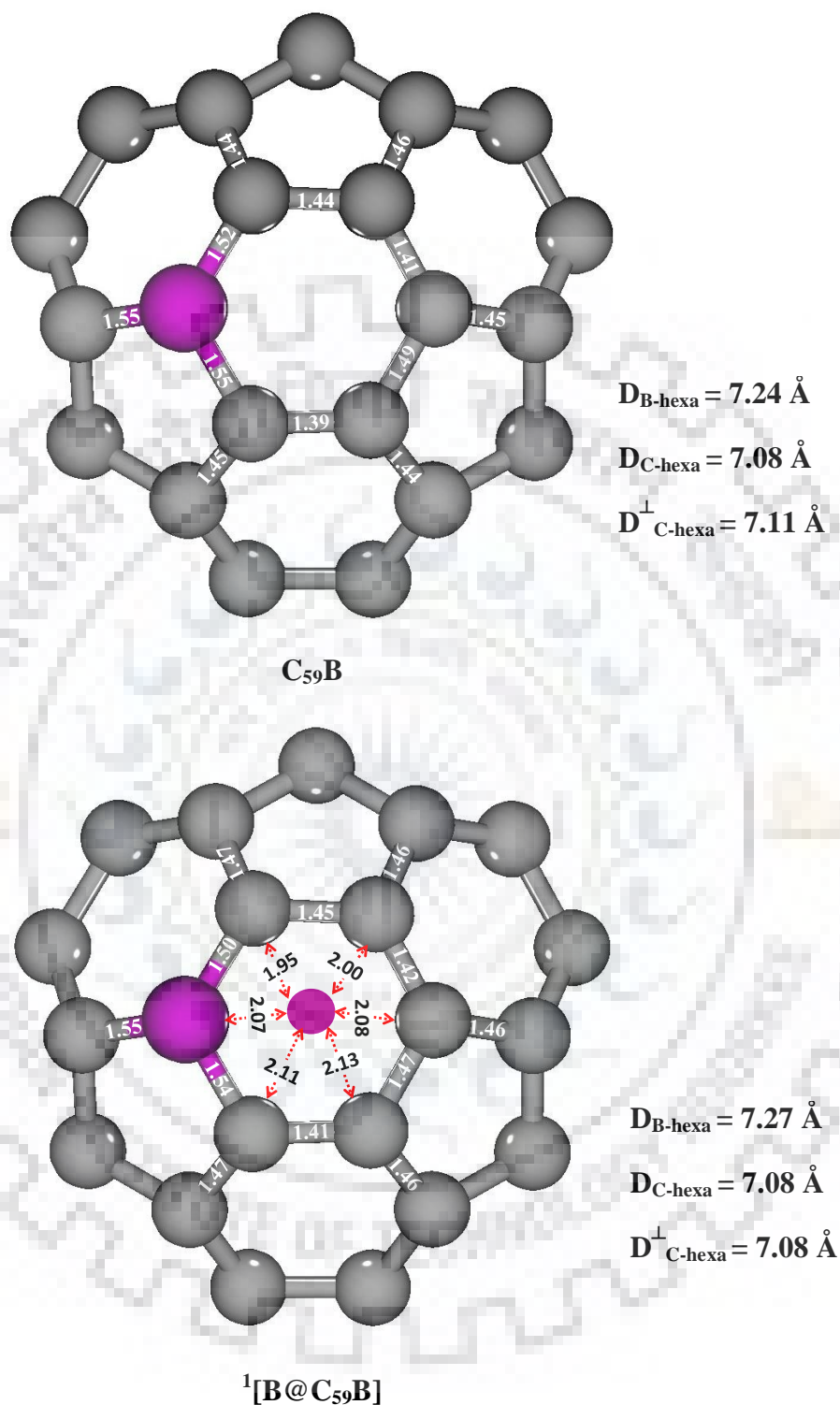
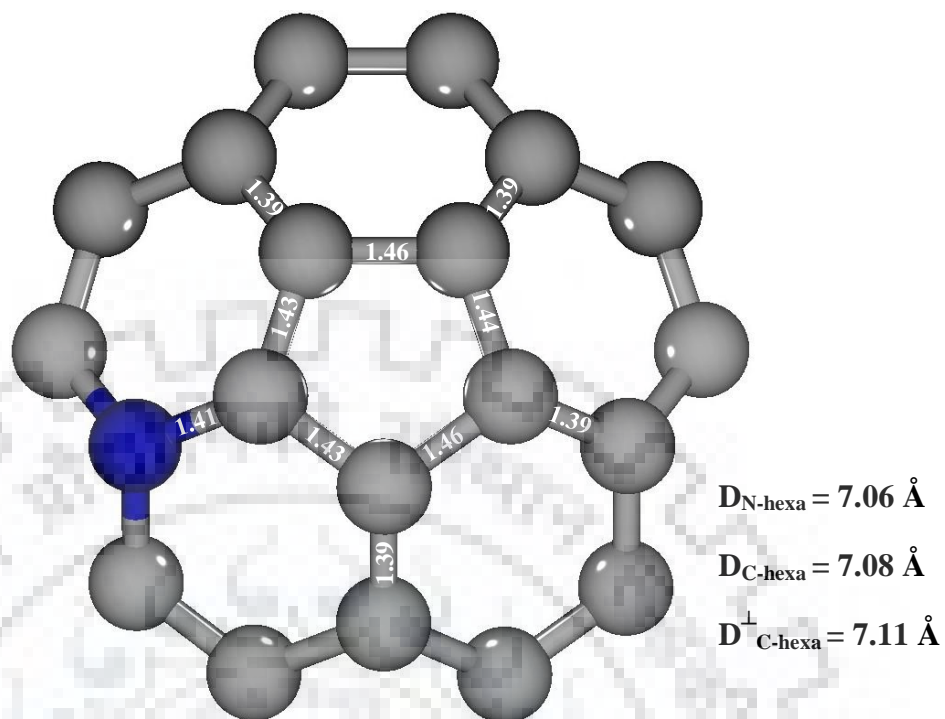
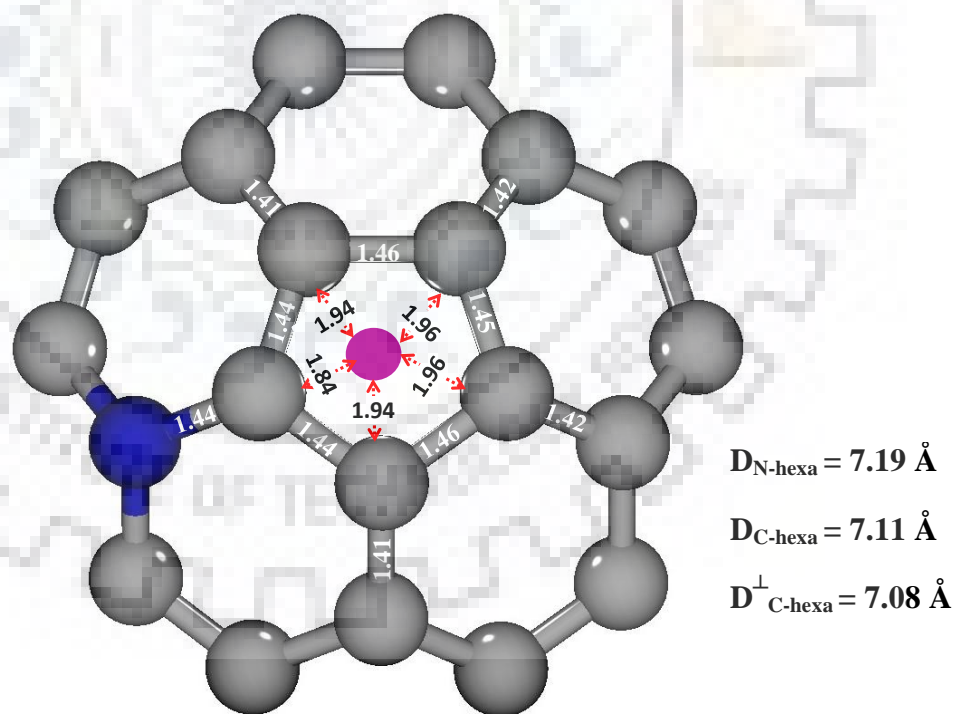


Figure 4.2. Figure illustrating the internuclear distances for some of the selected atoms of C₅₉B, C₅₉N and their complexes. The diameter of the cage with respect to the heteroatom, its nearest carbon and along the perpendicular direction is also shown in the right bottom of each panel.



$C_{59}N$



${}^1[B@C_{59}N]$

Figure 4.2. continued.

To get further insight on the nature of interaction, the natural bond orbital (NBO) analysis was carried out for the above complexes. The NBO analysis indicated strong interaction between the encapsulated boron and the nearby hexagonal or pentagonal rings of the cages mentioned above. The analysis also revealed that the interaction of guest atom with heteroatom of the cage is more prominent in $^1[\text{B}@\text{C}_{59}\text{B}]$ than in $^1[\text{B}@\text{C}_{59}\text{N}]$, leading to a higher stabilization energy for the former.

It should be mentioned that although the substitution of one of the carbon atoms of C_{60} by a heteroatom (B/N) causes slight distortion of the cage, encapsulation of boron atom inside the cage did not show significant distortion further. The changes in C–C and C–B (or C–N) bond lengths for the nearby hexagonal rings of $\text{B}@\text{C}_{59}\text{B}$ (or pentagonal ring of $\text{B}@\text{C}_{59}\text{N}$) are less than $\sim 0.03 \text{ \AA}$ as evident from figure 4.2. To know the effect of the encapsulation of guest boron on the size of cage, the diameter of the cage in different directions are determined for the complexes as well as for the free cage as shown in figure 4.2. The diameter of the cage C_{59}B (or C_{59}N) with respect to heteroatom of the cage and its nearest carbon are represented by $D_{\text{B-hexa}}$ (or $D_{\text{N-hexa}}$) and $D_{\text{C-hexa}}$, respectively, whereas the diameter along the perpendicular direction of heteroatom is represented by $D_{\text{C-hexa}}^{\perp}$. As expected, the change in size of the cage due to encapsulation of boron is negligible as reflected from the values of diameters.

4.3.2 Electronic properties

4.3.2.1 Electron affinity and ionization energy

To study the electronic properties of complexes, vertical electron affinity (VEA) and vertical ionization energy (VIE) of different spin states of the complexes are calculated and are listed in table 4.2. From the table, it can be seen that the values of VEA and VIE of C_{60} are -2.44 eV and 7.63 eV , respectively. On encapsulation of boron atom inside C_{60} , the value of VEA is decreased by 0.68 eV compared to that of C_{60} . On the other hand, the VIE of C_{60} is not much affected due to the encapsulation of boron atom. Similarly, the electron affinity of the most stable state of the complex $\text{B}@\text{C}_{59}\text{B}$ is 1.07 eV less than that of its host cage C_{59}B . With the encapsulation of boron, the vertical ionization energy of C_{59}B is increased by 0.21 eV for the most stable state of the resultant complex $\text{B}@\text{C}_{59}\text{B}$. This suggests that the electron donating propensity is reduced significantly with the encapsulation of boron, probably due to the electron deficiency of boron atom. On the other hand, the electron affinity and ionization energy for triplet state of $\text{B}@\text{C}_{59}\text{B}$ is

found to be nearly unchanged with respect to $C_{59}B$. The encapsulation of boron in $C_{59}N$ does not change the vertical electron affinity of $C_{59}N$ for any of the spin states of complex. In contrast, the vertical ionization energy of ${}^1[B@C_{59}N]$ is increased by 0.40 eV compared to that of free host cage although it is unaltered for triplet state of the complex. The ionization energy of most stable state of the resultant complex suggests that $C_{59}N$ has more tendency to donate an electron than that for $B@C_{59}N$. The heterofullerene $C_{59}B$ has more propensity to accept electrons among all the species considered.

4.3.2.2 Energy gap between HOMO and LUMO

To know more about electronic properties of the complexes, isodensity surfaces of HOMO and LUMO as well as the energy gap between them are analyzed. The isodensity surfaces of HOMO and LUMO of the complexes in their different spin states are depicted in figure 4.3. For the complexes with unpaired electrons, α -spin orbitals are shown in figure 4.3. The corresponding β -spin orbitals are shown in figure 4.4. The values of energy gap between the respective HOMO and LUMO of C_{60} , $C_{59}B$, $C_{59}N$, and their boron encapsulated complexes are listed in table 4.2. It can be inferred from the figure that HOMO corresponding to α -spin of $B@C_{60}$ is mainly formed by orbitals of boron atom. The LUMO of the above is formed by orbitals of carbon atoms of C_{60} and resembles LUMO of C_{60} . Because of the encapsulation of boron, HOMO–LUMO energy gap of C_{60} is decreased by ~ 1.0 eV.

It was also found that the HOMO–LUMO energy gap of the complexes varies with their spin states. For example, HOMO–LUMO energy gap of $B@C_{59}B$ is 2.52 eV for its singlet state, whereas that of triplet state is 1.79 eV. The frontier molecular orbitals of the singlet state of $B@C_{59}B$ are formed by the orbitals of both guest and host species whereas those for the triplet state are formed either by the orbitals of one of the guest or host species. The HOMO–LUMO energy gap of $B@C_{59}N$ in its triplet state remains nearly the same as that of $C_{59}N$. However, the HOMO–LUMO energy gap of $B@C_{59}N$ in its singlet state is increased slightly by 0.21 eV with respect to the host cage. It can be inferred from figure 4.3 that the frontier molecular orbitals of $B@C_{59}N$ in its singlet state are formed from orbitals of both components of the complex. For triplet state of $B@C_{59}N$, the frontier molecular orbitals are mainly formed by the contribution of host cage. The above results show that HOMO–LUMO energy gap for the singlet state of $B@C_{59}B$ and $B@C_{59}N$ is slightly more than that of the respective host cages.

Table 4.2. Values of vertical electron affinity (VEA), vertical ionization energy (VIE), and the energy gap between HOMO and LUMO ($\Delta E_{\text{HOMO-LUMO}}$) of complexes in their different spin states obtained at the B3LYP/6-311G* Level. The values obtained at B3LYP-GD2/6-311G* level are given in parentheses.

Complexes	Multiplicity	VEA (eV)	VIE (eV)	$\Delta E_{\text{HOMO-LUMO}}$ (eV)
C ₆₀	1	-2.44 (-2.44)	7.63 (7.62)	2.75 (2.74)
B@C ₆₀	2	-1.76 (-1.76)	7.72 (7.74)	$\alpha=1.77$ (1.78) $\beta=2.72$ (2.72)
C ₅₉ B	2	-3.59 (-3.59)	7.23 (7.23)	$\alpha=2.41$ (2.40) $\beta=1.54$ (1.54)
B@C ₅₉ B	1	-2.52 (-2.52)	7.44 (7.44)	2.52 (2.52)
	3	-3.58(-3.61)	7.17(7.17)	$\alpha=1.79$ (1.79) $\beta=1.53$ (1.53)
C ₅₉ N	2	-2.72 (-2.72)	6.19 (6.19)	$\alpha=1.27$ (1.27) $\beta=2.46$ (2.45)
B@C ₅₉ N	1	-2.72 (-2.72)	6.59 (6.60)	1.48 (1.48)
	3	-2.68(-2.68)	6.18(6.18)	$\alpha=1.26$ (1.26) $\beta=2.46$ (2.46)

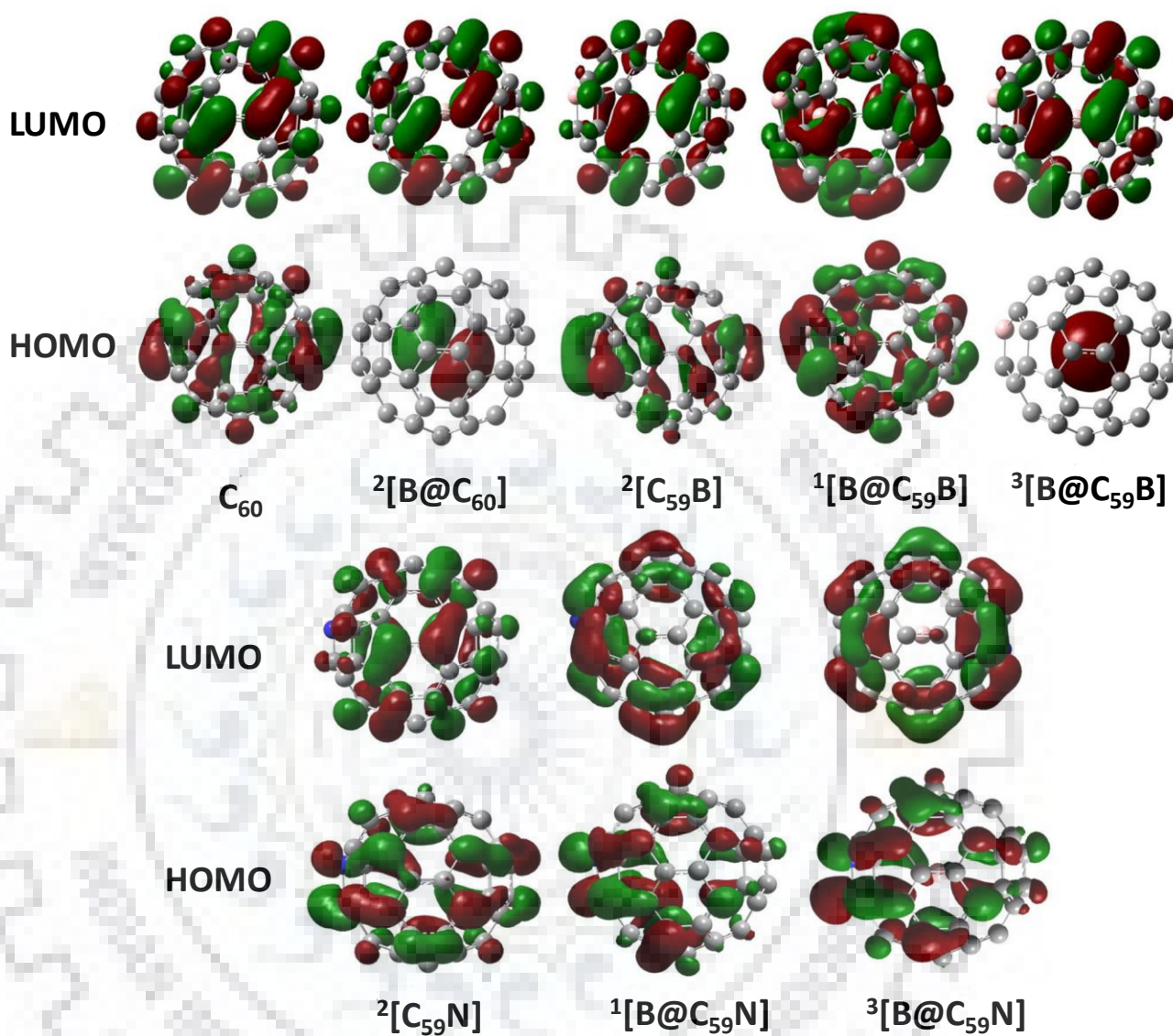


Figure 4.3. Isodensity surface plots of α -spin highest occupied and lowest unoccupied molecular orbitals of the complexes in their different spin states with an isodensity value of 0.02.

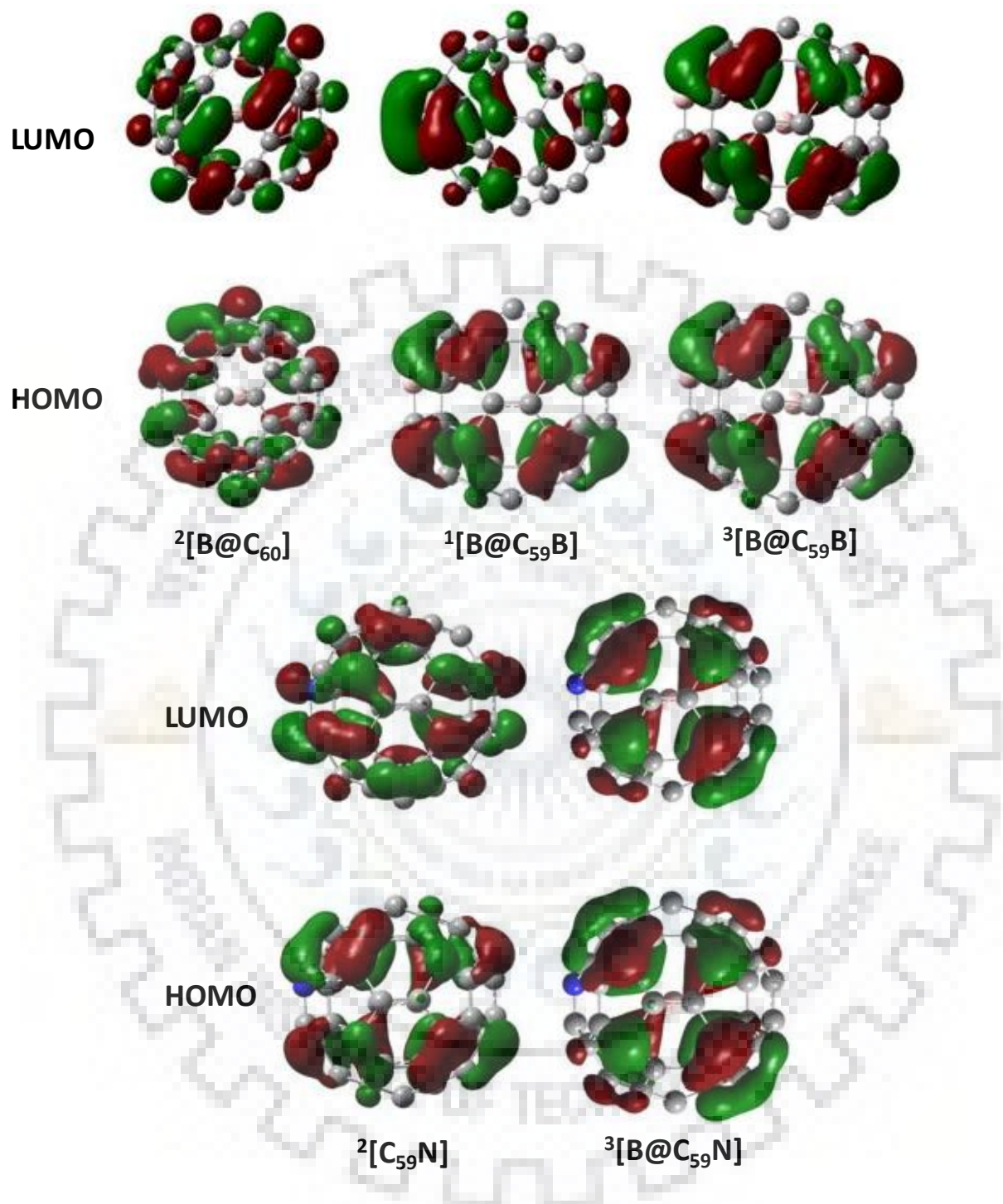


Figure 4.4. The β -spin isodensity surface of highest occupied and lowest unoccupied molecular orbitals of the paramagnetic species with an isodensity value of 0.02.

4.3.3 Spin–Spin coupling between guest and host

To get insight on spin–spin coupling and electron spin density transfer between guest and host cage, electron spin density of guest and heteroatoms of the cage for various complexes are calculated and are listed in table 4.3. The spin density difference plots for complexes are depicted in figure 4.5. It can be seen from the table that boron atom of $B@C_{60}$ has an electron spin density of $1.00 e/au^3$, keeping its original electronic configuration. This also indicates that there is no transfer of spin density from the trapped boron to the host cage or vice versa. It is also evident from spin density difference plot of the above complex that spin density is distributed only on the guest. For the triplet state of $B@C_{59}B$, spin of guest and that of host is ferromagnetically coupled without the transfer of spin density between guest and host. Similarly, ferromagnetic coupling also occurs in the triplet state of $B@C_{59}N$ without any spin density transfer between its components. Thus, the above observation clearly indicates the possibility of a core@shell type ferromagnetic coupling between guest and host cage in the triplet state of $B@C_{59}B$ and $B@C_{59}N$. It can also be concluded that the boron atom retains its atomic spin in ${}^2[B@C_{60}]$, ${}^3[B@C_{59}B]$ and ${}^3[B@C_{59}N]$.

In order to know the spin polarization in the complexes, the spin polarization parameter (ζ) for the complexes is calculated and is listed in table 4.3. The value of spin polarization parameter (ζ) for ${}^2[B@C_{60}]$ is 1.00 which indicates that the complex is spin polarized. Similarly, the complexes ${}^3[B@C_{59}B]$ and ${}^3[B@C_{59}N]$ are also spin polarized as reflected from corresponding spin polarization parameter (ζ) of 1.00.

4.3.4 Hyperfine coupling constant (hfcc)

The effect of confinement on the hyperfine coupling constant (hfcc) of boron due to the diamagnetic C_{60} cage as well as paramagnetic $C_{59}B$ and $C_{59}N$ cages was examined. In addition, the hfcc of the heteroatom of the cages in both the complexes and free state were calculated. The calculated values of hfcc for guest as well as for heteroatom of the cage of various complexes are listed in table 4.3. From the table, it can be seen that the value of hfcc obtained for free boron is 4.52 G at B3LYP/6-311G* and B3LYP-GD2/6-311G* levels of theory. The value of hfcc of boron is decreased to 1.07 G when it is encapsulated inside C_{60} , although there was no change in its electron spin density. For complexes ${}^3[B@C_{59}B]$ and ${}^3[B@C_{59}N]$, hfcc of trapped boron is further

Table 4.3. The spin density values (in e/au^3) and hyperfine coupling constant values ($hfcc$) (in Gauss) on the heteroatom of cage and encapsulated boron atom of various complexes along with the values of spin polarization parameter of the complexes.

Complexes	Multiplicity	B3LYP/6-311G*			B3LYP-GD2/6-311G*		
		Spin Density	$hfcc$	ζ	Spin Density	$hfcc$	ζ
B	2	1.00	4.52	1.00	1.00	4.52	1.00
B@C ₆₀	2	B _{encap} =1.00	B _{encap} =1.07	1.00	B _{encap} =1.00	B _{encap} =1.07	1.00
C ₅₉ B	2	B _{cage} =-0.14	B _{cage} =-1.09	1.00	B _{cage} =-0.14	B _{cage} =-1.08	1.00
B@C ₅₉ B	3	B _{encap} =1.00	B _{encap} =0.47	1.00	B _{encap} =1.00	B _{encap} =0.43	1.00
		B _{cage} =-0.14	B _{cage} =-0.54		B _{cage} =-0.14	B _{cage} =-0.54	
C ₅₉ N	2	N _{cage} =-0.08	N _{cage} =3.67	1.00	N _{cage} =-0.08	N _{cage} =3.63	1.00
B@C ₅₉ N	3	B _{encap} =1.00	B _{encap} =0.51	1.00	B _{encap} =1.00	B _{encap} =0.51	1.00
		N _{cage} =-0.08	N _{cage} =1.86		N _{cage} =-0.08	N _{cage} =1.86	

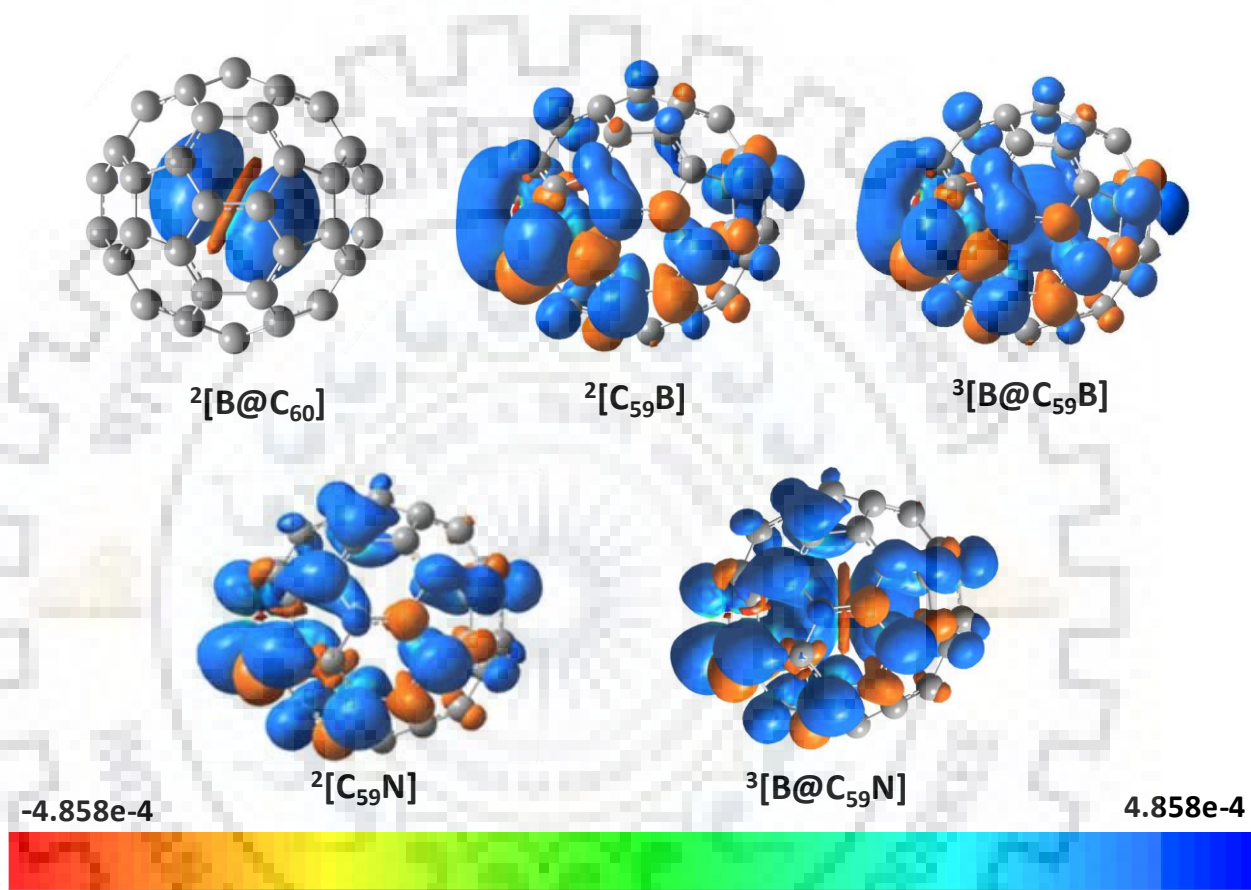


Figure 4.5. Spin density difference plots of various complexes in their different spin states with isodensity value of 0.0004. The blue color represents the excess of α -spin density, and the orange color represents the excess of β -spin density.

reduced to 0.47 G and 0.51 G, respectively, showing the effect of encapsulation by a paramagnetic cage. Despite a decrease in the value of hfcc, the electron spin density of encapsulated boron for the complexes $B@C_{59}B$ and $B@C_{59}N$ remained the same as in its free state. Further, the hyperfine coupling constant of heteroatoms of the cages $C_{59}B$ and $C_{59}N$ with and without guest species are also analyzed. As evident from table, the value of hfcc of boron in $C_{59}B$ is -1.09 G, which is increased to -0.54 G by encapsulating a boron atom inside. On the other hand, hfcc of nitrogen in $C_{59}N$ (3.67 G) is decreased to 1.86 G on encapsulating the guest species inside. Thus, hfcc of encapsulated boron atom of the complexes is decreased in the order $B@C_{60} > B@C_{59}N > B@C_{59}B$.

4.3.5 Thermodynamics of encapsulation of boron in fullerene derivatives

The thermodynamic feasibility of the encapsulation of boron atom in fullerene derivatives is investigated based on the values of the change in Gibbs free energy (ΔG) and change in enthalpy (ΔH). Therefore, the values of ΔG and ΔH associated with the encapsulation of boron atom inside fullerene derivatives are determined and are tabulated in table 4.4. As complexes were found to be stable at B3LYP-GD2/6-311G*, the values of ΔG and ΔH obtained at this level are discussed. The values of ΔG and ΔH for the complex $^2[B@C_{60}]$ are -5.92 and -11.64 kcal/mol indicated that the encapsulation of boron atom inside C_{60} is thermodynamically feasible. The encapsulation of boron atom inside $C_{59}B$ is thermodynamically feasible for the singlet and triplet states of resultant complex as reflected from their corresponding values of ΔG and ΔH . The formation of the singlet state of $B@C_{59}B$ is more feasible than its triplet state by 38.01 kcal/mol with respect to ΔG and 40.66 kcal/mol with respect to ΔH . The values of ΔG and ΔH for the singlet state of $B@C_{59}N$ are -14.52 and -23.97 kcal/mol, respectively, indicate the formation of complex. Similarly, the formation of its triplet state is also possible as reflected from the values of ΔG and ΔH (-5.95 and -12.10 kcal/mol, respectively). The formation of singlet state of $B@C_{59}N$ is more feasible than its triplet state as evident from the values of ΔG and ΔH . Thus, it can be concluded that the encapsulation of boron inside various fullerene derivatives is thermodynamically feasible.

Table 4.4. The change in Gibbs free energy (ΔG) and change in enthalpy (ΔH) due to the boron atom encapsulation in fullerene derivatives.

Complexes	Multiplicity	ΔG (kcal/mol)		ΔH (kcal/mol)	
		B3LYP/6-311G*	B3LYP-GD2/6-311G*	B3LYP/6-311G*	B3LYP-GD2/6-311G*
B@C ₆₀	2	12.52	-5.92	5.58	-11.64
B@C ₅₉ B	1	-33.07	-42.36	-42.42	-51.79
B@C ₅₉ B	3	13.15	-4.35	5.99	-11.13
B@C ₅₉ N	1	-4.60	-14.52	-13.90	-23.97
B@C ₅₉ N	3	12.24	-5.95	5.13	-12.10

4.4 Conclusion

In the present chapter, the structure as well as electronic, magnetic, and spectral properties of boron encapsulated C_{60} , $C_{59}B$, and $C_{59}N$ were investigated using density functional theoretical methods. The study showed that in $B@C_{60}$ the boron atom locates at the center of the cage. The complex was found to be stable due to dispersion interaction between the guest and the host. The complexes $B@C_{59}B$ and $B@C_{59}N$ exist in two different stable spin states, *viz.* singlet and triplet. For both types of complexes, the singlet state was found to be more stable than the triplet state analogue. The study also revealed that the size of the fullerene cage was unaffected due to the encapsulation of boron atom inside. The calculated values of vertical electron affinity (VEA) and vertical ionization energy (VIE) obtained for the complexes indicate that $C_{59}B$ has more propensity to accept the electrons than C_{60} , ${}^2[B@C_{60}]$, ${}^1[B@C_{59}B]$, $C_{59}N$, ${}^1[B@C_{59}N]$ and ${}^3[B@C_{59}N]$. On the other hand, $C_{59}N$ and ${}^3[B@C_{59}N]$ have more tendency to donate electrons. With the encapsulation of boron inside C_{60} , $C_{59}B$, and $C_{59}N$, the HOMO–LUMO energy gap of respective cages is either increased or decreased depending upon the spin states of complexes.

The calculated electron spin density values of guest and host indicated the absence of any spin density transfer between the component species. In ${}^2[B@C_{60}]$, ${}^3[B@C_{59}B]$ and ${}^3[B@C_{59}N]$, the boron atom retained its atomic spin as in its free state. The studies also showed ferromagnetic spin coupling between guest and host in triplet state of the complexes $B@C_{59}B$ and $B@C_{59}N$. The results also showed that the complexes ${}^2[B@C_{60}]$, ${}^3[B@C_{59}B]$ and ${}^3[B@C_{59}N]$ are spin polarized. The value of the hyperfine coupling constant of boron is decreased due to its encapsulation in a cage, and the change was found to be more prominent inside the paramagnetic cages. The calculated values of the thermodynamic parameters ΔG and ΔH for the boron encapsulated fullerene derivatives indicated that the encapsulation of boron atom inside the latter is thermodynamically feasible. The thermodynamic feasibility of the formation of the singlet states of the complexes $B@C_{59}B$ and $B@C_{59}N$ was found to be more compared to their respective triplet states.

Chapter-5

Structure, stability and properties of the dimers of $B@C_{59}N$ and $N@C_{59}B$

5.1 Introduction

In chapter 3, it was shown that the spins of the trapped nitrogen atom and the host $C_{59}N$ cage couple each other either antiferromagnetically or ferromagnetically without the transfer of spin density depending upon multiplicity of the complexes. It was also revealed that the anti-ferromagnetic and ferromagnetic states of $(N@C_{60})_2$ are isoenergetic and there is no spin density transfer between the guests or between the guest and the host. The above results also hold true for $(N@C_{59}N)_2$. Later in chapter 4, boron encapsulated in C_{60} , $C_{59}B$ and $C_{59}N$ were investigated. The ferromagnetic interaction was observed between the respective components of the complexes $B@C_{59}N$ and $B@C_{59}B$ in their triplet spin states. Interestingly, in this case also, spin density transfer was not observed between the components of the complexes.

Considering the lack of spin density transfer for the complexes studied in previous chapters, to seek the possibility of spin density transfer in the heterodimers of endohedral heterofullerenes $(B@C_{59}N)_2$, $(N@C_{59}B)_2$ and $(B@C_{59}N-N@C_{59}B)$ due to the presence of different types of heteroatoms on or inside the cage. The structure, stability and properties of the above complexes are studied in this chapter.

To investigate the spin polarization and spin degeneracy of the complexes, the spin polarization parameter is calculated and analyzed. The thermodynamic feasibility of the formation of the complexes both *via* the encapsulation of guest species in the host dimer $[(C_{59}B)_2, (C_{59}N)_2$ and $(C_{59}B-C_{59}N)]$ and *via* the dimerization of respective monomer units are studied. The effect of encapsulation of guest atoms on the electronic properties of the parent cage is also discussed in this chapter.

5.2 Computational methods

The electronic structure program Gaussian 09 was used for all of the calculations [261]. Considering the fact that B3LYP functional does not stabilize the endohedral complexes of fullerenes and heterofullerenes as mentioned in previous chapters, only the dispersion corrected B3LYP functional (B3LYP-GD2) in conjunction with the 6-311G* basis set was used for the present study [224, 240]. As was mentioned in chapters 3-4, the experimentally reported electronic properties of C₆₀ were in excellent agreement with the calculated values thereby justifying the level of calculation used. Like previous studies, all possible spin states of the complexes were considered. To confirm that the optimized geometries belong to minima on the potential energy surface, frequency calculations were performed. The stability of the wave functions of the complexes having unpaired electrons was also verified. The interaction between the radical centers was examined using the broken symmetry calculations as was explained in chapter 2.

The stabilization energy of various endohedral heterofullerenes was computed using the supermolecule approach by subtracting the energies of guest atoms and host cages from the energy of the respective complexes in their optimized geometries as was done in other chapters. To investigate the spin-spin interaction and spin density transfer, the spin density difference was calculated and plotted for various stable states. The spin density difference and molecular orbitals were plotted using the program GaussView5 [263]. To get more insight on the spin polarization of the complexes, the spin polarization parameter was calculated as discussed in chapter 2.

To determine the thermodynamic feasibility of complex formation, the change in Gibbs free energy (ΔG) and change in enthalpy (ΔH) associated with the encapsulation of guest species in the cage as well as those due to the dimerization of endohedral heterofullerenes were calculated using equation 3.2 and 3.3. The vertical ionization energy (VIE) and vertical electron affinity (VEA) of various species were computed using the energies of their neutral and ionic analogues

In chapter 3, it was reported that the nitrogen atom retained its spin inside C₅₉N, therefore it is important to study how the spins of atomic nitrogen behaves on encapsulating in C₅₉B. Thus, the structure, stability and properties of N@C₅₉B are investigated in the present study. The optimized geometries of the complex N@C₅₉B in its various spin states are shown in figure 5.1. The stabilization energy, spin density values of heteroatoms, spin polarization parameter (ζ), electronic properties (VIE, VEA and $\Delta E_{\text{HOMO-LUMO}}$) and thermodynamic parameters (ΔG and ΔH) of various complexes are tabulated in table 5.1. The stabilization energy for the singlet, triplet and quintet states of N@C₅₉B is -7.11, -9.96 and -10.02 kcal/mol suggesting that the complex is most stable in

its quintet state which is nearly isoenergetic with triplet state. The guest atom is located at the center of the host cage in $^3[\text{N@C}_{59}\text{B}]$ and $^5[\text{N@C}_{59}\text{B}]$, whereas it is located near inner surface of the host in $^1[\text{N@C}_{59}\text{B}]$. To investigate the spin-spin coupling and spin density transfer between nitrogen and C_{59}B , the spin density values on the heteroatoms of the complex are analyzed. The spin density distribution plots for the stable states of $\text{N@C}_{59}\text{B}$ are shown in figure 5.2. For $^3[\text{N@C}_{59}\text{B}]$, $^5[\text{N@C}_{59}\text{B}]$, the antiferromagnetic and ferromagnetic coupling occurs, respectively, between nitrogen and C_{59}B without any spin density transfer. As evident from the values listed in table 5.1, the nitrogen atom retained its atomic spin inside C_{59}B for triplet and quintet states of the resultant complex. The complex $\text{N@C}_{59}\text{B}$ is partially and fully spin polarized in its triplet ($\zeta=0.50$) and quintet ($\zeta=1.00$) states, respectively.

To know the effect of encapsulation of nitrogen on the electronic properties of C_{59}B , various electronic properties such as VIE, VEA and $\Delta E_{\text{HOMO-LUMO}}$ of the complex as well as that of host cage are calculated and are listed in table 5.1. The electron affinity of C_{59}B is -3.59 eV which is unaltered due to the encapsulation of nitrogen for the triplet and quintet states of the resultant complex. However, for $^1[\text{N@C}_{59}\text{B}]$, the electron affinity is decreased by 1.13 eV. On encapsulating nitrogen atom, the ionization energy of C_{59}B is not significantly changed for various spin states of the complex except for the triplet state for which it is increased slightly by 0.28 eV. For $^1[\text{N@C}_{59}\text{B}]$ and $^5[\text{N@C}_{59}\text{B}]$, the energy gap between HOMO and LUMO is found to be the same as that of C_{59}B , however, it is decreased by 0.86 eV for $^3[\text{N@C}_{59}\text{B}]$. To examine the thermodynamic feasibility of the formation of $\text{N@C}_{59}\text{B}$ for its various spin states, the change in Gibbs free energy (ΔG) and change in enthalpy (ΔH) associated with the encapsulation of nitrogen inside C_{59}B are calculated. From the values of ΔG and ΔH , it is found that the formation of $\text{N@C}_{59}\text{B}$ is thermodynamically feasible in its triplet and quintet states.

In order to investigate the homo and heterodimers of $\text{B@C}_{59}\text{N}$ and $\text{N@C}_{59}\text{B}$, the minimum energy structures of the host cages $(\text{C}_{59}\text{N})_2$, $(\text{C}_{59}\text{B})_2$ and $(\text{C}_{59}\text{N}-\text{C}_{59}\text{B})$ are selected. For this purpose, the relative energies of the cis and trans conformers of these host cages were calculated and are listed in table 5.2. As seen from table, trans-isomers of $(\text{C}_{59}\text{N})_2$, $(\text{C}_{59}\text{B})_2$ and $(\text{C}_{59}\text{N}-\text{C}_{59}\text{B})$ were found to be lower in energy by 8.45, 6.30 and 0.17 kcal/mol with respect to their respective cis-isomers. Thus, trans forms of the above species were selected for further studies.

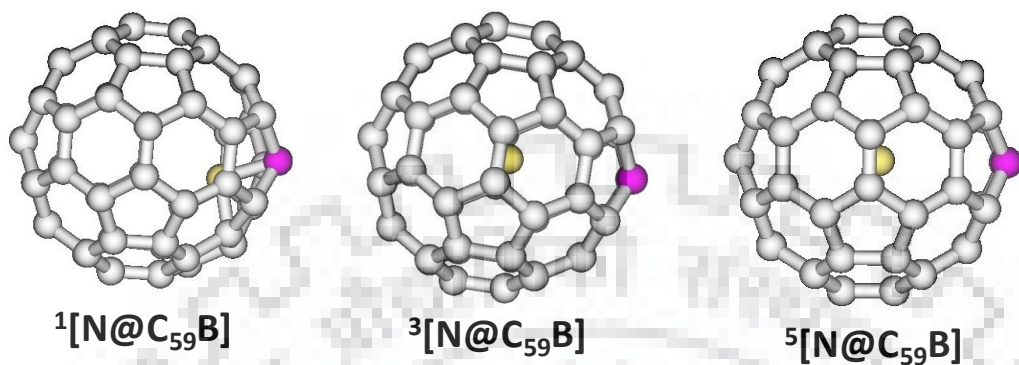


Figure 5.1. The optimized geometries of N@C₅₉B in its various spin states.

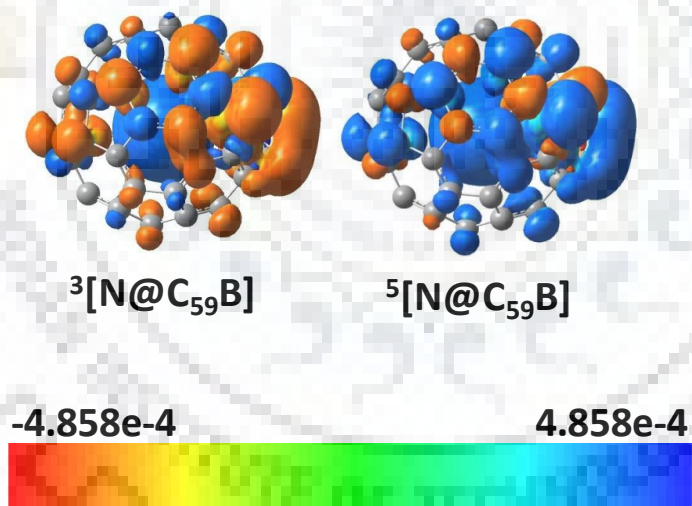


Figure 5.2. The spin density distribution plot of triplet and quintet states of N@C₅₉B with an isodensity value of 0.0004.

Table 5.1. The stabilization energy and various properties of C₅₉B and its nitrogen encapsulated complex. The value of stabilization energy with BSSE corrections are given in parenthesis.

System	Multiplicity	Stabilization energy(kcal/mol)		
N@C ₅₉ B	1	-7.11 (-3.08)		
	3	-9.96 (-7.77)		
	5	-10.02 (-7.83)		
		Spin density (e/au ³)	Spin polarization parameter (ζ)	
C ₅₉ B	2	B _{cage} =0.14	1.00	
N@C ₅₉ B	3	N _{encap} =2.97		
		B _{cage} =-0.15	0.50	
	5	N _{encap} =2.97 B _{cage} =0.14	1.00	
		VEA (eV)	VIE (eV)	$\Delta E_{\text{HOMO-LUMO}}$ (eV)
C ₅₉ B	2	-3.59	7.23	$\alpha=2.40$ $\beta=1.54$
	1	-2.46	7.29	2.44
	3	-3.59	7.51	$\alpha=1.54$ $\beta=2.34$
N@C ₅₉ B	5	-3.59	7.23	$\alpha=2.41$ $\beta=1.54$
		ΔG (kcal/mol)	ΔH (kcal/mol)	
N@C ₅₉ B	1	4.81	-5.91	
	3	-2.87	-9.45	
	5	-3.20	-9.50	

Table 5.2 Relative energies (kcal/mol) of cis and trans form of (C₅₉N)₂, (C₅₉B)₂ and (C₅₉B-C₅₉N).

System	Trans	Cis
(C ₅₉ N) ₂	0.00	8.45
(C ₅₉ B) ₂	0.00	6.30
C ₅₉ B-C ₅₉ N	0.00	0.17

5.3 Results and discussion

5.3.1 Structure and stability of the complexes

The calculated stabilization energies for all possible spin states of the dimers of various endohedral heterofullerenes are listed in table 5.3. The optimized geometries of the stable states of the above complexes are shown in figure 5.3. The complex (B@C₅₉B)₂ is found to be stable in its singlet state with a stabilization energy of -62.35 kcal/mol. The triplet state of the above complex is also stable, although the stabilization energy of the latter is decreased by ~37.5 kcal/mol. For the singlet state, the encapsulated boron atoms are close to the cage, whereas they are near to the centre of the cage for the triplet state. Unlike singlet and triplet states of (B@C₅₉B)₂, the complexes ¹[(B@C₅₉N)₂] and ³[(B@C₅₉N)₂] were found to be isoenergetic with the stabilization energy of -24.23 kcal/mol and the guest species are located close to the centre of the cage. The stabilization energy of triplet and quintet states of B@C₅₉N-N@C₅₉B is -22.20 and -22.22 kcal/mol, respectively, which indicated that they are nearly isoenergetic. The guest atoms reside at the centre of respective cages in the triplet and quintet states of B@C₅₉N-N@C₅₉B. The stabilization energy of the singlet state of the above complex is -6.15 kcal/mol, which is ~16.0 kcal/mol less than its triplet and quintet states. The complex (N@C₅₉B)₂ is stable in its septet state, for which the guest species are located at the centre of the host cages, although the complex (N@C₅₉N)₂ was stable in both the singlet and septet state as discussed in chapter 3. In the complex (B@C₆₀)₂, the guest atoms occupy at the centre of C₆₀ cage similar to (N@C₆₀)₂ reported in chapter 3. The singlet and triplet states of the complex (B@C₆₀)₂ are isoenergetic with the stabilization energy of -24.75 kcal/mol.

Table 5.3. Stabilization energies (ΔE_{stab}) of various endohedral heterofullerenes for their different spin states obtained at B3LYP-GD2/6-311G* level. The basis set superposition error (BSSE) corrected values of stabilization energies are given in parenthesis.

Complexes	Multiplicity	ΔE_{stab} (kcal/mol)
(B@C ₅₉ B) ₂	1	-62.35
	3	-24.89 (-20.92)
	5	14.76
(B@C ₅₉ N) ₂	1	-24.23
	3	-24.23 (-20.33)
	5	10.17
N@C ₅₉ B-B@C ₅₉ N	1	-6.15
	3	-22.20 (-18.19)
	5	-22.22 (-18.18)
	7	14.46
(N@C ₅₉ B) ₂	1	2.54
	3	29.76
	5	17.74
	7	-20.05 (-15.70)
	9	18.68
(B@C ₆₀) ₂	1	-24.75
	3	-24.75 (-20.43)
	5	14.69

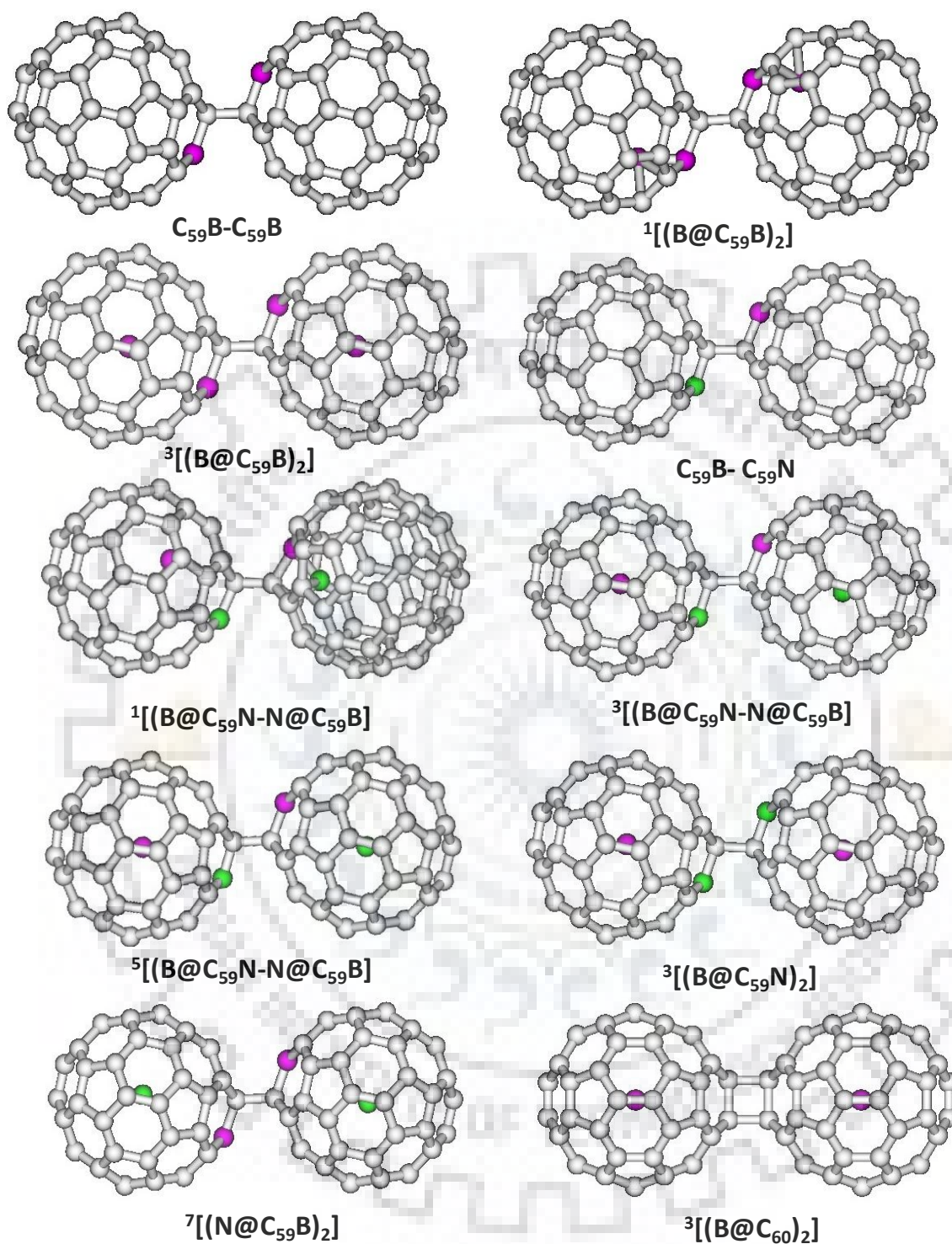


Figure 5.3. Optimized geometries of various stable spin states of different endohedral heterofullerenes. The grey, violet and green colored spheres represent carbon, boron and nitrogen atoms, respectively. The multiplicity of the complexes is given in superscript.

5.3.2 Spin polarization and transfer of spin density

The values of spin density of the heteroatoms present in various complexes are given in table 5.4. The calculated values of spin polarization parameter (ζ) for the stable states of complexes are also provided in the table. The plots of spin density distribution for various complexes are shown in figure 5.4. For $^1[(B@C_{59}B)_2]$, the values of spin density on the encapsulated boron atoms are -0.68 and 0.68 e/au³, respectively, which indicate that the spin density is shifted from the guest atom to the respective host cage, followed by antiferromagnetic spin coupling between two monomer units. In $^3[(B@C_{59}B)_2]$, such a shift in spin density is not observed, rather the spins of the encapsulated boron atoms are ferromagnetically coupled. Depending upon the spin states of $(B@C_{59}N)_2$, the interaction between unpaired electrons of the encapsulated boron atoms and their respective host cage is either antiferromagnetic or ferromagnetic without any shift of spin density between them. As discussed in chapter 3, the spin density transfer between guest and host species was not observed for the analogous $(N@C_{59}N)_2$ or $(N@C_{60})_2$. In triplet state of the heterodimer $B@C_{59}N-N@C_{59}B$, the value of spin density on encapsulated boron and nitrogen atoms are -1.00 and 2.97 e/au³ suggesting the encapsulated atoms are antiferromagnetically coupled, whereas in its quintet state, the coupling is ferromagnetic without spin density transfer. The values of spin density on trapped boron and nitrogen are 1.00 and 2.97 e/au³. In contrast to $^3[B@C_{59}N-N@C_{59}B]$ and $^5[B@C_{59}N-N@C_{59}B]$, the spin density is shifted from trapped nitrogen to its host cage in singlet state. Similarly, a shift of spin density is observed from the encapsulated boron to its host cage followed by antiferromagnetic coupling between two monomer units. The spin of guest nitrogen atoms in $^7[(N@C_{59}B)_2]$ interact ferromagnetically without spin density transfer between guest and host. In $(B@C_{60})_2$, the spin of each boron atom interacts anti-ferromagnetically and ferromagnetically in its singlet and triplet states, respectively, without spin transfer as reflected from the values of spin density.

Table 5.4. The spin density of various heteroatoms and the spin polarization parameter (ζ) for the stable endohedral complexes

Complexes	Multiplicity	Spin Density ($e/a.u.^3$)	Spin Polarization Parameter (ζ)
$(B@C_{59}B)_2$	1	$(B_{encap})_1=-0.68, (B_{encap})_2=0.68$ $(B_{cage})_1=-0.09, (B_{cage})_2=0.09$	0.00
	3	$(B_{encap})_1=(B_{encap})_2=0.95$ $(B_{cage})_1=(B_{cage})_2=0.04$	1.00
$(B@C_{59}N)_2$	1	$(B_{encap})_1=1.00, (B_{encap})_2=-1.00$ $(N_{cage})_1=(N_{cage})_2=0.00$	0.00
	3	$(B_{encap})_1=(B_{encap})_2=1.00$ $(N_{cage})_1=(N_{cage})_2=0.00$	1.00
$N@C_{59}B-B@C_{59}N$	1	$(N_{encap})=-0.13, (B_{encap})=0.0$ $(N_{cage})=(B_{cage})=0.00$	0.00
	3	$(N_{encap})=2.97, (B_{encap})=-1.00$ $(N_{cage})=(B_{cage})=0.00$	0.50
	5	$(N_{encap})=2.97, (B_{encap})=1.00$ $(N_{cage})=(B_{cage})=0.00$	1.00
$(N@C_{59}B)_2$	7	$(N_{encap})_1=(N_{encap})_2=2.97$ $(B_{cage})_1=(B_{cage})_2=0.00$	1.00
$(B@C_{60})_2$	1	$(B_{encap})_1=1.00, (B_{encap})_2=-1.00$	0.00
	3	$(B_{encap})_1=(B_{encap})_2=1.00$	1.00

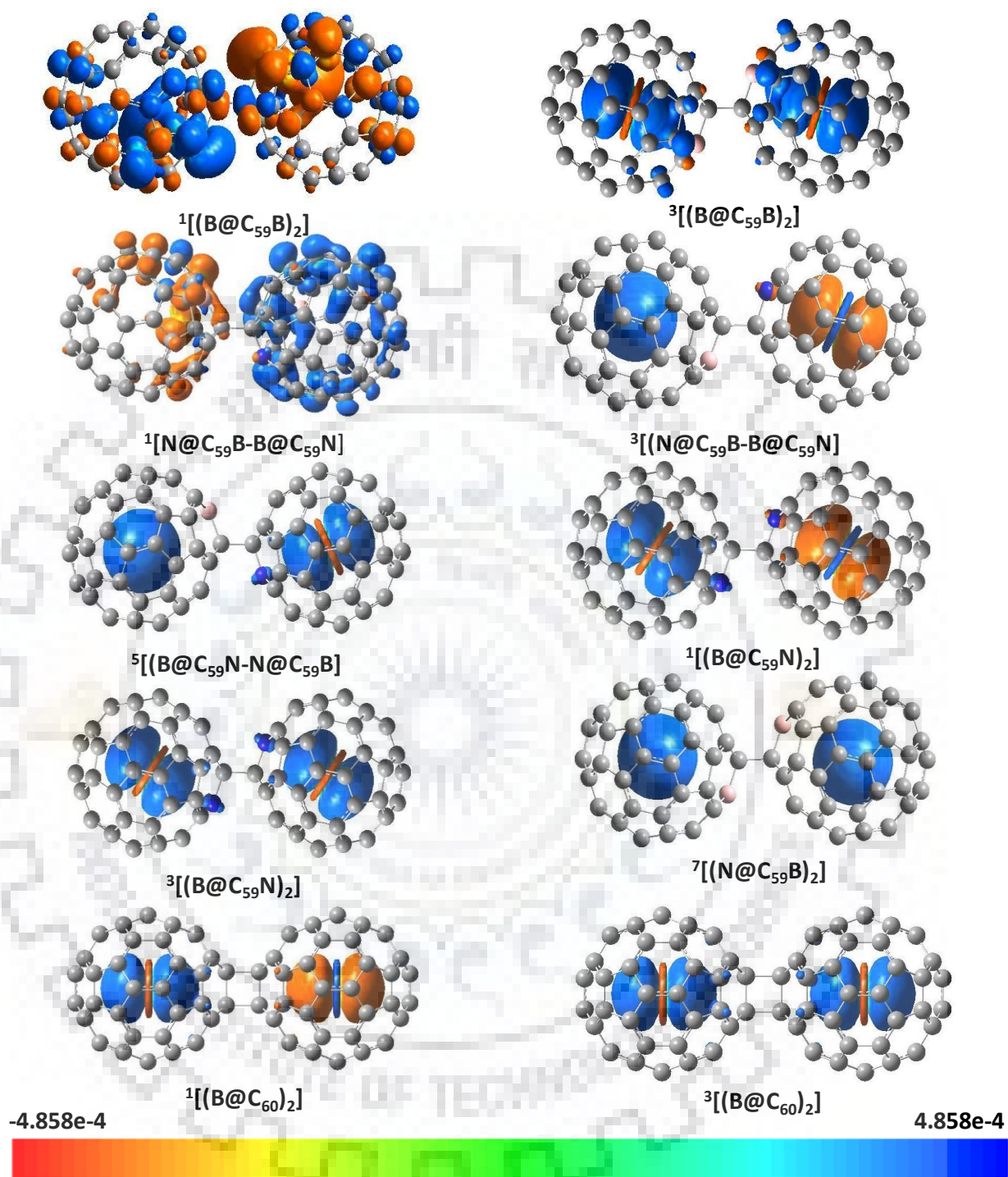
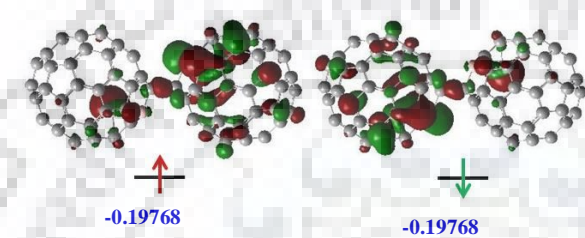
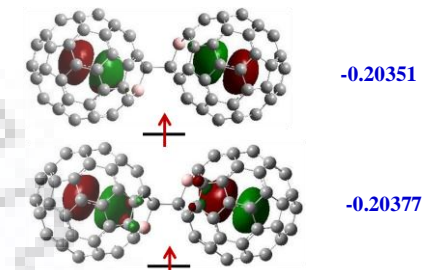
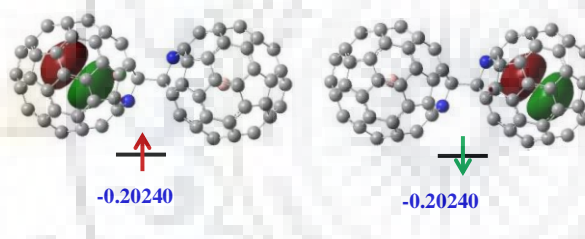
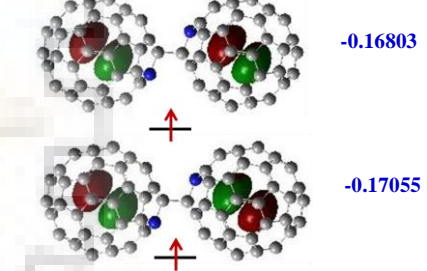
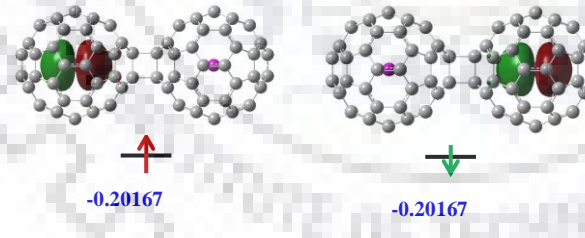
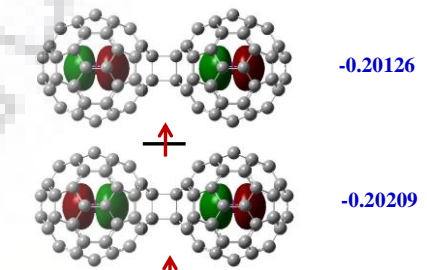


Figure 5.4. Spin density difference plots for various endohedral heterofullerenes in their stable spin states for an isodensity value of 0.0004. The blue color represents an excess of α -spin density, and the orange color represents an excess of β -spin density. The multiplicity of the complexes is given in superscript.

To know more about the spin polarization and spin density transfer, the spin polarization parameter was calculated as mentioned in chapter 2 and the results are listed in table 5.4. The relevant molecular orbitals of these species are depicted in table 5.5. The highest occupied molecular orbitals (degenerate α - and β -spin orbitals) of $^1[(B@C_{59}B)_2]$ suggest that the electron density is distributed on guest as well as on host species. In addition, the spin density values given in table 5.4 clearly indicate the transfer of spin density from guest to host in $^1[(B@C_{59}B)_2]$. Moreover, the zero value of the spin polarization parameter and the degeneracy of the α - and β -spin orbitals of $^1[(B@C_{59}B)_2]$ confirm the spin degeneracy of the complex. In contrast to the singlet state, the unpaired electrons are localized only on guest boron in its triplet state, leading to ferromagnetic coupling. The spin polarization parameter of 1.00 for $^3[(B@C_{59}B)_2]$ suggests that the complex is fully spin polarized. The complexes $^1[(B@C_{59}N)_2]$ and $^3[(B@C_{59}N)_2]$ are spin degenerate and fully spin polarized as reflected from the corresponding values of spin polarization parameter (0.00 and 1.00). Further, the respective molecular orbitals of $^1[(B@C_{59}N)_2]$ and $^3[(B@C_{59}N)_2]$ suggest the antiferromagnetic and ferromagnetic spin coupling between guest atoms of the complexes, respectively.

The spin density transfer from guest to host followed by the antiferromagnetic coupling between two units occurs in $^1[B@C_{59}N-N@C_{59}B]$. The zero value of spin polarization parameter (table 5.4) for the complex also indicates that the complex is spin degenerated. In contrast to singlet state of $B@C_{59}N-N@C_{59}B$, for the triplet and quintet states, the unpaired electrons are localized only on guest atoms leading to their antiferromagnetic and ferromagnetic coupling for these states (table 5.5). Further, as reflected from the values of spin polarization parameter listed in table 5.4, the complex $B@C_{59}N-N@C_{59}B$ in its triplet state ($\zeta = 0.50$) is partially spin polarized, whereas the quintet state ($\zeta = 1.00$) is fully spin polarized. The spin polarization parameter value of 1.00 and relevant molecular orbitals of $^7[(N@C_{59}B)_2]$ reveal that the complex is fully spin polarized along with the ferromagnetic coupling between encapsulated nitrogen atoms. The spin degeneracy of the singlet state of $(B@C_{60})_2$ and the fully spin polarized nature of its triplet state are evident from the values of table 5.4 and 5.5.

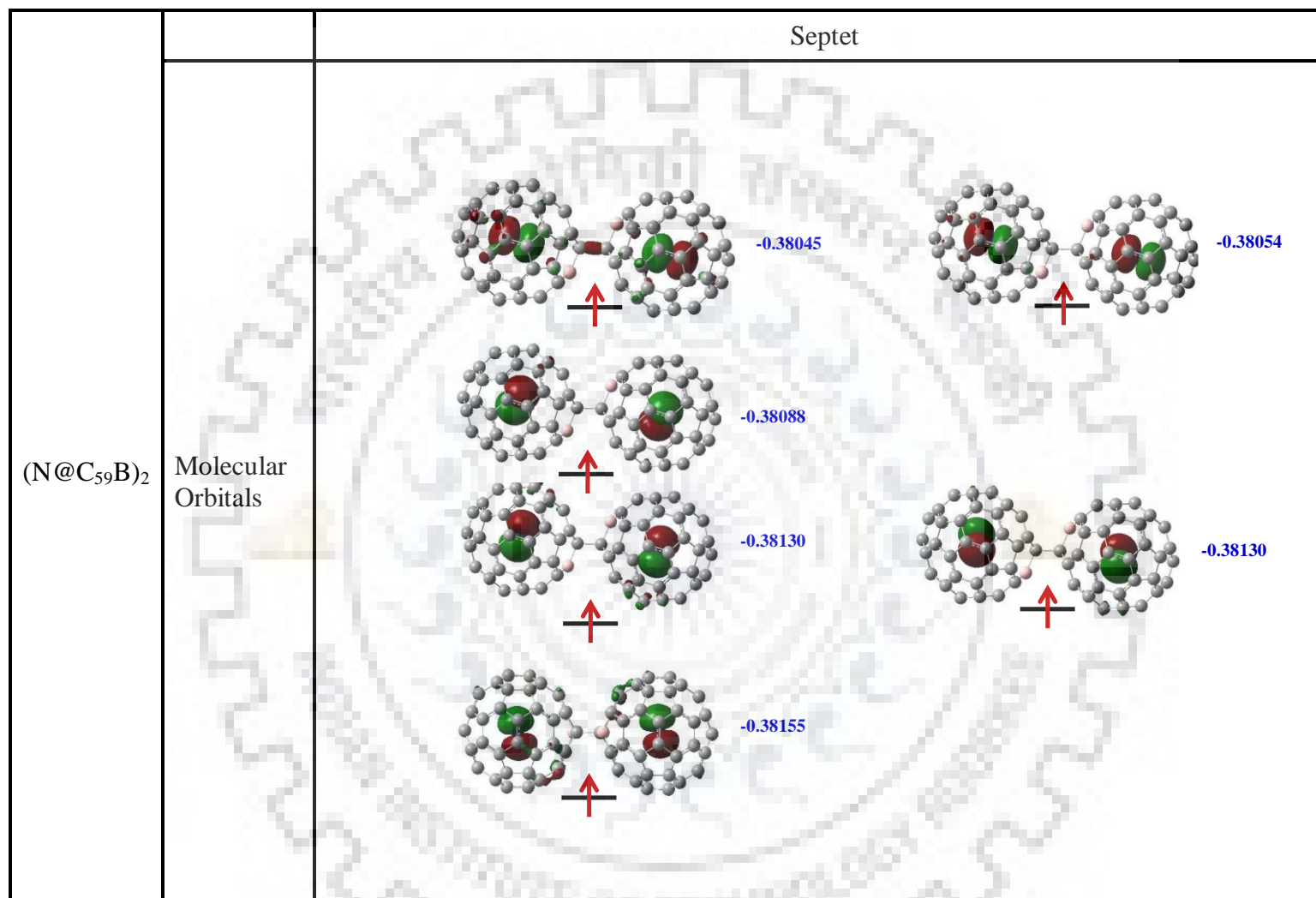
Table 5.5. The relevant molecular orbitals showing the spin density distribution for an isodensity value of 0.02 of stable spin states of various endohedral heterofullerenes. The energies of molecular orbitals are given in Hartree.

		Singlet	Triplet
$(B@C_{59}B)_2$	Molecular Orbital	 -0.19768 -0.19768	 -0.20351 -0.20377
$(B@C_{59}N)_2$	Molecular Orbital	 -0.20240 -0.20240	 -0.16803 -0.17055
$(B@C_{60})_2$	Molecular Orbital	 -0.20167 -0.20167	 -0.20126 -0.20209

(...continued)

		Singlet	Triplet	Quintet
B@C ₅₉ N- N@C ₅₉ B	Molecular Orbital	<p>-0.18693 -0.19905</p>	<p>-0.38157 -0.38181 -0.38213</p>	<p>-0.20247 -0.38112 -0.38161 -0.38196</p>

(...continued)



5.3.3 Thermodynamic feasibility of the formation of the complexes

To investigate the thermodynamic feasibility of the formation of the complexes, the values of ΔG and ΔH were computed and are listed in table 5.6. For the complex $(B@C_{59}B)_2$, the values of ΔG and ΔH suggest that the encapsulation of boron atoms inside $(C_{59}B)_2$ is feasible leading to the formation of a stable complex. However, the formation of $(B@C_{59}B)_2$ is more feasible *via* dimerization of $B@C_{59}B$ as reflected from the respective ΔG and ΔH values. On the other hand, the encapsulation of boron atoms inside $(C_{59}N)_2$ is not a thermodynamically feasible process, although formation of the complex $(B@C_{59}N)_2$ is feasible *via* dimerization of $B@C_{59}N$. From table 5.6, it can also be inferred that formation of the heterodimer $B@C_{59}N-N@C_{59}B$ is thermodynamically feasible. The dimer $(N@C_{59}B)_2$ can be obtained either by dimerization of $N@C_{59}B$ or by encapsulating nitrogen atoms inside $(C_{59}B)_2$. The above holds true for the formation of $(B@C_{60})_2$.

5.3.4 Electronic properties

5.3.4.1 Electron affinity and ionization energy

To get more insight on the properties of the above endohedral heterofullerenes, vertical electron affinity (VEA), vertical ionization energy (VIE) and dipole moment (μ) were calculated for various complexes in their distinct stable states and are given in table 5.7. The value of VEA for $^1[(B@C_{59}B)_2]$ is -3.18 eV which is 0.25 eV more than that of $(C_{59}B)_2$. However, VIE of the complexes is less by 0.92 eV compared to $(C_{59}B)_2$. The higher VEA and lower VIE values of $^1[(B@C_{59}B)_2]$ compared to the respective host cage is due to the encapsulation of electron deficient boron atoms close to the surface of the cage, resulting strong interactions with the cage. The VEA of $^3[(B@C_{59}B)_2]$ is the same as that of its free host cage. The VIE of the above complex is decreased by 0.22 eV when the encapsulated boron atoms occupy at the centre of the respective host cages. There is no significant change in VEA and VIE of $^3[(B@C_{59}N)_2]$ due to relatively weak interactions between its components. For the triplet and quintet states of the heterodimer $B@C_{59}N-N@C_{59}B$, the electron affinity and ionization energies remain nearly the same as those of the host cage $C_{59}N-C_{59}B$. On encapsulating nitrogen atoms, the electronic properties VEA and VIE of $(C_{59}B)_2$ were not affected, probably due to the weak interactions between the component species. Similar to $(C_{59}B)_2$, the electronic properties of $(C_{60})_2$ were not changed due to the encapsulation of boron atoms in adjacent cages.

The systems $(C_{59}B)_2$, $(C_{59}N)_2$ and their encapsulated complexes have no dipole moment due to the presence of an inversion centre. The dipole moment of the heterofullerene $C_{59}N-C_{59}B$ is 0.66 Debye. For triplet and quintet states of $B@C_{59}N-N@C_{59}B$, the dipole moment is found to be unaltered on encapsulating boron and nitrogen atoms in $C_{59}N$ and $C_{59}B$ cages, respectively, as guest atoms remained at the centre of the respective cages. On the other hand, a large dipole moment (16.62 Debye) for ${}^1[B@C_{59}N-N@C_{59}B]$ arises due to the rotation of dihedral angle ϕ_{NCCB} by $\sim 20^\circ$ indicating the polarity of the system and hence its possible separation.

5.3.4.2 Energy gap between HOMO and LUMO

To investigate more about the electronic properties, the calculated energy gap between HOMO and LUMO ($\Delta E_{\text{HOMO-LUMO}}$) of various species considered is listed in table 5.7. The energy gap between HOMO and LUMO of $(C_{59}B)_2$ is 2.43 eV. For ${}^1[(B@C_{59}B)_2]$, $\Delta E_{\text{HOMO-LUMO}}$ was decreased by 1.07 eV compared to that of $(C_{59}B)_2$, although it is decreased only by 0.71 eV for the triplet state of the complex. Similarly, the value of $\Delta E_{\text{HOMO-LUMO}}$ for ${}^3[(B@C_{59}N)_2]$ is 1.75 eV which is 0.45 eV less than that of its host cage $(C_{59}N)_2$. On encapsulating guest atoms inside $C_{59}N-C_{59}B$, the values of $\Delta E_{\text{HOMO-LUMO}}$ of singlet and quintet states of the resultant complex $(B@C_{59}N-N@C_{59}B)$ are reduced by 1.74 and 0.47 eV, respectively, whereas it is unchanged for the triplet state of the complex. The energy gap between HOMO and LUMO of $(C_{59}B)_2$ is unaffected due to the encapsulation of nitrogen atoms inside. The calculated value of $\Delta E_{\text{HOMO-LUMO}}$ of ${}^3[(B@C_{60})_2]$ is 1.73 eV that indicates that $\Delta E_{\text{HOMO-LUMO}}$ of $(C_{60})_2$ is decreased by 0.74 eV due to the encapsulation of boron. Thus, it can be concluded that the energy gap between HOMO and LUMO of complexes depends on their various spin states. The boron atom encapsulation inside various fullerenes derivatives changed $\Delta E_{\text{HOMO-LUMO}}$, although it was unaffected by encapsulating nitrogen atoms in consistent with the results of the complexes studied in chapters 3 and 4.

Table 5.6. The change in Gibbs free energy (ΔG) and change in enthalpy (ΔH) for the formation of the complexes by encapsulating guest atoms in the host cage of the heterofullerene dimer as well as by the dimerization of their respective monomers.

Complexes	Multiplicity	ΔG (kcal/mol)		ΔH (kcal/mol)	
		$\Delta G_{\text{encapsulation}}$	$\Delta G_{\text{dimerization}}$	$\Delta H_{\text{encapsulation}}$	$\Delta H_{\text{dimerization}}$
$(B@C_{59}B)_2$	1	-33.61	-53.23	-47.94	-70.81
	3	-10.05	-29.67	-24.24	-47.11
$(B@C_{59}N)_2$	3	14.56	-5.37	1.74	-20.63
$N@C_{59}B-B@C_{59}N$	1	12.87	-9.77	-5.89	-30.22
	3	-6.67	-29.30	-21.00	-45.32
	5	-8.98	-31.61	-21.40	-45.72
$(N@C_{59}B)_2$	7	-7.18	-29.11	-19.21	-45.34
$(B@C_{60})_2$	3	-8.87	4.67	-23.55	-13.42

Table 5.7. The values of vertical electron affinity (VEA), vertical ionization energy (VIE), energy gap between HOMO and LUMO ($\Delta E_{\text{HOMO-LUMO}}$) and dipole moment (μ) for various heterofullerenes and their complexes.

Systems	Multiplicity	VEA (eV)	VIE (eV)	$\Delta E_{\text{HOMO-LUMO}}$ (eV)	Dipole Moment (Debye)
(C ₅₉ B) ₂	1	-2.93	7.11	2.43	0.0
	1	-3.18	6.19	1.36	0.0
(B@C ₅₉ B) ₂	3	-2.94	6.89	$\alpha=1.72$ $\beta=2.43$	0.0
(C ₅₉ N) ₂	1	-2.83	6.80	2.20	0.0
(B@C ₅₉ N) ₂	3	-2.77	6.88	$\alpha=1.75$ $\beta=2.19$	0.0
C ₅₉ B-C ₅₉ N	1	-2.94	6.93	2.16	0.66
	1	-3.76	5.97	$\alpha=0.42$ $\beta=0.90$	16.62
N@C ₅₉ B-	3	-2.95	6.93	$\alpha=2.16$ $\beta=1.66$	0.67
B@C ₅₉ N	5	-2.95	6.89	$\alpha=1.69$ $\beta=2.13$	0.59
(N@C ₅₉ B) ₂	7	-2.93	7.11	$\alpha=2.43$ $\beta=2.37$	0.0
(C ₆₀) ₂	1	-2.84	7.07	2.47	0.0
(B@C ₆₀) ₂	3	-2.80	7.00	$\alpha=1.73$ $\beta=2.45$	0.0

5.4 Conclusions

In the present chapter, the dispersion corrected density functional method (B3LYP-GD2/6-311G*) was applied on endohedral heterofullerenes $(B@C_{59}B)_2$, $(B@C_{59}N)_2$, $(B@C_{59}N-N@C_{59}B)$ and $(N@C_{59}B)_2$ to investigate their structure, stability and various properties. The study was initiated with the investigation of $N@C_{59}B$ which was found to be stable in its various spin states. In $^3[N@C_{59}B]$ and $^5[N@C_{59}B]$, the core and shell are coupled antiferromagnetically and ferromagnetically, respectively. The complex is partially spin polarized in triplet state whereas it is fully spin polarized in quintet state. The encapsulation of nitrogen atom in $C_{59}B$ was thermodynamically feasible.

The investigations on the homo and heterodimers of $B@C_{59}N$ and $N@C_{59}B$ showed that the complexes are stable in their various spin states. In $^1[(B@C_{59}B)_2]$ and $^1[(B@C_{59}N-N@C_{59}B)]$, the guest atoms are positioned near to the inner surface of the host cages, while for their high spin states the guest atoms are positioned near to the centre of the cages. For $^1[(B@C_{59}N)_2]$, $^3[(B@C_{59}N)_2]$, $^7[(N@C_{59}B)_2]$, $^1[(B@C_{60})_2]$ and $^3[(B@C_{60})_2]$, the encapsulated atoms occupy at the centre of the cages. The spin-spin coupling and transfer of spin density between the component species of various complexes were analyzed. Interestingly, for $^1[(B@C_{59}B)_2]$ and $^1[(B@C_{59}N-N@C_{59}B)]$, the spin density was found to shifted from guest to host. Based on the spin states of the complexes, spins of two monomer units of complexes interacted either anti-ferromagnetically or ferromagnetically without spin density transfer between the components. The study showed that the complexes with their higher spin states are fully spin polarized, although they are either partially spin polarized or spin degenerate for lower spin states.

To determine the feasibility of formation of various complexes, the thermodynamic parameters ΔG and ΔH *via* encapsulation of guest species inside host dimers as well as *via* dimerization of endohedral heterofullerenes were calculated. The values of thermodynamic parameters for the complexes indicated that the formation of a dimer of endohedral heterofullerenes is thermodynamically feasible either of the ways as mentioned above. To determine the effect of encapsulation of guest atoms on the properties of various heterofullerenes, the values of VEA, VIE, $\Delta E_{\text{HOMO-LUMO}}$ and μ were calculated and it was found that the properties can be tuned by encapsulating suitable guest atoms inside heterofullerenes. The study showed that the energy gap between HOMO and LUMO depends on the spin states of the complexes. Moreover, on encapsulating boron atoms inside various dimers of fullerene derivatives, the value of $\Delta E_{\text{HOMO-LUMO}}$ is significantly decreased. However, the nitrogen atom encapsulation inside $(C_{59}B)_2$ does not alter its $\Delta E_{\text{HOMO-LUMO}}$. The high dipole moment of $B@C_{59}N-N@C_{59}B$ indicated the polarity of the complex and hence its separation.

Chapter-6

Structure, stability and properties of the nitrogen encapsulated carbon and boron nitride nanotubes

6.1 Introduction

As was mentioned in chapter 1, the nanotubes can accommodate various molecules and clusters inside the cavity. Earlier, studies on endohedral complexes of carbon nanotubes showed that such complexes attain stability due to the dispersion interaction between the guest and the host. The properties of carbon nanotubes are reported to be altered because of the encapsulation of guest species. In chapter 3, the spin-spin coupling and spin polarization for the nitrogen encapsulated C_{60} , $C_{59}N$ and their respective dimers were investigated. The study revealed that the spins of respective guest nitrogen atoms of $(N@C_{60})_2$ and $(N@C_{59}N)_2$ are either antiferromagnetically or ferromagnetically coupled based on the spin state of the complexes. The results also suggested that the higher spin states of the complexes are spin polarized whereas the complexes of lower spin states are spin degenerated. Therefore, it is interesting to know how the spins of encapsulated nitrogen atoms interact with each other when they are confined in adjacent nanotubes. Although several studies have been done on endohedral complexes of carbon nanotubes [179-200], the encapsulation of paramagnetic nitrogen atoms inside carbon nanotube, boron nitride nanotube and their respective dimers as well as the subsequent interactions between host-guest and guest-guest are not yet reported.

In the present chapter, the structure, stability and properties of nitrogen atom encapsulated carbon nanotube, boron nanotube and their respective dimers are investigated. The spin-spin coupling between the guest and the host and that between guest species are examined. To investigate the spin polarization and spin degeneracy of the stable states of the complexes, spin polarization parameter is calculated and the relevant molecular orbitals to the spin density are analyzed. The effect of encapsulated nitrogen atoms on the electronic properties of the carbon and boron nitride nanotubes is examined. For this purpose, the vertical electron affinity (VEA), vertical ionization energy (VIE) and energy gap between HOMO and LUMO ($\Delta E_{\text{HOMO-LUMO}}$) are determined for all the species mentioned above. The effect of confinement by both types of nanotubes on the hyperfine coupling constant of nitrogen is examined. The role of cavity size of the nanotube on the spin-spin coupling between the components of the complexes is studied using (6,6)- and (5,5)-carbon nanotubes as the host cages.

6.2 Computational methods

The calculations were performed using the computational chemistry package Gaussian 09 [261]. The hybrid functional B3LYP with dispersion correction (B3LYP-GD2) in conjunction with 6-311G** was used [224, 240]. The functional chosen have already found suitable to describe spin-spin coupling in similar complexes discussed in previous chapters. The terminals of the carbon nanotubes and boron nitride nanotubes (BNNT) used in the present study were passivated by hydrogen atoms. The calculated values of energy gap between HOMO and LUMO of (6,6)- and (5,5)-carbon nanotubes are 2.30 and 2.16 eV, respectively, which are in agreement with those values reported earlier at B3LYP/6-31G* level [265].

Similar to previous chapters, various possible spin states of the complexes are considered. The stability of wave function of the systems having unpaired electrons was verified. The energy of the antiferromagnetic singlet was calculated using broken symmetry approach as was discussed in chapter 2.

The stabilization energy of nitrogen atom encapsulated complexes of CNT, BNNT and their respective dimers were calculated using the supermolecule approach as in equation 3.1. To study the spin-spin coupling in the above complexes, spin density values of the encapsulated nitrogen atoms were determined. The program GaussView5 was used to plot the spin density difference and molecular orbitals of the systems [263]. The spin polarization parameter was determined as discussed in chapter 2. The values of vertical ionization energy (VIE) and vertical electron affinity (VEA) for the species considered are calculated using the respective energies of their neutral, cationic, and anionic analogues as was done for the fullerene complexes in chapters 3-5.

6.3 Results and discussion

6.3.1 Structure and stability of the complexes

The optimized geometries of free as well as nitrogen atom encapsulated (6,6)-carbon nanotube (CNT), (6,6)-boron nitride nanotube (BNNT) and their respective dimers are shown in figure 6.1. As indicated in the figure, the diameter and length of CNT are 8.16 Å and 9.21 Å, respectively. The size of BNNT is approximately the same as that of CNT with diameter 8.44 Å and length 9.18 Å. The distance between CNTs in (CNT)₂ is 3.22 Å. For (BNNT)₂, the above distance is 2.88 Å. The energy of dimerization for (CNT)₂ is -14.66 kcal/mol and that for (BNNT)₂ is -33.95 kcal/mol.

The stabilization energies associated with the encapsulation of atomic nitrogen in various host cavities are listed in table 6.1. The stabilization energy of the complex ${}^4[\text{N}@\text{CNT}]$ is -3.02 kcal/mol. This is much lower than that of -9.69 kcal/mol obtained for ${}^4[\text{N}@\text{C}_{60}]$ and is expected because of the weaker interactions between guest and host in ${}^4[\text{N}@\text{CNT}]$ due to the relatively large cavity size of CNT (by 1.07 Å). The stabilization energy of -4.09 kcal/mol for ${}^4[\text{N}@\text{BNNT}]$ arises from the weak van der Waals interaction between the component units. In ${}^4[\text{N}@\text{CNT}]$ and ${}^4[\text{N}@\text{BNNT}]$, the guest atoms are located at the centre of the respective host cages. The complexes $(\text{N}@\text{CNT})_2$ is found to be stable in its septet state with the stabilization energy of -12.95 kcal/mol which is significantly less than that of ${}^7[(\text{N}@\text{C}_{60})_2]$ (-20.75 kcal/mol) due to large cavity of nanotube. In contrast to ${}^4[\text{N}@\text{CNT}]$, each of the guest atoms are shifted towards the surface of CNT by ~ 0.76 Å in ${}^7[(\text{N}@\text{CNT})_2]$, thereby decreasing the distance between nitrogen atoms of adjacent CNTs. Moreover, the distance between the nanotubes is decreased by 0.15 Å on encapsulating nitrogen atoms inside. The broken symmetry calculation of $(\text{N}@\text{CNT})_2$ suggested that the singlet state of the complex is isoenergetic to its septet state. Similar to $(\text{N}@\text{CNT})_2$, the complex $(\text{N}@\text{BNNT})_2$ is also stable in its septet state with the stabilization energy of -10.58 kcal/mol. In ${}^7[(\text{N}@\text{BNNT})_2]$, the guest nitrogen atoms are shifted from the centre of the host cage by 1 Å in contrast to its monomer units. However, the separation between the nanotubes remained the same in $(\text{N}@\text{BNNT})_2$ as was in its free dimer. The broken symmetry calculations revealed that the singlet state of the complex $(\text{N}@\text{BNNT})_2$ is isoenergetic to its septet state.

As evident from the above analysis, the encapsulation energy of ${}^7[(\text{N}@\text{CNT})_2]$ and ${}^7[(\text{N}@\text{BNNT})_2]$ is more than twice as that of their respective monomer units. In order to know the factors responsible for the additional stability of the above complexes, the stabilization energies of related complexes were calculated and are listed in table 6.2. The stabilization energy of ${}^4[\text{N}@(\text{CNT})_2]$ in which nitrogen atom is shifted towards the inner surface of CNT is -4.47 kcal/mol. The stabilization energy of ${}^4[\text{N}@(\text{CNT})_2]$ in which nitrogen atom is at the center of one of the CNTs is -3.35 kcal/mol. This difference in the energy of -1.12 kcal/mol is due to the shift of guest atom from the center towards the surface of CNT.

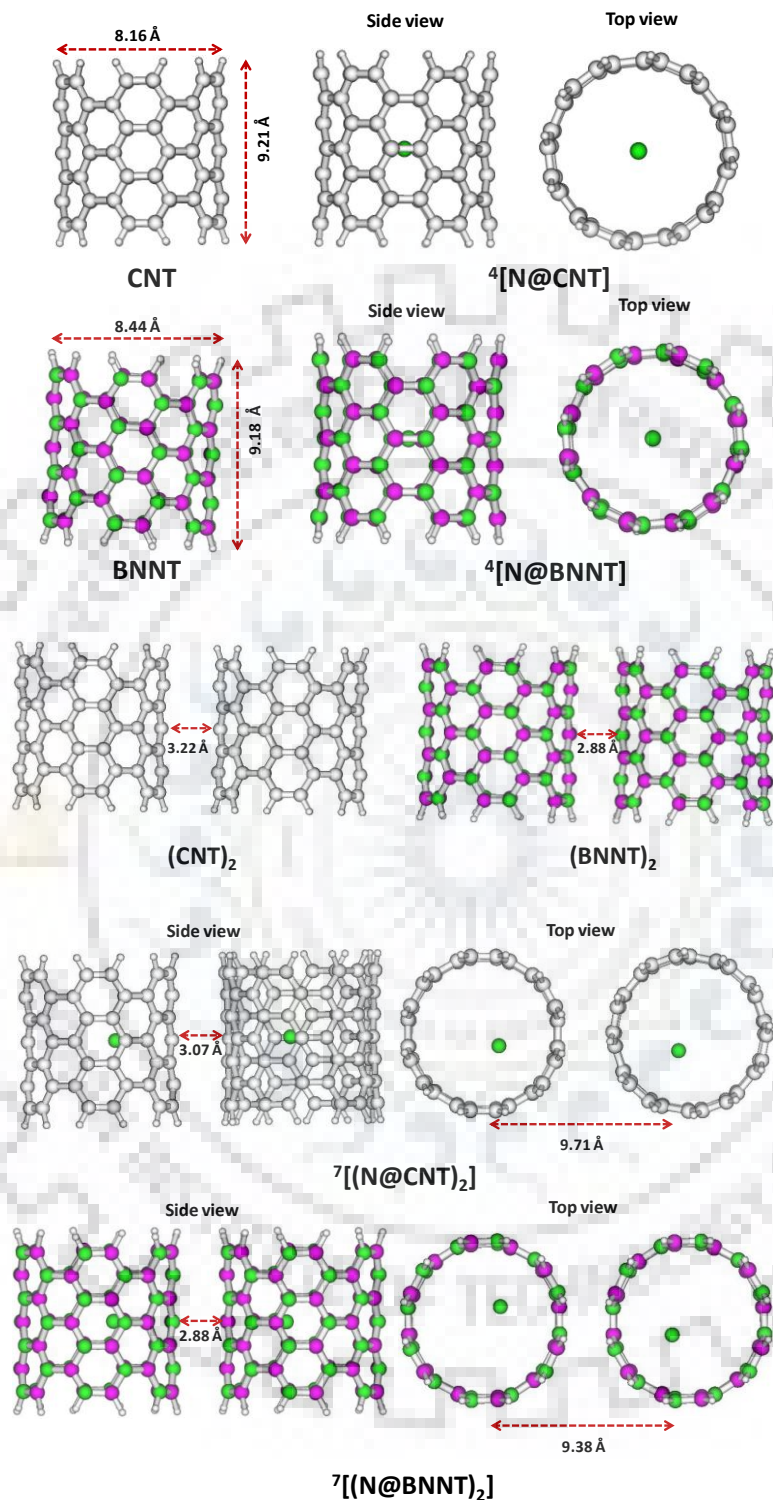


Figure 6.1. Optimized geometries of CNT, BNNT, (CNT)₂, (BNNT)₂ and their respective nitrogen atom encapsulated complexes. The grey, violet and green colored spheres represent carbon, boron and nitrogen atoms, respectively. The multiplicity for each of the complexes is given in superscript.

Table 6.1. The stabilization energies of the nitrogen atom encapsulated complexes of nanotubes in their different spin states at B3LYP-GD2/6-311G** level. The values of BSSE corrected stabilization energies are given in parenthesis for the stable states of the complexes.

Complexes	Multiplicity	Stabilization Energy (kcal/mol)
N@CNT	4	-3.02(-2.21)
	1	-12.95
	3	---a
(N@CNT) ₂	5	25.52
	7	-12.95(-9.01)
	9	20.60
	4	-4.09(-2.74)
N@BNNT	1	-10.58
	3	39.09
	5	17.43
(N@BNNT) ₂	7	-10.58(-5.34)
	9	107.65

a-Convergence error

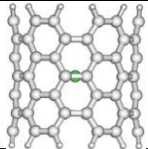
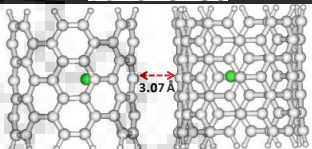
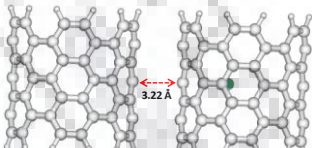
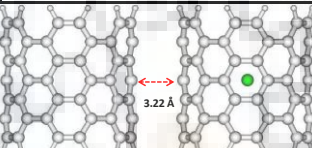
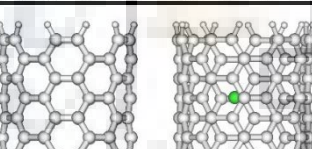
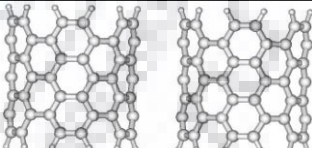
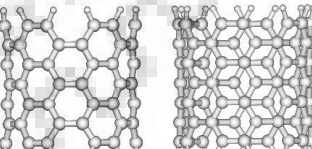
In the optimized geometry of ${}^7[(\text{N@CNT})_2]$, one of the CNTs is rotated along their tube axis similar to benzene dimer in its slipped parallel form as shown in figure 6.2 [266]. This contributes to an additional stabilization of -3.65 kcal/mol. Thus, the stabilization energy of ${}^7[(\text{N@CNT})_2]$ can be attributed to the encapsulation of nitrogen atoms along with their shift towards each other in two cages ($2 \times -4.47 \text{ kcal/mol} = -8.94 \text{ kcal/mol}$) and the stabilization due to the rotation of one of the nanotubes (-3.65 kcal/mol). The stabilization energy due to the single occupancy of nitrogen inside $(\text{CNT})_2$, out of which one CNT is rotated is -8.35 kcal/mol. This is approximately equal to the sum of the stabilization energies due to the encapsulation of nitrogen (-3.02 kcal/mol), its shift inside $(\text{CNT})_2$ (-1.12 kcal/mol) and the rotation of nanotubes (-3.65 kcal/mol).

For ${}^4[\text{N@}(\text{BNNT})_2]$, in which guest atom is shifted near to the surface of BNNT, the stabilization energy is -5.29 kcal/mol. The stabilization energy reduces to -4.24 kcal/mol on displacing the guest atom to the center of BNNT. Hence, the energy of -1.05 kcal/mol can be attributed to the shift of guest atom from the center of BNNT. In contrast to ${}^7[(\text{N@CNT})_2]$, both nanotubes are aligned parallel to each other in ${}^7[(\text{N@BNNT})_2]$ similar to the most stable structure of borazine dimer in which the individual borazine units are stacked parallel to each other (figure 6.2) [267-268]. Thus, the stabilization energy of ${}^7[(\text{N@BNNT})_2]$ can be attributed due to the encapsulation of nitrogen atoms inside adjacent BNNTs as well as to their shift towards each other.

6.3.2 Spin-Spin coupling in complexes

The spin density of guest atoms in various endohedral complexes mentioned above in their stable spin states are given in table 6.3. The spin density distribution plots of these complexes are shown in figure 6.3. The spin density value of 2.99 e/au^3 on nitrogen of ${}^4[\text{N@CNT}]$ suggests that the nitrogen atom retains its atomic spin state after encapsulation in CNT. It is also confirmed from its spin density distribution plot. This also holds true for ${}^4[\text{N@BNNT}]$, suggesting that the guest nitrogen retains its spin states irrespective of the type of confinement (at least by C_{60} , CNT and BNNT).

Table 6.2. The stabilization energy of various complexes associated with the encapsulation of nitrogen atom at B3LYP-GD2/6-311G level. For (CNT)₂ and rotated-(CNT)₂, their relative energy with respect to each other is given.**

Complex	Stabilization Energy (kcal/mol)	Geometries
⁴ [N@CNT]	-3.02	
⁷ [(N@CNT) ₂]	-12.95	
⁴ [(N@(CNT) ₂)]	-4.47	
⁴ [(N@(CNT) ₂)] (nitrogen at the centre)	-3.35	
⁴ [(N@(CNT) ₂)] (CNT is rotated on encapsulation)	-8.35	
(CNT) ₂	0.00	
rotated-(CNT) ₂	-3.65	

...continued.

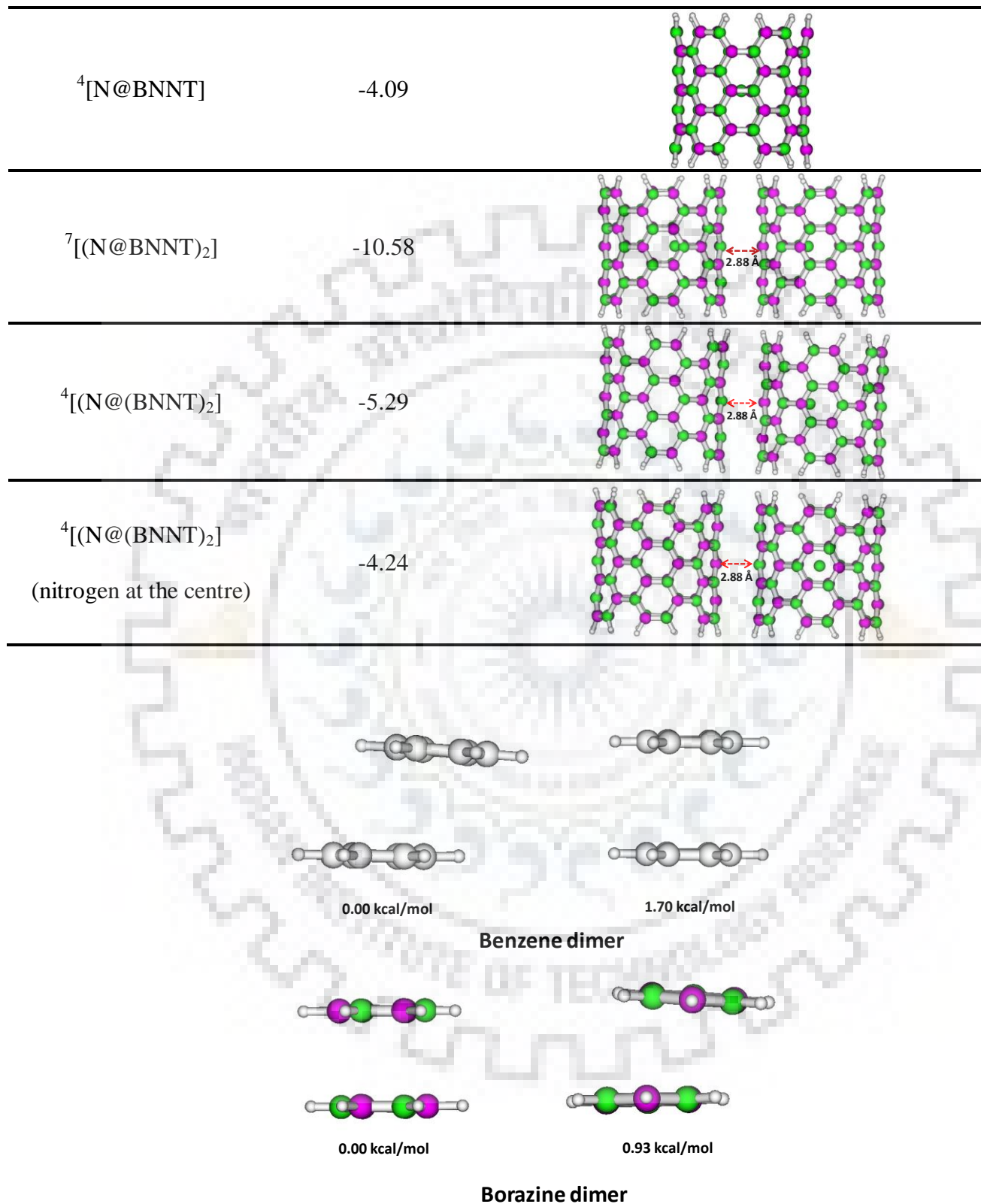


Figure 6.2. The geometries and relative energies of parallel and slipped parallel form of respective dimers of benzene and borazine at B3LYP-GD2/6-311G** level

To investigate how the spins of guest atoms interact in $(\text{N@CNT})_2$ and $(\text{N@BNNT})_2$, the spin-spin coupling in the stable states of the above complexes are analyzed. In $^7[(\text{N@CNT})_2]$, the values of spin density of nitrogen atoms are equal to that of nitrogen in $^4[\text{N@CNT}]$ and $^7[(\text{N@C}_{60})_2]$. The values of spin density of both nitrogen atoms and their spin density distribution plot suggest ferromagnetic spin coupling between guest atoms on confining in CNT cages. In case of singlet state of $(\text{N@CNT})_2$, the spins of both guest atoms are antiferromagnetically coupled as inferred from their spin density values 2.97 e/au^3 and -2.97 e/au^3 . This is also confirmed from its spin density distribution plot. Similar results are also obtained for stable states of $(\text{N@BNNT})_2$. As in monomers, both nitrogen atoms retained their spin inside CNT and BNNT dimers. It should be also mentioned that the spins of guest species in the respective septet states of both $(\text{N@CNT})_2$ and $(\text{N@BNNT})_2$ are ferromagnetically coupled in septet state whereas they are antiferromagnetically coupled in their singlet states similar to the case of $(\text{N@C}_{60})_2$ and $(\text{N@C}_{59}\text{N})_2$ reported in chapter 3.

6.3.3 Spin polarization in complexes

To know about the spin polarization and spin degeneracy in the complexes, the spin polarization parameter (ζ) for stable states of the complexes is calculated and is listed in table 6.3. To get more insight on the spin polarization and spin degeneracy of the complexes, the spin density distribution of various orbitals are shown in figure 6.4 and are analyzed. It was revealed from the spin density distribution plots of $^4[\text{N@CNT}]$ and $^4[\text{N@BNNT}]$ that the unpaired electrons are mainly localized on encapsulated nitrogen atoms. Moreover, the atomic orbitals of nitrogen become non-degenerated when it is confined in nanotubes. As indexed in table 6.3, the value of spin polarization parameter is 1.00 for $^4[\text{N@CNT}]$ and $^4[\text{N@BNNT}]$ indicating the complexes are spin polarized. In the septet states of $(\text{N@CNT})_2$ and $(\text{N@BNNT})_2$, the unpaired electrons are occupied in non-degenerate orbitals of guest atoms. The atomic orbitals of guest atoms of $^7[(\text{N@CNT})_2]$ and $^7[(\text{N@BNNT})_2]$ are also non-degenerate. The value of spin polarization parameter (ζ) for both $^7[(\text{N@CNT})_2]$ and $^7[(\text{N@BNNT})_2]$ is 1.00 indicating that the complexes are spin polarized. In contrast to septet state, the complexes $(\text{N@CNT})_2$ and $(\text{N@BNNT})_2$ are spin degenerated in their singlet state as inferred from the zero value of spin polarization parameter. The spin polarization and spin degeneracy in nitrogen encapsulated CNT, BNNT and their respective dimers are in similar to the observations of nitrogen encapsulated fullerene analogues discussed in chapters 3 and 5.

Table 6.3. The spin density on encapsulated nitrogen atoms and the spin polarization parameter (ζ) for the stable endohedral nanotubes.

Complexes	Spin densities (e/eu^3)	Spin polarization parameter (ζ)
N	3.00	1.00
$^4[\text{N@CNT}]$	$(N_{\text{encap}})=2.99$	1.00
$^1[(\text{N@CNT})_2]$	$(N_{\text{encap}})_1=2.97$ $(N_{\text{encap}})_2=-2.97$	0.00
$^7[(\text{N@CNT})_2]$	$(N_{\text{encap}})_1=(N_{\text{encap}})_2=2.97$	1.00
$^4[\text{N@BNNT}]$	$(N_{\text{encap}})=2.98$	1.00
$^1[(\text{N@BNNT})_2]$	$(N_{\text{encap}})_1=2.97$ $(N_{\text{encap}})_2=-2.97$	0.00
$^7[(\text{N@BNNT})_2]$	$(N_{\text{encap}})_1=(N_{\text{encap}})_2=2.97$	1.00

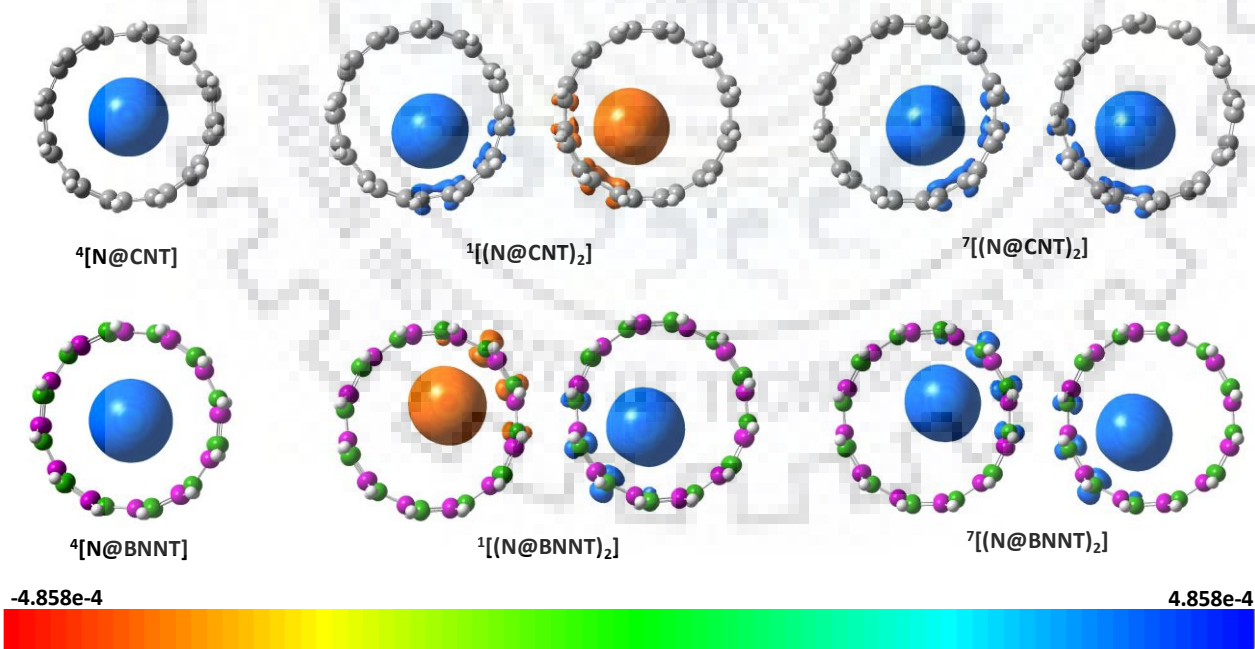


Figure 6.3. Spin density difference plots for endohedral nanotubes in their stable spin states for an isodensity value of 0.0004.

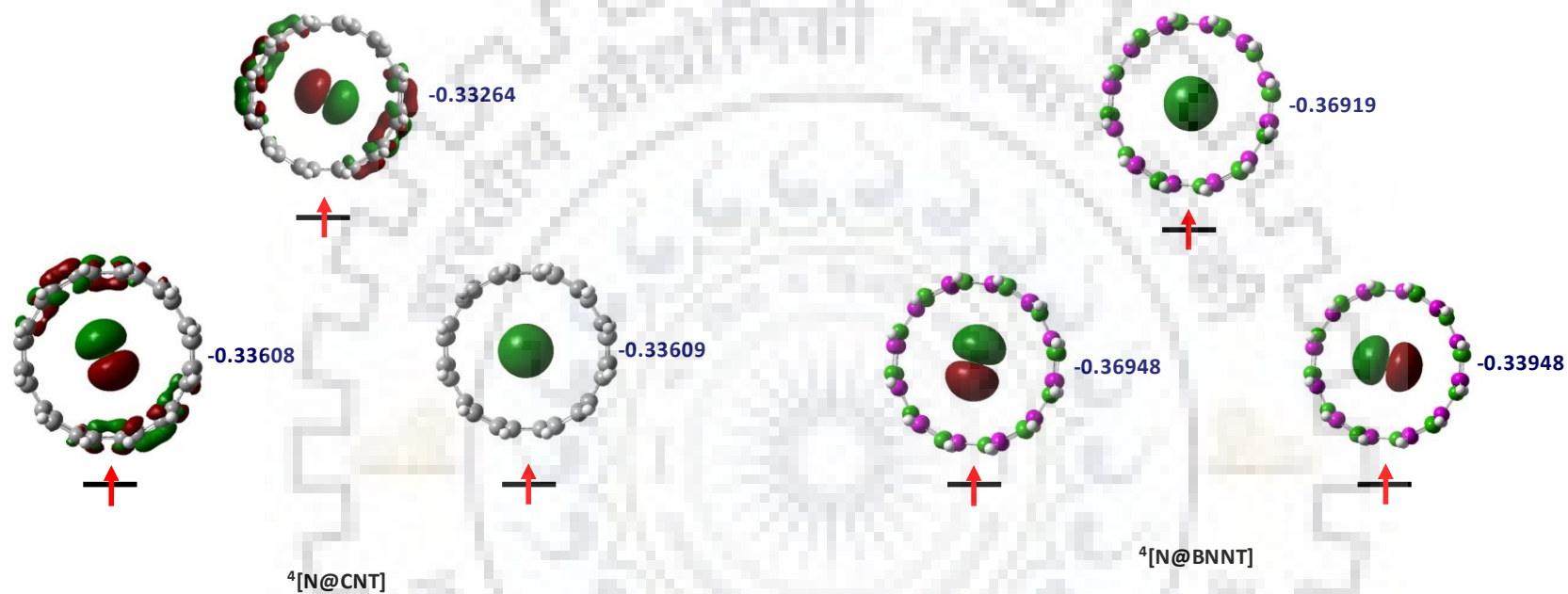


Figure 6.4. The relevant molecular orbitals showing spin density distribution for the stable spin states of various endohedral nanotubes with an isodensity value of 0.02. The energies of orbitals are given in Hartree.

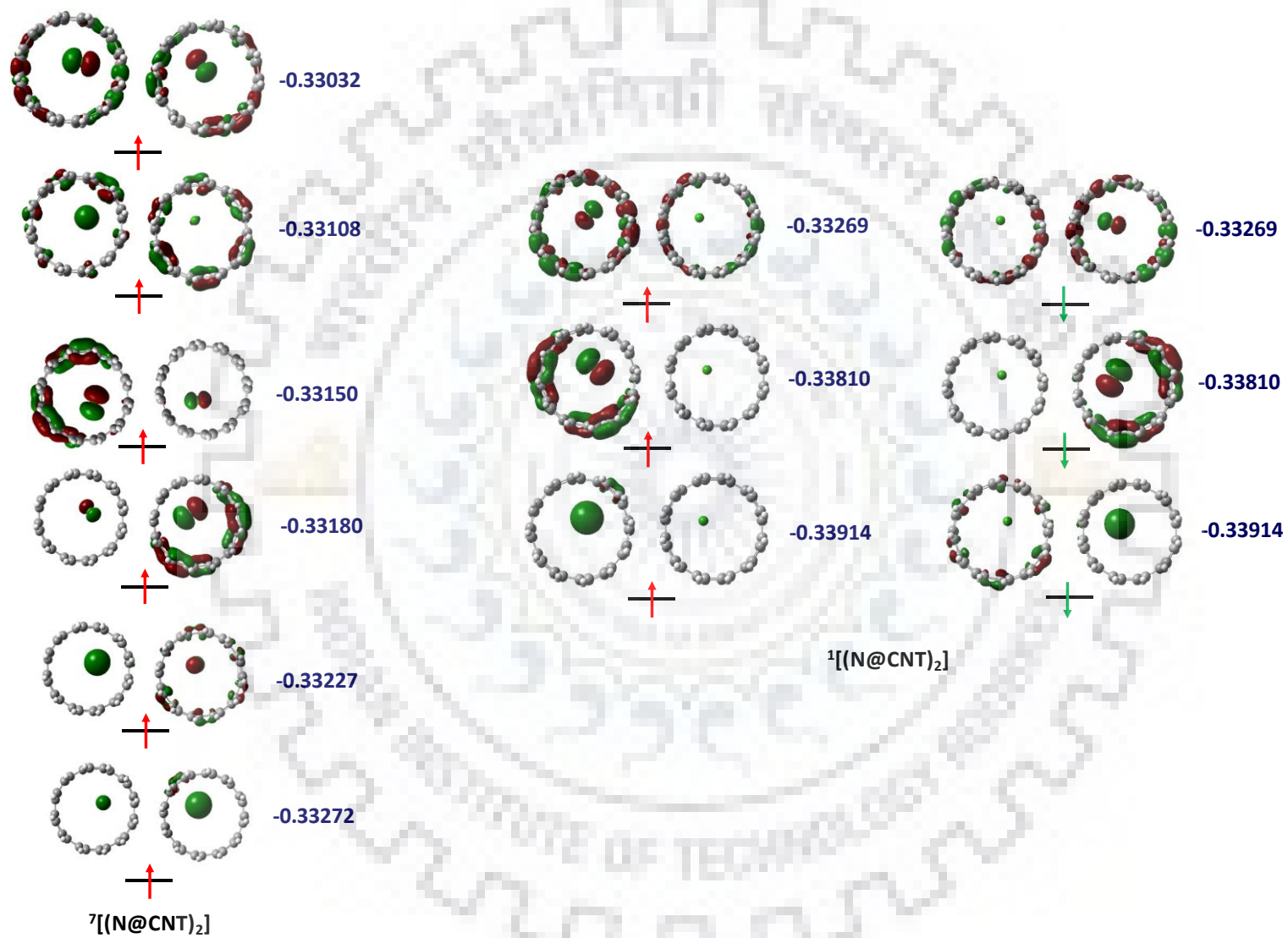


Figure 6.4. Continued.

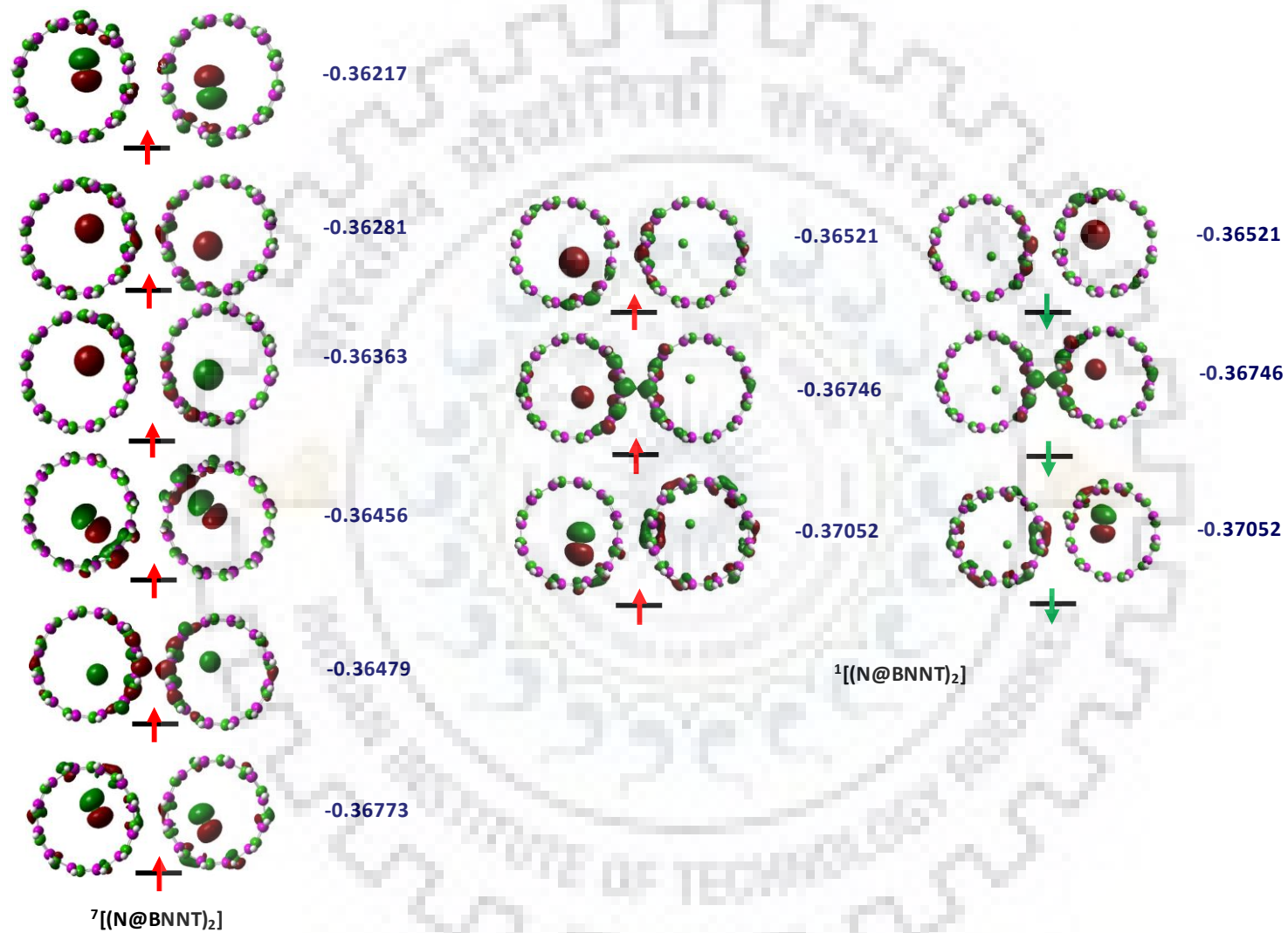


Figure 6.4. Continued.

6.3.4 Hyperfine coupling constant

To investigate the effect of confinement by nanotubes on the hyperfine coupling constant (hfcc) of guest nitrogen atoms, the values of hfcc of the latter in complexes as well as in free states are calculated and are listed in table 6.4. The value of hfcc of nitrogen in its free state is 1.84 Gauss (G) which remained nearly the same after its encapsulation in CNT. However, hfcc of nitrogen in ${}^7[(\text{N@CNT})_2]$ is decreased to 0.90 G, although the spin density values remained the same (table 6.3). The decrease in hfcc of nitrogen atoms of ${}^7[(\text{N@CNT})_2]$ is due to the ferromagnetic spin coupling between the guest atoms. In ${}^4[\text{N@BNNT}]$, the value of hfcc of encapsulated nitrogen is increased by 0.26 G due to the confinement of BNNT despite the same value of spin density in its free state. On encapsulating nitrogen atoms in adjacent BNNT, the hfcc of nitrogen atoms is reduced by 0.99 G due to the ferromagnetic spin coupling between trapped nitrogen atoms. Thus, the confinement by different nanotubes alters the hfcc of nitrogen atom.

Table 6.4. The calculated values of hyperfine coupling constant (hfcc) of encapsulated nitrogen atom in various endohedral nanotubes

Complexes	hfcc (Gauss)
N	1.84
${}^4[\text{N@CNT}]$	$(N_{\text{encap}})=1.87$
${}^7[(\text{N@CNT})_2]$	$(N_{\text{encap}})_1=0.90$ $(N_{\text{encap}})_2=0.89$
${}^4[\text{N@BNNT}]$	$(N_{\text{encap}})=2.10$
${}^7[(\text{N@BNNT})_2]$	$(N_{\text{encap}})_1=(N_{\text{encap}})_2=0.85$

6.3.5 Electronic properties

6.3.5.1 Electron affinity and ionization energy

In order to investigate the electronic properties of the complexes, the vertical electron affinity (VEA) and vertical ionization energy for the stable states of the complexes are calculated and are listed in table 6.5. The values of electron affinity and ionization energy of CNT are -1.67 and 5.85 eV, respectively. The electron affinity and ionization energy of CNT were found to be unaltered with the encapsulation of nitrogen. Similarly, VEA and VIE of (CNT)₂ were also not changed by encapsulating nitrogens in adjacent cages. On encapsulating nitrogen, electron affinity of BNNT is decreased by 1.37 eV, although the ionization energy remained the same. The electron affinity of (BNNT)₂ is 0.30 eV which is reduced to -1.76 eV by encapsulating nitrogen atom in both of the tubes. As in the case of BNNT, the encapsulation of nitrogen does not change the ionization energy.

6.3.5.2 Energy gap between HOMO and LUMO

To know more about the electronic properties of the complexes, the energy gap between HOMO and LUMO ($\Delta E_{\text{HOMO-LUMO}}$) is calculated and is tabulated in table 6.5. The corresponding molecular orbitals are shown in figure 6.5. The energy gap between HOMO and LUMO of CNT is 2.30 eV which is not changed due to encapsulation of nitrogen inside. The analysis showed that the respective frontier molecular orbitals of CNT and ⁴[N@CNT] are formed by the contribution of carbon atoms of CNT which is expected as the orbitals of nitrogen are relatively lower in energy due to its high electronegativity. The value of $\Delta E_{\text{HOMO-LUMO}}$ of ⁷[(N@CNT)₂] is 2.24 eV and is nearly the same (2.11 eV) as that of its free host (CNT)₂. Likewise, the electron density of frontier molecular orbitals of ⁷[(N@CNT)₂] is mainly distributed over the carbon atoms of CNTs. The energy gap between HOMO and LUMO of BNNT is 6.31 eV which was unaffected due to the encapsulation of nitrogen inside. Similar to ⁴[N@CNT], the encapsulation of nitrogen in BNNT does not perturb the frontier molecular orbitals of the latter as inferred from figure 6.5. The energy gap between HOMO and LUMO of (BNNT)₂ and their corresponding molecular orbitals are unaffected by the encapsulation of nitrogen atom inside adjacent cages.

In order to know the effect of dimerization of CNT, N@CNT, BNNT and N@BNNT on their $\Delta E_{\text{HOMO-LUMO}}$, the respective values $\Delta E_{\text{HOMO-LUMO}}$ for monomers and dimers are compared. The energy gap between HOMO and LUMO of CNT was decreased by 0.19 eV on its dimerization. The dimerization of $^4[\text{N@CNT}]$ also leads to a decrease in $\Delta E_{\text{HOMO-LUMO}}$ by 0.07 eV. The energy gap between HOMO and LUMO of BNNT and $^4[\text{N@BNNT}]$ is reduced by 0.09 eV on forming their respective dimers.

Table 6.5. The values of vertical electron affinity (VEA), vertical ionization energy (VIE), energy gap between HOMO and LUMO ($\Delta E_{\text{HOMO-LUMO}}$) of various nanotubes and their nitrogen atom encapsulated complexes.

System	VIE (eV)	VEA (eV)	$\Delta E_{\text{(HOMO-LUMO)}}$ (eV)
CNT	5.85	-1.67	2.30
$^4[\text{N@CNT}]$	5.85	-1.68	2.31(α) 2.30(β)
$(\text{CNT})_2$	5.43	-1.94	2.11
$^7[(\text{N@CNT})_2]$	5.48	-1.87	2.24(α) 2.21(β)
BNNT	7.62	0.50	6.31
$^4[\text{N@BNNT}]$	7.62	-0.87	6.31(α) 3.30(β)
$(\text{BNNT})_2$	7.33	0.30	6.22
$^7[(\text{N@BNNT})_2]$	7.33	-1.76	6.22(α) 3.40(β)

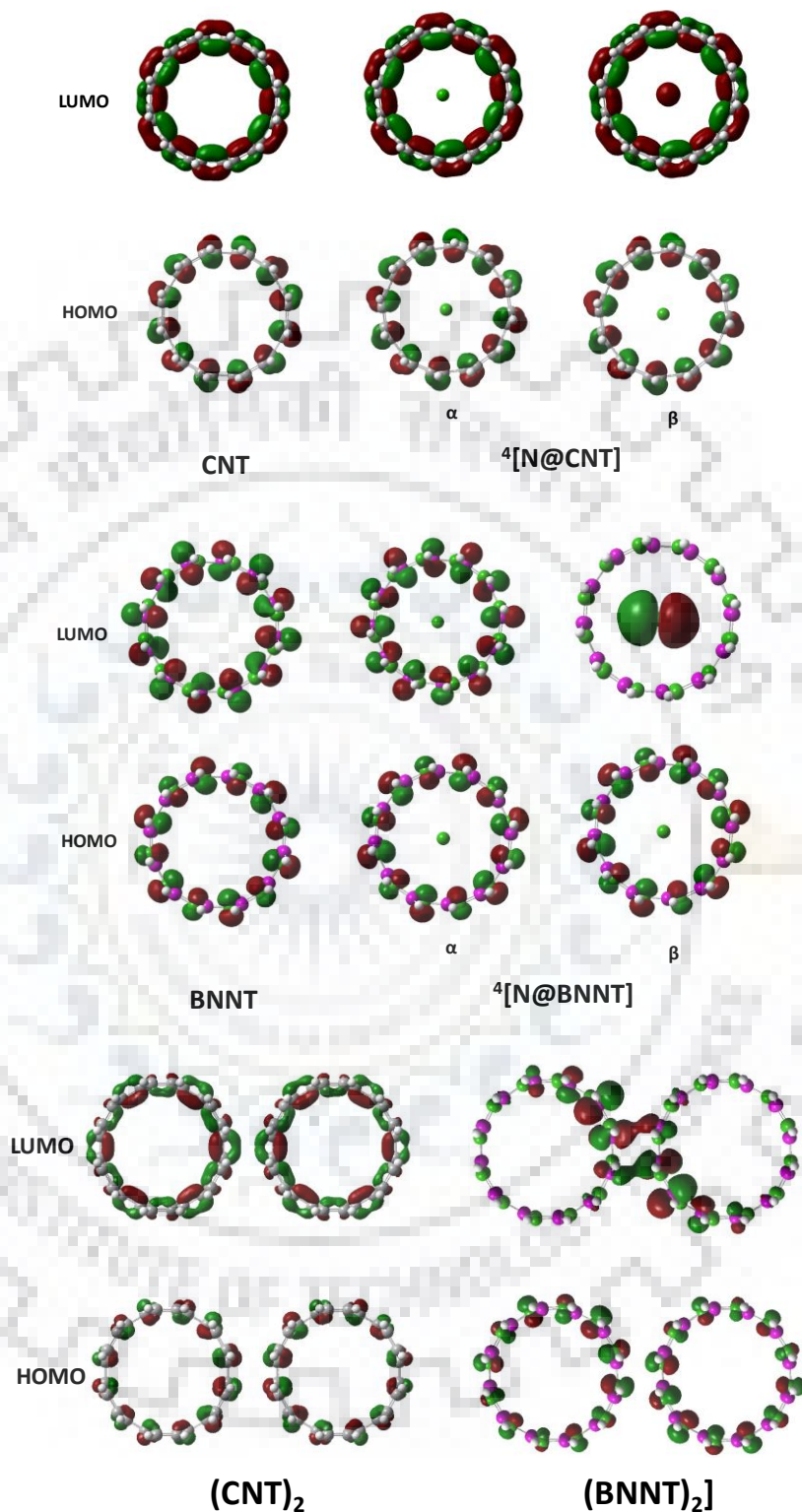


Figure 6.5. Isodensity surface plots of highest occupied and lowest unoccupied molecular orbitals of the complexes in their stable spin states with an isodensity value of 0.02.

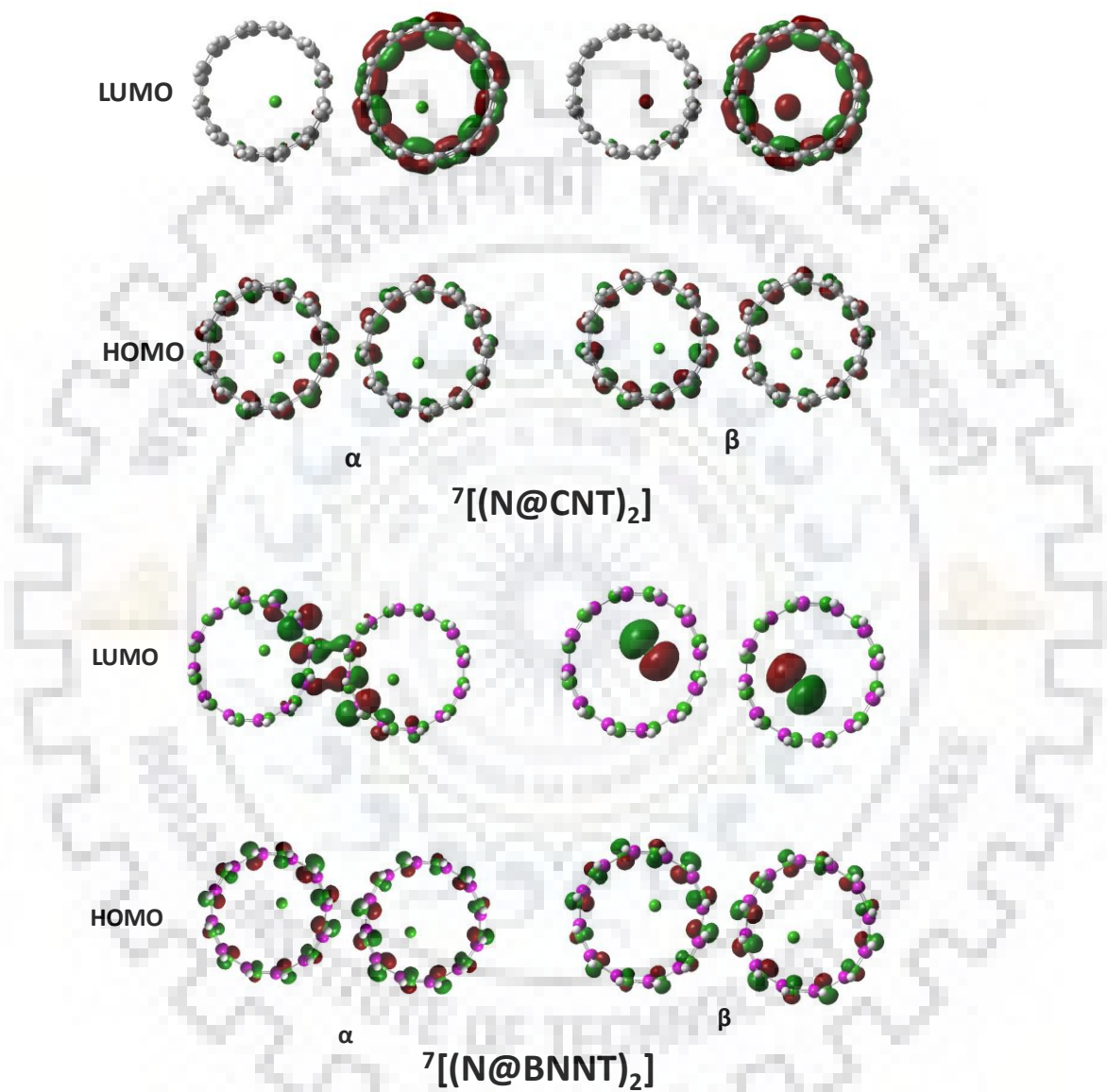


Figure 6.5. Continued.

6.3.6 Effect of the size of cavity on the spin-spin coupling between guest atoms

To investigate the effect of size of cavity on the spin-spin coupling between the guest and the host as well as that between guests, the structure and properties of nitrogen encapsulated (5,5)-carbon nanotube of same length as that of the tube considered before was also investigated. The optimized geometries of (5,5)-CNT, its dimer and their respective nitrogen encapsulated complexes are shown in figure 6.6. As shown in figure, the diameter of (5,5)-CNT is 6.98 Å which is 1.18 Å less than that of (6,6)-CNT used before. The distance between two (5,5)-CNT in its dimer is 3.49 Å which is 0.27 Å more than that between two (6,6)-CNTs. The dimerization energy of ((5,5)-CNT)₂ is -14.32 kcal/mol indicating that the dimerization is energetically possible.

The stabilization energies of N@(5,5)-CNT and its dimer (N@(5,5)-CNT)₂ in their possible spin states are listed in table 6.6. The spin density plots for these states of the complexes as well as the values of spin density on nitrogen atoms and spin polarization parameter (ζ) are shown in figure 6.7. The stabilization energy of the complex N@(5,5)-CNT in its quartet spin state is -7.64 kcal/mol, where the guest atom is occupied at the centre of the nanotube. The value of spin density of nitrogen is 2.97 e/au³, same as that obtained for CNT of larger diameter suggesting that the spin density of nitrogen atom is unaltered inside (5,5)-CNT. The spin polarization was also unaffected with a decrease in the cavity size as can be seen from figure 6.7. The complex (N@(5,5)-CNT)₂ is stable in its isoenergetic singlet and septet states with the stabilization energy of -13.89 kcal/mol. In ⁷[(N@(5,5)-CNT)₂], the guest atoms are located at the centre of respective nanotubes unlike in ⁷[(N@(6,6)-CNT)₂]. The distance between nitrogen atoms in ⁷[(N@(5,5)-CNT)₂] is 9.90 Å which is 0.19 Å more than that in its larger nanotube analogue. The spin density on the nitrogen atoms are unaffected by using CNT of smaller diameter as inferred from table 6.3 and figure 6.7. The antiferromagnetic and ferromagnetic spin coupling occur between guest atoms in ¹[(N@(5,5)-CNT)₂] and ⁷[(N@(5,5)-CNT)₂], respectively, an observation similar to (6,6)-CNT analogue. The spin polarization in complexes was also unaffected with a decrease in the diameter of the carbon nanotube. Thus, the size of carbon nanotube did not affect the spin-spin coupling between encapsulated nitrogen atoms.

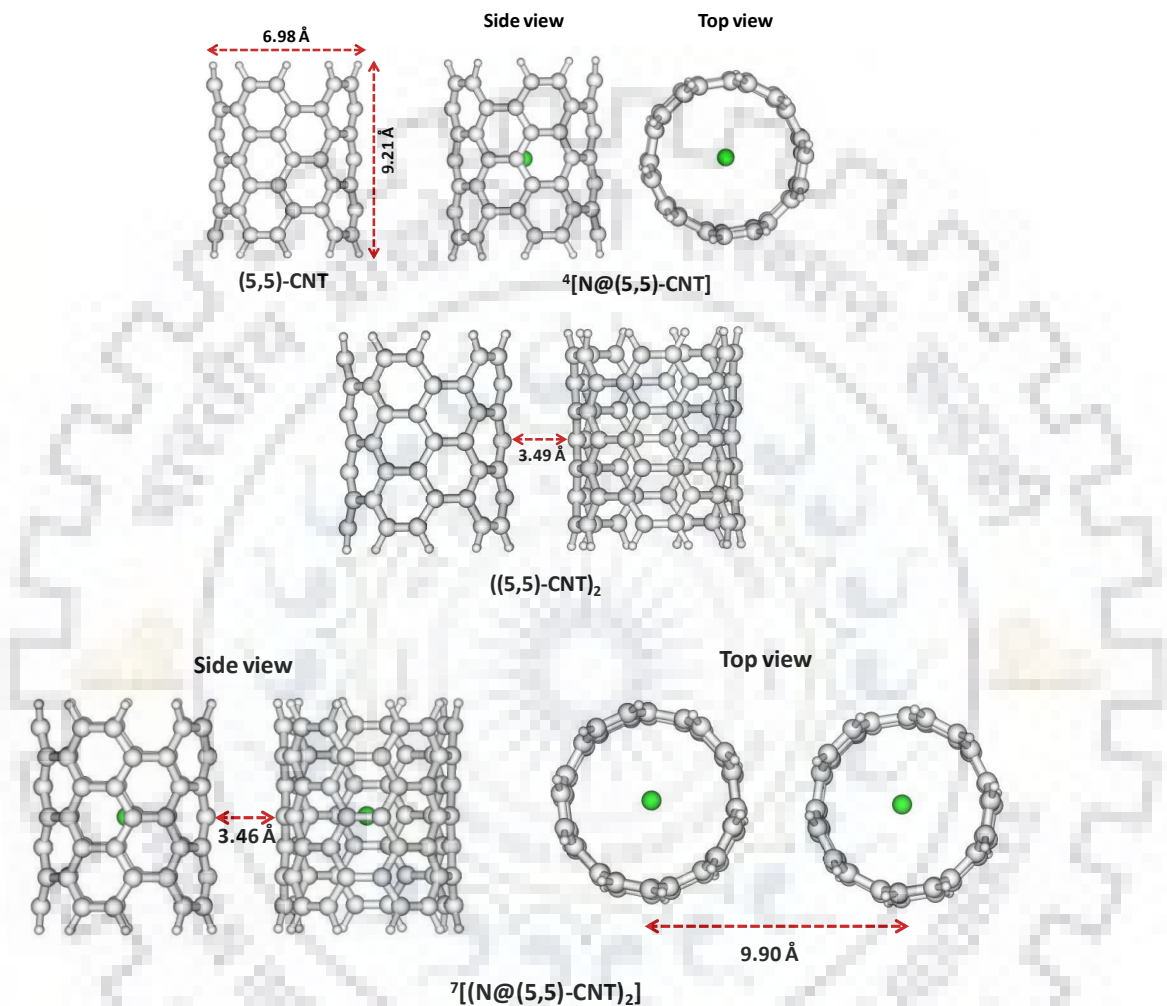


Figure 6.6. Optimized geometries of (5,5)-CNT, N@(5,5)-CNT and their respective dimers. The grey, violet and green colored spheres represent carbon, boron and nitrogen atoms, respectively. The multiplicity of the complexes is given in superscript.

Table 6.6. The calculated stabilization energies of the nitrogen atom encapsulated complexes of (5,5)-CNT in their different spin states at B3LYP-GD2/6-311G** level. The values of BSSE corrected stabilization energies for the stable spin states of the complexes are given in parenthesis.

Complexes	Multiplicity	Stabilization Energy (kcal/mol)
N@(5,5)-CNT	4	-7.64 (-5.93)
	1	-13.89
	3	35.93
(N@(5,5)-CNT) ₂	5	14.84
	7	-13.89(-11.04)
	9	15.66

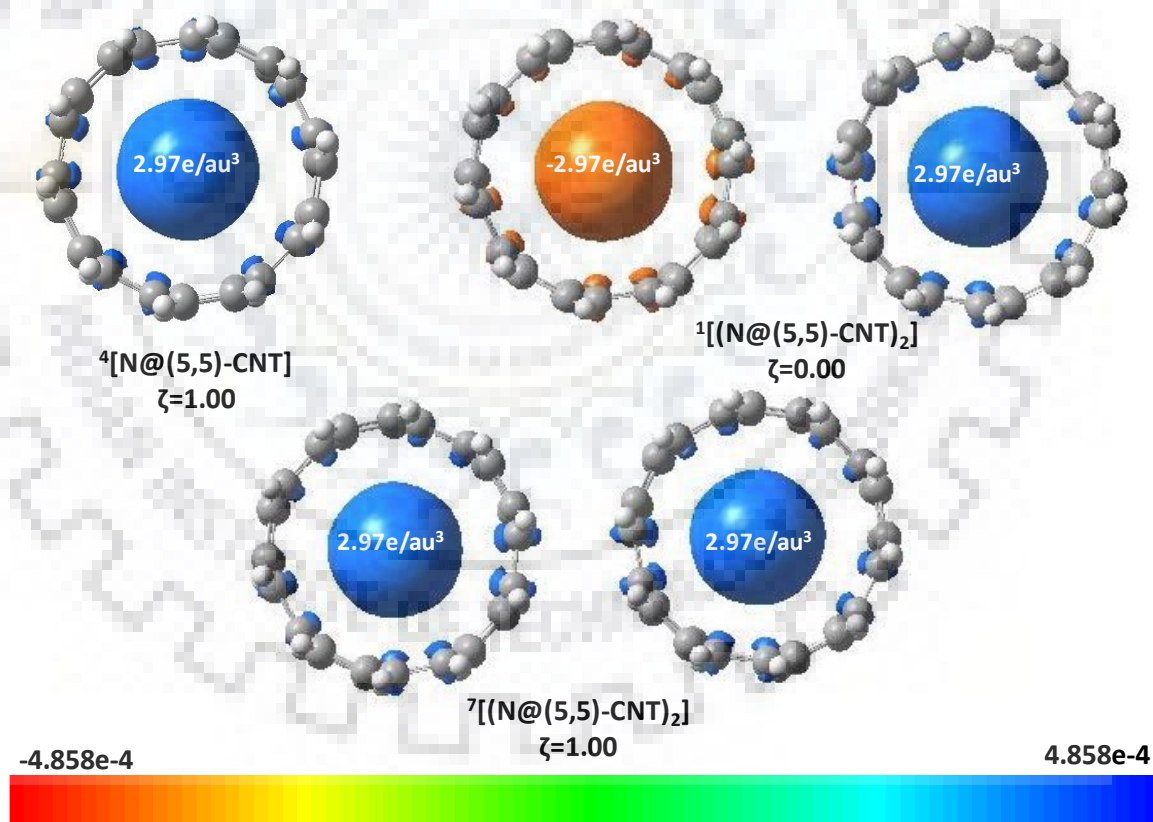


Figure 6.7. The spin density difference plots of $^4[\text{N}@(5,5)\text{-CNT}]$, $^1[(\text{N}@(5,5)\text{-CNT})_2]$ and $^7[(\text{N}@(5,5)\text{-CNT})_2]$ for an isodensity value of 0.0004. The spin density values (e/au^3) on guest nitrogen atoms along with the spin polarization parameter (ζ) are also given.

6.4 Conclusions

In the present chapter, the structure, stability and properties of nitrogen atom encapsulated complexes of CNT, BNNT and their respective dimers were investigated using the dispersion corrected density functional B3LYP-GD2 and 6-311G** basis set. The study showed that in $^4[\text{N@CNT}]$ and $^4[\text{N@BNNT}]$, the guest atom is located at the centre of respective hosts. The stability of the complexes arises due to the van der Waals interaction between guest and host species where guest atom retained its electronic configuration. The complexes $(\text{N@CNT})_2$ and $(\text{N@BNNT})_2$ were found to be stable in their singlet and septet spin states. In the stable states of $(\text{N@CNT})_2$ and $(\text{N@BNNT})_2$, the guest atoms are shifted towards each other from the centre of adjacent CNTs providing additional stability to the complexes. This stabilization energy is more than twice as that of monomer analogues. The spins of respective guest atoms of $(\text{N@CNT})_2$ and $(\text{N@BNNT})_2$ are antiferromagnetically and ferromagnetically coupled in their singlet and septet states, respectively. The study revealed that $^4[\text{N@CNT}]$ and $^4[\text{N@BNNT}]$ exhibit spin polarization. For $(\text{N@CNT})_2$ and $(\text{N@BNNT})_2$, the septet states are spin polarized although their singlet spin states are spin degenerated. The effect of confinement by nanotubes on hyperfine coupling constant of encapsulated nitrogen atom was examined and for the complexes $^7[(\text{N@CNT})_2]$ and $^7[(\text{N@BNNT})_2]$, the value of hyperfine coupling constant of the encapsulated nitrogen was significantly reduced due to the ferromagnetic spin coupling between them. In general, on encapsulating nitrogen atom inside CNT, BNNT and their respective dimers, the electronic properties such as VEA, VIE and $\Delta E_{\text{HOMO-LUMO}}$ of the respective hosts were found to be unaffected except VEA of BNNT and $(\text{BNNT})_2$ for which it was significantly decreased.

The effect of cavity size of nanotubes on spin-spin coupling between the guest and the host as well as that between guests in endohedral complexes of nanotubes was analyzed. The analysis showed that the spin-spin coupling and spin polarization of nitrogen encapsulated nanotubes are not affected due to a decrease in size of nanotubes.

The nitrogen encapsulated complexes of CNT, BNNT and their respective dimers showed similar spin-spin coupling and spin polarization as that of the complexes of C_{60} and $(\text{C}_{60})_2$.

Chapter-7

Conclusions and future scope

In the present thesis, the density functional theoretical studies were performed to investigate the structure, stability and properties of the heteroatom encapsulated complexes of various derivatives of fullerenes and nanotubes. For this purpose, the nitrogen (and boron) atom encapsulated C_{60} , $C_{59}N$, $C_{59}B$ and their respective dimers were considered. The heterodimer $B@C_{59}N-N@C_{59}B$ was also investigated. The nitrogen atom encapsulated carbon nanotube, boron nitride nanotube and their respective dimers were also studied.

The study showed that the guest atoms were located at the center of C_{60} in $^4[N@C_{60}]$ and $^2[B@C_{60}]$. For nearly isoenergetic $^3[N@C_{59}N]$ and $^5[N@C_{59}N]$, the guest was occupied nearly at the center of the cage. Like in triplet and quintet states of $N@C_{59}N$, the guest was located at the center of $C_{59}B$ in $^3[N@C_{59}B]$ and $^5[N@C_{59}B]$, whereas it was located near to inner surface of the cage in its singlet state. The nearly isoenergetic triplet and quintet states of $N@C_{59}B$ are more stable than that of its singlet state. The boron encapsulated complexes of $C_{59}B$ and $C_{59}N$ are found to be stable in their singlet and triplet states. The results also revealed that the singlet states of both the complexes are more stable than their respective triplet states.

The complexes $(N@C_{60})_2$ and $(N@C_{59}N)_2$ are stable in their respective isoenergetic singlet and septet states, however, for $(N@C_{59}B)_2$ only the septet state is stable. The guest atoms were located at the center of each of the host cages in the stable states of the above complexes. The complexes $(B@C_{60})_2$ and $(B@C_{59}N)_2$ are stable in their isoenergetic singlet and triplet states with the guests at the center of host cages. Similarly, the complex $(B@C_{59}B)_2$ are stable in its singlet and triplet states although the former is more stable than the latter. The heterodimer $(B@C_{59}N-N@C_{59}B)$ is stable in its various spin states. In the singlet states of the complexes $(B@C_{59}B)_2$ and $(B@C_{59}N-N@C_{59}B)$, the guest atoms occupy near the inner surfaces of the host cages, although in their high spin states they locate at the center of respective host cages. Studies showed that in $^4[N@CNT]$ and $^4[N@BNNT]$, the guest atoms prefer to be at the center of the respective nanotubes. It was also revealed that the singlet and septet states of both $(N@CNT)_2$ and $(N@BNNT)_2$ are stable where the guest atoms were shifted towards each other from the centre of adjacent nanotubes which results into an additional stabilization energy than twice of the stabilization energy of respective monomer analogue.

The studies on the spin-spin coupling and spin density transfer revealed that the nitrogen and boron atom retained their atomic spin inside C_{60} and hence no spin density transfer was observed from guest to host or vice versa. For $(N@C_{59}N)$ and $(N@C_{59}B)$, the spins of guest nitrogen atoms are either antiferromagnetically or ferromagnetically coupled with that of the respective host cage in their triplet and quintet states in order. However, the spins of guest and host are only ferromagnetically coupled in $^3[B@C_{59}N]$ and $^3[B@C_{59}B]$. The study showed that there is no spin density transfer between the respective component species of $N@C_{59}N$, $N@C_{59}B$, $B@C_{59}N$ and $B@C_{59}B$.

In $^1[(N@C_{60})_2]$, the spins of guest nitrogen atoms are antiferromagnetically coupled whereas they are ferromagnetically coupled in $^7[(N@C_{60})_2]$. Likewise, the interaction between guest atoms is antiferromagnetic and ferromagnetic in singlet and triplet states of $(B@C_{60})_2$, respectively. Thus, changing the guest atom inside $(C_{60})_2$ does not affect spin-spin interaction between guest species.

To get more insight onto the spin-spin coupling and spin density transfer between guest and host as well as those between guest species, various endohedral heterofullerenes such as $(N@C_{59}N)_2$, $(N@C_{59}B)_2$, $(B@C_{59}N)_2$, $(B@C_{59}B)_2$ and $(B@C_{59}N-N@C_{59}B)$ were studied. The results showed that the guest atoms are antiferromagnetically or ferromagnetically coupled in both $(N@C_{59}N)_2$ and $(B@C_{59}N)_2$ depending upon their spin states suggesting that substitution of carbon atom of $(C_{60})_2$ by nitrogen atom also does not affect the spin-spin coupling between guest species. However, the spin-spin interaction was affected when the carbon atom of $(C_{60})_2$ was substituted by boron atom as the interaction between spins of respective guest species of $^7[(N@C_{59}B)_2]$ and $^3[(B@C_{59}B)_2]$ is only ferromagnetic. For $B@C_{59}N-N@C_{59}B$, the spins of guest species are antiferromagnetically and ferromagnetically coupled in its triplet and quintet states, respectively. Interestingly, the spin density transfer occurs from the guest to the host of $^1[(B@C_{59}B)_2]$ and $^1[B@C_{59}N-N@C_{59}B]$ followed by the antiferromagnetic coupling between their respective monomers.

The effect of confinement by different nanotubes on the spins of nitrogen atom was studied. The nitrogen atom retained its atomic spin inside both CNT and BNNT. The spins of the corresponding guest atoms of each of the complexes $^1[(N@CNT)_2]$ and $^7[(N@CNT)_2]$ coupled antiferromagnetically and ferromagnetically, respectively. This holds true for singlet and septet states of $(N@BNNT)_2$. Thus, spin-spin interaction between the respective guest atoms of $(N@CNT)_2$ and $(N@BNNT)_2$ is similar to that of C_{60} analogue. In all of the above complexes, the spin of guest atom was found to be retained except in $^1[(B@C_{59}B)_2]$ and $^1[B@C_{59}N-N@C_{59}B]$ where spin is transferred from guest to host. Thus, the spin-spin interactions and spin density

transfer between the components of the complexes depend on the encapsulated atom as well as on the heteroatoms of the cage.

The analysis of spin polarization parameter of the above complexes showed that the complexes are spin polarized when the spins of their component species are ferromagnetically coupled. Whereas, the complexes are spin degenerate when the antiferromagnetic coupling occurs between the component species except for $^3[\text{N}@C_{59}\text{N}]$, $^3[\text{N}@C_{59}\text{B}]$ and $^3[\text{B}@C_{59}\text{N}-\text{N}@C_{59}\text{B}]$ which are partially spin polarized.

The calculated values of change in the Gibbs free energy (ΔG) and change in enthalpy (ΔH) associated with the encapsulation of guest species as well as dimerization of endohedral fullerene derivatives showed that the encapsulation of nitrogen and boron atoms inside C_{60} , $C_{59}\text{B}$, $C_{59}\text{N}$ and their respective dimer is thermodynamically feasible. It was also revealed that the formation of the dimer of endohedral fullerene derivatives is also thermodynamically feasible.

The energy gap between HOMO and LUMO of various derivatives of fullerene was unaffected due to the encapsulation of nitrogen atom inside. Based on the spin states of the complexes, the energy gap between HOMO and LUMO was altered on encapsulating boron atom inside fullerene derivatives. The investigation on other electronic properties (VEA and VIE) of the derivatives of fullerene showed that the properties can be tuned by the encapsulation of suitable guest species. The dipole moment of $\text{B}@C_{59}\text{N}-\text{N}@C_{59}\text{B}$ is found to be the highest suggesting the polarity of the complex and hence its separation. On the other hand, the electronic properties such as VEA, VIE and $\Delta E_{\text{HOMO-LUMO}}$ of the host nanotubes remain the same on encapsulation of atoms except VEA of BNNT and $(\text{BNNT})_2$ which are significantly reduced due to encapsulation.

The results obtained from the present thesis are expected to trigger several experimental studies on the development and applications of endohedral complexes of fullerenes, heterofullerenes, carbon nanotubes and boron nitride nanotubes. The study can be extended to the encapsulation of other paramagnetic atomic and molecular species inside fullerenes and nanotubes of various size and shape.





Bibliography

1. Georgakilas, V.; Perman, J. A.; Tucek, J.; Zboril, R. Broad family of carbon nanoallotropes: classification, chemistry, and application of fullerenes, carbon dots, nanotubes, graphene, nanodiamonds, and combined superstructures. *Chem. Rev.* **2015**, 115, 4744-4822.
2. Kroto, H. W.; Heath, J. R.; O'Brien, S. C.; Curl, R. F.; Smalley, R.E. C₆₀: buckminsterfullerene. *Nature* **1985**, 318, 162-163.
3. Ijima, S. Helical microtubules of graphitic carbon. *Nature* **1991**, 354, 56-58.
4. Krätschmer, W.; Lamb, D. L.; Fostiropoulos, K.; Huffman D. R. Solid C₆₀: a new form of carbon. *Nature* **1990**, 347, 354-358.
5. Gerhardt, Ph.; Löffler, S.; Homann, K. H. Polyhedral carbon ions in hydrocarbon flames. *Chem. Phys. Lett.* **1987**, 137, 306-310.
6. Homann, K. H. Fullerenes and soot formation-new pathways to large particles in flames. *Angew. Chem. Int. Ed.* **1998**, 37, 2434-2451.
7. Buseck, P. R.; Tsipursky, S. J., Hettich, R. Fullerenes from the geological environment. *Science* **1992**, 257, 215-217.
8. Heath, J. R.; O'Brien, S. C.; Zhang, Q.; Liu, Y.; Curl, R. F.; Kroto, H. W.; Tittel, F. K.; Smalley, R. E. Lanthanum Complexes of Spheroidal Carbon Shells. *J. Am. Chem. Soc.* **1985**, 107, 7779-7780.
9. Lu, X.; Feng, L.; Akasaka, T.; Nagase, S. Current status and future developments of endohedral metallofullerenes. *Chem. Soc. Rev.* **2012**, 41, 7723-7760.
10. Popov, A. A.; Yang, S.; Dunsch, L. Endohedral fullerenes. *Chem. Rev.* **2013**, 113, 5989-6113.
11. Almeida Murphy, T.; Pawlik, Th.; Weidinger, A.; Höhne, M.; Alcalá, R.; Spaeth, J.-M. Observation of atomlike nitrogen-implanted solid C₆₀. *Phys. Rev. Lett.* **1996**, 77, 1075- 1078.
12. Komatsu, K.; Murata, M.; Murata, Y. Encapsulation of molecular hydrogen in fullerenes C₆₀ by organic synthesis. *Science* **2005**, 307, 238-240.
13. Iwamatsu, S.; Uozaki, T.; Kobayashi, K.; Re, S.; Nagase, S.; Murata, S. A bowl-shaped fullerene encapsulates a water into the cage. *J. Am. Chem. Soc.* **2004**, 126, 2668-2669.

BIBLIOGRAPHY

14. Rubin, Y.; Jarrosson, T.; Wang, G.; Bartberger, M. D.; Houk, K. N.; Schick, G.; Saunders, M.; Cross, R. J. Insertion of helium and molecular hydrogen through the orifice of an open fullerene. *Angew. Chem., Int. Ed.* **2001**, 40, 1543-1546.
15. Darzynkiewicz, R. B.; Scuseria, G. E. Noble gas endohedral complexes of C₆₀ buckminsterfullerene. *J. Phys. Chem. A* **1997**, 101, 7141-7144.
16. Bloodworth, S.; Sitinova, G.; Alom, Vidal, S.; Bacanu, G. R.; Elliott, S. J.; Light, M. E.; Herniman, J. M.; Langley, G. J.; Levitt, M. H.; Whitby R. J. First synthesis and characterization of CH₄@C₆₀. *Angew. Chem. Int. Ed.* **2019**, 58, 5038-5043.
17. Krachmalnicoff, A.; Bounds, R.; Mamone, S.; Alom, S.; Concistrè, M.; Meier, B.; Kouřil, K.; Light, M. E.; Johnson, M. R.; Rols, S.; Horsewill, A. J.; Shugai, A.; Nagel, U.; Rõõm, T.; Carravetta, M.; Levitt, M. H.; Whitby, R. J. The dipolar endofullerene HF@C₆₀. *Nat. Chem.* **2016**, 8, 953-957.
18. Bloodworth, S.; Gråsvik, J.; Alom, S.; Kouřil, K.; Elliott, S. J.; Wells, N. J.; Horsewill, A. J.; Mamone, S.; Jiménez-Ruiz, M.; Rols, S.; Nagel, U.; Rõõm, T.; Levitt, M. H.; Whitby, R. J. Synthesis and properties of open fullerenes encapsulating ammonia and methane. *ChemPhysChem* **2018**, 19, 266-276.
19. Fagan, P. J.; Calabrese, J. C.; Malone, B. The chemical nature of buckminsterfullerene (C₆₀) and the characterization of a platinum derivative. *Science* **1991**, 252, 1160-1161.
20. Fagan, P. J.; Calabrese, J. C.; Malone, B. Metal complexes of buckminsterfullerene (C₆₀). *Acc. Chem. Res.* **1992**, 25, 134-142.
21. Bashilov, V. V.; Petrovskii, P. V.; Sokolov, V. I.; Lindeman, S. V.; Guzey, I. A.; Struchkov, Yu. T. Synthesis, crystal, and molecular structure of the palladium(0)-fullerene derivative (η^2 -C₆₀)Pd(PPh₃)₂. *Organometallics* **1993**, 12, 991-992.
22. Hideo, N.; Yoshiyuki, K.; Hirofumi, Y.; Eiji, K.; Teruhiko, K.; Masanao, K.; Yahachi, S.; Masaaki, H.; Kenji, I. Synthesis and reactions of organoplatinum compounds of C₆₀, C₆₀Pt_n. *Chem. Lett.* **1994**, 23, 1207-1210.
23. Loboda, O. *Quantum-chemical studies on porphyrins, fullerenes and carbon nanostructures*, Springer, Hardcover XVII, **2013**.
24. Wohlers, M.; Herzog, B.; Belz, T.; Bauer, A.; Braun, Th.; Rühle, Th.; Schlögl, R. Ruthenium-C₆₀ compounds: properties and catalytic potential. *Synth. Met.* **1996**, 77, 55-58.
25. Dresselhaus, M. S.; Dresselhaus, G.; Eklund, P. C. *Science of fullerenes and carbon nanotubes*. Academic press Inc., San Diego, **1996**.

26. Lerke, S. A.; Parkinson, B. A.; Evans, D. H.; Fagan, P. J. Electrochemical studies on metal derivatives of buckminsterfullerene (C_{60}). *J. Am. Chem. Soc.* **1992**, 114, 7807-7813.
27. Fagan, P. J.; Calabrese, J. C.; Malone, B. A multiply-substituted buckminsterfullerene (C_{60}) with an octahedral array of platinum atoms. *J. Am. Chem. Soc.* **1991**, 113, 9408-9409.
28. Talyzin, A.V.; Jansson, U. A comparative Raman study of some transition metal fullerenes. *Thin Solid Films* **2003**, 429, 96-101.
29. Kroto, H. W.; Jura, M. Circumstellar and interstellar fullerenes and their analogues. *Astron. Astrophys.* **1992**, 263, 275-280.
30. Bühl, M.; Hirsch, A. Spherical aromaticity of fullerenes. *Chem. Rev.* **2001**, 101, 1153-1184.
31. Baei, M. T.; Peyghan, A. A.; Bagheri, Z. Electronic, energetic, and geometric properties of methylene-functionalized C_{60} . *J. Clust. Sci.* **2013**, 24, 669-678.
32. Lee, K. H.; Suh, Y. S.; Park, S. S.; Lüthi, H. P.; Kim, D. H. Structures and energetics of pentahaptofullerene metal complexes. *Synth. Met.* **2001**, 121, 1163-1164.
33. Van Lier, G.; Cases, M.; Ewels, C. P.; Taylor, R.; Geerlings, P. Theoretical study of the addition patterns of C_{60} fluorination: $C_{60}F_n$ ($n = 1 - 60$). *J. Org. Chem.* **2005**, 70, 1565-1579.
34. Van Lier, G.; De Vleschouwer, F.; De Pril, P.; Geerlings, P. Theoretical prediction of the solubility of fluorinated C_{60} . *Phys. Chem. Chem. Phys.* **2009**, 11, 5175-5179.
35. Ravinder, P.; Subramanian, V. Density functional theory studies on the Diels–Alder reaction of [3]dendralene with C_{60} : an attractive approach for functionalization of fullerene. *Theor Chem Acc* **2012**, 131, 1128.
36. Muhr, H.-J.; Nesper, R.; Schnyder, B.; Kötz, R. The boron heterofullerenes $C_{59}B$ and $C_{69}B$: generation, extraction, mass spectrometric and XPS characterization. *Chem. Phys. Lett.* **1996**, 249, 399-405.
37. Kozlova, O.; Tamuliene, J. Modeling and investigations of the heterofullerenes. *Mater. Phys. Mach.* **2013**, 18, 63-69.
38. Lu, J.; Zhou, Y.; Luo, Y.; Huang, Y.; Zhang, X.; Zhao, X. Structural and electronic properties of heterofullerenes $C_{59}P$. *Mol. Phys.* **2001**, 99, 1203-1207.
39. Butcher, M. J.; Jones, F. H.; Beton, P. H.; Moriarty, P.; Cotier, B. N.; Upward, M. D.; Prassides, K.; Kordatos, K.; Tagmatarchis, N.; Wudl, F. et. al. $C_{59}N$ Monomers: Stabilization through Immobilization. *Phys. Rev. Lett.* **1999**, 83, 3478-3481.
40. Glenis, S.; Cooke, S.; Chen, X.; Labes, M. M. Photophysical properties of fullerenes prepared in an atmosphere of pyrrole. *Chem. Mater.* **1994**, 6, 1850-1853.

41. Guo, T.; Jin, C.; Smalley, R. E. Doping bucky: formation and properties of boron-doped buckminsterfullerene. *J. Phys. Chem.* **1991**, 95, 4948-4950.
42. Hummelen, J. C.; Knight, B.; Pavlovich, J.; Wudl, F. Isolation of the heterofullerene C₅₉N as its dimer (C₅₉N)₂. *Science* **1995**, 269, 1554-1556.
43. Batirev, I. G.; Lee, K. H.; Leiro, J. A. Atomic structure and chemical bonding of boro- and azafullerene dumb-bells. *J. Phys. Chem. Solids* **2000**, 61, 695-699.
44. Yadav, B. C.; Kumar, R. Structure, properties and applications of fullerenes. *Int. J. Nanotechnol. Applications* **2008**, 2, 15-24.
45. Collavini, S.; Delgado, J. L. Fullerenes: the stars of photovoltaics. *Sustainable Energy Fuels* **2018**, 2, 2480-2493.
46. Gokhale, M. M.; Somani, R. R. Fullerenes: chemistry and its applications. *Mini-Rev. Org. Chem.* **2015**, 12, 355-366.
47. Spohn, P.; Hirsch, C.; Hasler, F.; Bruinink, A.; Krug, H. F.; Wick, P. C₆₀ fullerene: a powerful antioxidant or a damaging agent? the importance of an in-depth material characterization prior to toxicity assays. *Environmental Pollution* **2009**, 157, 1134-1139.
48. Bakry, R.; Vallant, R. M.; Najam-Ul-Haq, M.; Rainer, M.; Szabo, Z.; Huck, C. W.; Bonn, G. K. Medicinal applications of fullerenes. *Int. J. Nanomed.* **2007**, 2, 639-649.
49. Mattesini, M.; Ahuja, R. Sab, L.; Hugosson, H.W.; Johansson, B.; Eriksson, O. Electronic structure and optical properties of solid C₆₀. *Physica B* **2009**, 404, 1776-1780.
50. Scheicher, R. H.; Li, S.; Araujo, C. M.; Blomqvist, A.; Ahuja, R.; Jena, P. Theoretical study of C₆₀ as catalyst for dehydrogenation in LiBH₄. *Nanotechnology* **2011**, 22, 335401.
51. Sutradhar, P.; Chauhan, V.; Khanna, S. N.; Atulasimha, J. Magnetic behavior of superatomic fullerene assemblies. *Phys. Chem. Chem. Phys.* **2017**, 19, 996-1002.
52. Chauhan, V.; Sahoo, S.; Khanna, S. N. Ni₉Te₆(PEt₃)₈C₆₀ Is a superatomic superalkali superparamagnetic cluster assembled material (S³-CAM). *J. Am. Chem. Soc.* **2016**, 138, 1916-1921.
53. Sitharaman, B.; Wilson, L. J. Gadofullerenes and gadonanotubes: a new paradigm for high-performance magnetic resonance imaging contrast agent probes. *J. Biomed. Nanotechnol.* **2007**, 3, 342-352.
54. Anilkumar, P.; Lu, F.; Cao, L.; Luo, P. G.; Liu, J.-H.; Sahu, S.; K., N. T., II; Wang, Y.; Sun, Y.-P. Fullerenes for applications in biology and medicine. *Curr. Med. Chem.* **2011**, 18, 2045-2059.

55. Zhang, J.; Liu, K. M.; Xing, G. M.; Ren, T. X.; Wang, S. K. J. Synthesis and in vivo study of metallofullerene based MRI contrast agent. *Radioanal. Nucl. Chem.* **2007**, 272, 605-609.
56. Iezzi, E. B.; Duchamp, J. C.; Fletcher, K. R.; Glass, T. E.; Dorn, H. C. Lutetium-based trimetallic nitride endohedral metallofullerenes: new contrast agents. *Nano Lett.* **2002**, 2, 1187-1190.
57. Kobayashi, K.; Kuwano, M.; Sueki, K.; Kikuchi, K.; Achiba, Y.; Nakahara, H.; Kananishi, N.; Watanabe, M.; Tomura, K. Activation and tracer techniques for study of metallofullerenes. *J. Radioanal. Nucl. Chem.* **1995**, 192, 81-89.
58. Horiguchi, Y.; Kudo, S.; Nagasaki, Y. Gd@C₈₂ metallofullerenes for neutron capture therapy-fullerene solubilization by poly(ethylene glycol)-block-poly(2-(N, N- diethylamino)ethyl methacrylate) and resultant efficacy in vitro. *Sci. Technol. Adv. Mater.* **2011**, 12, 044607.
59. Wang, J. X.; Chen, C. Y.; Li, B.; Yu, H. W.; Zhao, Y. L.; Sun, J.; Li, Y. F.; Xing, G. M.; Yuan, H.; Tang, J.; Chen, Z.; Meng, H.; Gao, Y. X.; Ye, C.; Chai, Z. F.; Zhu, C. F.; Ma, B. C.; Fang, X. H.; Wan, L. Antioxidative function and biodistribution of [Gd@C₈₂(OH)₂₂]_n nanoparticles in tumor-bearing mice. *Biochem. Pharmacol.* **2006**, 71, 872-881.
60. Yin, J.-J.; Lao, F.; Meng, J.; Fu, P. P.; Zhao, Y.; Xing, G.; Gao, X.; Sun, B.; Wang, P. C.; Chen, C.; Liang, X.-J. Inhibition of tumor growth by endohedral metallofullerenol nanoparticles optimized as reactive oxygen species scavenger. *Mol. Pharmacol.* **2008**, 74, 1132-1140.
61. Yakigaya, K.; Takeda, A.; Yokoyama, Y.; Ito, S.; Miyazaki, T.; Suetsuna, T.; Shimotani, H.; Kakiuchi, T.; Sawa, H.; Takagi, H.; Kitazawa, K.; Dragoe, N. Superconductivity of doped Ar@C₆₀. *New J. Chem.* **2007**, 31, 973-979.
62. Cioslowski, J. Endohedral chemistry: electronic structures of molecules trapped inside the C₆₀ cage. *J. Am. Chem. Soc.* **1991**, 113, 4139-4141.
63. Cioslowski, J.; Nanayakkara, A. Endohedral fullerites: A new class of ferroelectric materials. *Phys. Rev. Lett.* **1992**, 69, 2871-2873.
64. Feng, M.; Twamley, J. Readout scheme of the fullerene-based quantum computer by a single-electron transistor. *Phys. Rev. A* **2004**, 70, 030303.
65. Feng, M.; Twamley, J. Selective pulse implementation of two-qubit gates for spin-3/2-based fullerene quantum-information processing. *Phys. Rev. A* **2004**, 70, 032318.
66. Harneit, W.; Meyer, C.; Weidinger, A.; Suter, D.; Twamley, J. Architectures for a spin quantum computer based on endohedral fullerenes. *Phys. Status Solidi B* **2002**, 233, 453-461.

67. Tripathi, M. K.; Chandrakumar, K. R. S. The exemplary role of nanoconfinement in the proton transfer from acids to ammonia. *Phys. Chem. Chem. Phys.* **2017**, *19*, 19869-19872.
68. Esrafil, M. D.; Heidari, S. CO catalytic oxidation over C₅₉X heterofullerenes (X=B, Si, P, S): A DFT study. *Comp. Theor. Chem.* **2019**, 1151, 50-57.
69. Esrafil, M. D.; Heidari, S. C₅₉N heterofullerene: A promising catalyst for NO conversion into N₂O. *ChemistrySelect* **2019**, *4*, 4308-4315.
70. Esrafil, M. D.; Heidari, S. C₅₉X heterofullerenes (X=N, B, Si, P and S) as catalysts for reduction of N₂O: A comparative DFT study. *ChemistrySelect* **2019**, *4*, 2267-2274.
71. Cimpoesu, F.; Ito, S.; Shimotani, H.; Takagi, H.; Dragoe, N. Vibrational properties of noble gas endohedral fullerenes. *Phys. Chem. Chem. Phys.* **2011**, *13*, 9609-9615.
72. Felker, P. M.; Vlček, V.; Hietanen, I.; FitzGerald, S.; Neuhauser, D.; Bačić, Z. Explaining the symmetry breaking observed in the endofullerenes H₂@C₆₀, HF@C₆₀, and H₂O@C₆₀. *Phys. Chem. Chem. Phys.* **2017**, *19*, 31274-31283.
73. Tishchenko, O.; Truhlar, D. G. Atom-cage charge transfer in endohedral metallofullerenes: trapping atoms within a sphere-like ridge of avoided crossings. *J. Phys. Chem. Lett.* **2013**, *4*, 422-425.
74. Zhong, X.; Pandey, R.; Rocha, A. R.; Karna, S. P. Can single-atom change affect electron transport properties of molecular nanostructures such as C₆₀ fullerene? *J. Phys. Chem. Lett.* **2010**, *1*, 1584-1589.
75. Shameema, O.; Ramachandran, C. N.; Sathyamurthy, N. Blue-shift in X-H stretching frequency of molecules due to confinement. *J. Phys. Chem. A* **2006**, *110*, 2-4.
76. Khatua, M.; Pan, S.; Chattaraj, P. K. Movement of Ng₂ molecules confined in a C₆₀ cage: an Ab initio molecular Dynamics Study. *Chem. Phys. Lett.* **2014**, 610-611, 351-356.
77. Khatua, M.; Pan, S.; Chattaraj, P. K. Confinement of (HF)₂ in C_n (n = 60, 70, 80, 90) cages. *Chem. Phys. Lett.* **2014**, 616-617, 49-54.
78. Singh, M. K.; Rajaraman, G. Acquiring a Record Barrier Height for Magnetization Reversal in Lanthanide Encapsulated Fullerene Molecules Using DFT and Ab Initio Calculations. *Chem. Commun.* **2016**, *52*, 14047-14050.
79. Kaneko, S.; Hashikawa, Y.; Fujii, S.; Murata, Y.; Kiguchi, M. Single molecular junction study on H₂O@C₆₀: H₂O is electrostatically isolated. *ChemPhysChem* **2017**, *18*, 1229-1233.

80. Frecus, B.; Buta, C. M.; Oprea, C. I.; Stroppa, A.; Putz, M. V.; Cimpoesu, F. Noble gas endohedral fullerenes, Ng@C₆₀ (Ng=Ar, Kr): a particular benchmark for assessing the account of non-covalent interactions by density functional theory calculations. *Theor. Chem. Acc.* **2016**, 135,133.
81. Ravinder, P.; Subramanian, V. Fullerene based endohedral metallocenes. *Comp. Theor. Chem.* **2012**, 998, 106-112.
82. Cioslowski, J.; Fleischmann, E. D. Endohedral complexes: atoms and ions inside the C₆₀ cage. *J. Chem. Phys.* **1991**, 94, 3730-3734.
83. Weidinger, A.; Waiblinger, M.; Pietzak, B.; Almeida Murphy, T. Atomic nitrogen in C₆₀:N@C₆₀. *Appl. Phys. A: Mater. Sci. Process.* **1998**, 66, 287-292.
84. Wan, Z.; Christian, J. F.; Anderson, S. L. Collision of Li⁺ and Na⁺ with C₆₀: insertion, fragmentation, and thermionic emission. *Phys. Rev. Lett.* **1992**, 69, 1352-1355.
85. Wang, L. S.; Alford, J. M.; Chai, Y.; Diener, M.; Zhang, J.; McClure, S. M.; Guo, T.; Scuseria, G. E.; Smalley, R. E. The electronic structure of Ca@C₆₀. *Chem. Phys. Lett.* **1993**, 207, 354-359.
86. Lu, J.; Zhang, X.; Zhao, X. Metal-cage hybridization in endohedral La@C₆₀, Y@C₆₀ and Sc@C₆₀. *Chem. Phys. Lett.* **2000**, 332, 51-57.
87. Lu, J.; Zhou, Y.; Zhang, X.; Zhao, X. Density functional theory studies of beryllium-doped endohedral fullerene Be@C₆₀: on centre displacement of beryllium inside the C₆₀ cage. *Chem. Phys. Lett.* **2002**, 352, 8-11.
88. Türker, L. Certain endohedrally hydrogen doped Be@C₆₀ systems-a theoretically study. *J. Mol. Struct.: THEOCHEM* **2002**, 577, 205-211.
89. Ren, X.; Liu, Z.; Zhu, M.; Zheng, K. DFT studies on endohedral fullerene C@C₆₀: C centres the C₆₀ cage. *J. Mol. Struct.: THEOCHEM* **2004**, 710, 175-178.
90. Campbell, E. E. B.; Fanti, M.; Hertel, I. V.; Mitzner, R.; Zerbetto, F. The hyperpolarisability of an endohedral fullerene: Li@C₆₀. *Chem. Phys. Lett.* **1998**, 288, 131-137.
91. Naydenov, B.; Mende, J.; Harneit, W.; Mehring, M. Entanglement in P@C₆₀ encapsulated in a solid state matrix. *Phys. Status Solidi B* **2008**, 245, 2002-2005.
92. Rao, A. M.; Zhou, P.; Wang, K.; Hager, G. T.; Holden, J. M.; Wang, Y.; Lee, W.-T.; Bi, X.; Eklund, P. C.; Cornett, D. S. Photoinduced polymerization of solid C₆₀ films. *Science* **1993**, 259, 955-957.

93. Sheka E. H. Donor–acceptor interaction and fullerene C₆₀ dimerization. *Chem. Phys. Lett.* **2007**, 438, 119-126.
94. Pekker, S.; Jánossy, A.; Mihaly, L.; Chauvet, O.; Carrard, M.; Forró, L. Single-crystalline (KC₆₀)_n: a conducting linear alkali fulleride polymer. *Science* **1994**, 265, 1077-1078.
95. Iwasa, Y.; Arima, T.; Fleming, R. M.; Siegrist, T.; Zhou, O.; Haddon, R. C.; Rothberg, L. J.; Lyons, K. B.; Carter Jr., H. L.; Hebard, A. F.; Tycko, R.; Dabbagh, G.; Krajewski, J. J.; Thomas, G. A.; Yagi, T. New phases of C₆₀ synthesized at high pressure. *Science* **1994**, 264, 1570-1572.
96. Takahashi, N.; Dock, H.; Matsuzawa, N.; Ata, M. Plasma-polymerized C₆₀/C₇₀ mixture films: electric conductivity and structure. *J. Appl. Phys.* **1993**, 74, 5790-5798.
97. Zhao, Y. B.; Poirier, D. M.; Pechman, R. J.; Weaver, J. H. Electron stimulated polymerization of solid C₆₀. *Appl. Phys. Lett.* **1994**, 64, 577-579.
98. Zhou, P.; Dong, Z.-H.; Rao, A. M.; Eklund, P. C. Reaction mechanism for the photopolymerization of solid fullerene C₆₀. *Chem. Phys. Lett.* **1993**, 211, 337-340.
99. Strout, D. L.; Murry, R. L.; Xu, C.; Eckhoff, W. C.; Odom, G. K.; Scuseria, G. E. A theoretical study of buckminsterfullerene reaction products: C₆₀+C₆₀. *Chem. Phys. Lett.* **1993**, 214, 576-582.
100. Menon, M.; Subbaswamy, K. R. Structure and properties of C₆₀ dimers by generalized tight-binding molecular dynamics. *Phys. Rev. B* **1994**, 49, 13966-13969.
101. Adams, G. B.; Page, J. B.; Sankey, O. F.; O’Keeffe, M. Polymerized C₆₀ studied by first-principles molecular dynamics. *Phys. Rev. B* **1994**, 50, 17471-17479.
102. Wang, G.-W.; Komatsu, K.; Murata, Y.; Shiro, M. Synthesis and X-ray structure of dumbbell-shaped C₁₂₀. *Nature* **1997**, 387, 583-586.
103. Farrington, B. J.; Jevric, M.; Rance, G. A.; Ardavan, A.; Khlobystov, A. N.; Briggs, G. A. D.; Porfyakis, K. Chemistry at the nanoscale: synthesis of an N@C₆₀-N@C₆₀ endohedral fullerene dimer. *Angew. Chem., Int. Ed.* **2012**, 51, 3587-3590.
104. Park, J. M.; Tarakeshwar, P.; Kim, K. S.; Clark, T. Nature of the interaction of paramagnetic atoms (A = ⁴N, ⁴P, ³O, ³S) with π systems and C₆₀: A theoretical investigation of A···C₆H₆ and endohedral fullerenes A@C₆₀. *J. Chem. Phys.* **2002**, 116, 10684-10691.
105. Lu, J.; Zhang, X.; Zhao, X. Electronic structure of endohedral N@C₆₀, O@C₆₀, and F@C₆₀. *Chem. Phys. Lett.* **1999**, 312, 85-90.

106. Chi, M.; Han, P.; Fang, X.; Jia, W.; Liu, X.; Xu, B. Density functional theory of polonium-doped endohedral fullerenes Po@C_{60} . *J. Mol. Struct.: THEOCHEM* **2007**, 807, 121-124.
107. Equbal, A.; Srinivasan, S.; Ramachandran, C. N.; Sathyamurthy, N. Encapsulation of paramagnetic diatomic molecules B_2 , O_2 , and Ge_2 inside C_{60} . *Chem. Phys. Lett.* **2014**, 610, 251-255.
108. Lu, J.; Zhang, X.; Zhao, X. Electronic structure of endohedral Ca@C_{60} , Sc@C_{60} and Y@C_{60} . *Solid State Commun.* **1999**, 110, 565-568.
109. Lu, J.; Mei, W. N.; Gao, Y.; Zeng, X.; Jing, M.; Li, G.; Sabirianov, R.; Gao, Z.; You, L.; Xu, J. Structural and electronic properties of Gd@C_{60} : all-electronic relativistic total-energy study. *Chem. Phys. Lett.* **2006**, 425, 82-84.
110. Dai, X.; Cheng, C.; Zhang, W.; Xin, M.; Huai, P.; Zhang, R.; Wang, Z. Defect induced electronic structure of uranofullerene. *Sci. Rep.* **2013**, 3, 1341.
111. Dai, X.; Xin, M.; Meng, Y.; Han, J.; Gao, Y.; Zhang, W.; Jin, M.; Wang, Z.; Zhang, R. Stable electronic structure of a defective uranofullerene. *Carbon* **2014**, 78, 19-25.
112. Nakagawa, A.; Nishino, M.; Niwa, H.; Ishino, K.; Wang, Z.; Omachi, H.; Furukawa, K.; Yamaguchi, T.; Kato, T.; Bandow, S.; Rio, J.; Ewels, C. P.; Aoyagi, S.; Shinohara, H. Crystalline functionalized endohedral C_{60} metallofullerides. *Nat. Comm.*, **2018**, 9, 3073.
113. Qian, M.; Ong, S. V.; Khanna, S. V.; Knickelbein, M. B. Magnetic endohedral metallofullerenes with floppy interiors. *Phys. Rev. B.* **2007**, 75, 104424.
114. Vostrowsky, O.; Hirsch, A. Heterofullerenes. *Chem. Rev.* **2006**, 106, 5191-5207.
115. Ewels, C. P.; Cheikh, H. E.; Suarez-Martinez, I.; Van Lier, G. Oxidation and reactivity of nitrogen- and phosphorus-doped heterofullerenes. *Phys. Chem. Chem. Phys.* **2008**, 10, 2145-2148.
116. Jing-Nan, L.; Bing-Lin, G.; Ru-Shan, H. Electronic structures of doped fullerenes with boron and nitrogen atoms. *Solid State Commun.* **1992**, 84, 807-810.
117. Andreoni, W.; Gygi, F.; Parrinello, M. Impurity states in doped fullerenes: C_{59}B and C_{59}N . *Chem. Phys. Lett.* **1992**, 190, 159-162.
118. Mekky, A. H.; Elhaes, H.; El-Oker, M. M.; Ibrahim, M. A. Electronic properties of substituted C_{59}X ($\text{X} = \text{C}, \text{B}, \text{Al}, \text{Ga}, \text{In}$) fullerene. *Mater. Sci.: Indian J.* **2016**, 2, 50-55.
119. Bai, H.; Ji, W.; Liu, X.; Wang, L.; Yuan, N.; Ji, Y. Doping the buckminsterfullerene by substitution: density functional theory studies of C_{59}X ($\text{X} = \text{B}, \text{N}, \text{Al}, \text{Si}, \text{P}, \text{Ga}, \text{Ge}, \text{and As}$). *J. Chem.* **2012**, 2013, 1-9.

120. Ramachandran, C. N.; Sathyamurthy, N. Time-dependent density functional theoretical study of the absorption properties of BN-substituted C_{60} fullerenes. *J. Phys. Chem. A* **2007**, *111*, 6901-6903.
121. Simon, F.; Arcon, D.; Tagmatarchis, N.; Garaj, S.; Forro, L.; Prassides, K. ESR signal in azafullerene $(C_{59}N)_2$ induced by thermal homolysis. *J. Phys. Chem. A* **1999**, *103*, 6969-6971.
122. Schrier, J.; Whaley, K. B. Hyperfine coupling constants of the azafullerenes $C_{19}N$, $C_{59}N$, $C_{69}N$, and $C_{75}N$. *J. Phys. Chem. A* **2006**, *110*, 5386-5390.
123. Pichler, T.; Knupfer, M.; Golden, M. S.; Haffner, S.; Friedlein, R.; Fink, J. On-ball doping of fullerenes: The electronic structure of $C_{59}N$ dimers from experiment and theory. *Phys. Rev. Lett.* **1997**, *78*, 4249-4252.
124. Hirsch, A.; Nuber, B. Nitrogen heterofullerenes. *Acc. Chem. Res.* **1999**, *32*, 795-804.
125. Tenne, R. Doped and heteroatom-containing fullerene-like structures and nanotubes. *Adv. Mater.* **1995**, *7*, 965-995.
126. Huczko, A. Heterohedral fullerenes and nanotubes: formation and characteristics. *Fullerene Sci. Technol.* **1997**, *5*, 1091-1131.
127. Ying, Z. C.; Zhu, J. G.; Compton, R. N.; Allard, L. F., Jr.; Hettich, R. L.; Haufler, R. E. Synthesis of doped fullerene clusters and boron-nitrogen tubules using laser ablation. *ACS Symp. Ser.* **1997**, *679*, 169-182.
128. Mattay, J.; Torres-Garcia, G.; Averdung, J.; Wolff, C.; Schlachter, I.; Luftmann, H.; Siedschlag, C.; Luger, P.; Ramm, M. Progress in fullerene chemistry: exohedral functionalization of first and second generation and a new approach to aza-heterofullerenes. *J. Phys. Chem. Solids* **1997**, *58*, 1929-1937.
129. Hirsch, A. Aspects of organic chemistry of fullerenes. *J. Phys. Chem. Solids* **1997**, *58*, 1729-1740.
130. Bellavia-Lund, C.; Hummelen, J. C.; Keshavarz-K., M.; González, R.; Wudl, F. New developments in the organic chemistry of fullerenes. *J. Phys. Chem. Solids* **1997**, *58*, 1983-1990.
131. Bellavia-Lund, C.; Keshavarz-K., M.; González, R.; Hummelen, J. C.; Hicks, R.; Wudl, F. Heterocyclic and heteroatom derivatives of buckminsterfullerene C_{60} . *Phosphorus, Sulfur Silicon Relat. Elem.* **1997**, *120*, 107-119.
132. Kuzmany, H. Fullerenforschung in der zweiten generation. *Physik in unserer Zeit* **1998**, *29*, 16-21.

133. Reuther, U.; Hirsch, A. Synthesis, properties and chemistry of aza[60]fullerene. *Carbon* **2000**, 38, 1539-1549.
134. Averdung, J.; Torres-Garcia, G.; Luftmann, H.; Luger, P.; Schlachter, I.; Mattay, J. Progress in fullerene chemistry: from exohedral functionalization to heterofullerenes. *Fullerene Sci. Technol.* **1996**, 4, 633-654.
135. Buchachenko, A. L.; Breslavskaya, N. N. Chemical bond inside endohedral complexes H@C₅₉B and H@C₅₉P. *Russ. Chem. Bull.* **2007**, 56, 1283-1288.
136. Hashikawa, Y.; Murata, M.; Wakamiya, A.; Murata, Y. Synthesis and properties of endohedral aza[60]fullerenes: H₂O@C₅₉N and H₂@C₅₉N as their dimers and monomers. *J. Am. Chem. Soc.* **2016**, 138, 4096-4104.
137. Hashikawa, Y.; Murata, M.; Wakamiya, A.; Murata, Y. Orientation of a water molecule: effects on electronic nature of the C₅₉N Cage. *J. Org. Chem.* **2017**, 82, 4465-4469.
138. Hashikawa, Y.; Murata, Y. Facile access to azafullerenyl cation C₅₉N⁺ and specific interaction with entrapped molecules. *J. Am. Chem. Soc.* **2017**, 139, 18468-18471.
139. Guo-Zhu Zhu, G.-Z.; Liu, Y.; Hashikawa, Y.; Zhang, Q.-F.; Murata, Y.; Wang, L.-S. Probing the interaction between the encapsulated water molecule and the fullerene cages in H₂O@C₆₀⁻ and H₂O@C₅₉N⁻. *Chem. Sci.* **2018**, 9, 5666-5671.
140. Singh, M. K.; Yadav, N.; Rajaraman, G. Record high magnetic exchange and magnetization blockade in Ln₂@C₇₉N (Ln = Gd(III) and Dy(III)) molecules: a theoretical perspective. *Chem. Commun.* **2015**, 51, 17732-17735.
141. Dresselhaus, M. S.; Dresselhaus, G.; Saito, R. Physics of carbon nanotubes. *Carbon* **1995**, 33, 883-891.
142. Dalton, A. B.; Collins, S.; Muñoz, E.; Razal, J. M.; Ebron, V. H.; Ferraris, J. P.; Coleman, J. N.; Kim, B. G.; Baughman, R. H. Super-tough carbon-nanotube fibres. *Nature* **2003**, 423, 703.
143. Tasis, D.; Tagmatarchis, N.; Bianco, A.; Prato, M. Chemistry of carbon nanotubes. *Chem. Rev.* **2006**, 106, 1105-1136.
144. Yu, L.; Shearer, C.; Shapter, J. Recent development of carbon nanotube transparent conductive films. *Chem. Rev.* **2016**, 116, 13413-13453.
145. Janas, D. Towards monochiral carbon nanotubes: a review of progress in the sorting of single-walled carbon nanotubes. *Mater. Chem. Front.* **2018**, 2, 36-63.

146. Tiano, A. L.; Park, C.; Lee, J. W.; Luong, H. H.; Gibbons, L. J.; Chu, S.-H.; Applin, S.; Gnoffo, P.; Lowther, S.; Kim, H. J.; Boron nitride nanotube: synthesis and applications. Varadan, V. K., Ed.; Springer: San Diego, California, USA, 2014; 906006.
147. Kim, J. H.; Pham, T. V.; Hwang, J. H.; Kim, C. S.; Kim, M. J. Boron nitride nanotubes: synthesis and applications. *Nano Converg.* **2018**, 5, 17.
148. Kalay, S.; Yilmaz, Z.; Sen, O.; Emanet, M.; Kazanc, E.; Çulha, M. Synthesis of boron nitride nanotubes and their applications. *Beilstein J. Nanotechnol.* **2015**, 6, 84-102.
149. Chopra, N. G.; Luyken, R. J.; Cherrey, K.; Crespi, V. H.; Cohen, M. L.; Louie, S. G.; Zettl, A. Boron nitride nanotubes. *Science* **1995**, 269, 966-967.
150. Guo, T.; Nikolaev, P.; Rinzler, A. G.; Tomànek, D.; Colbert, D. T.; Smalley, R. E. Self-assembly of tubular fullerenes. *J. Phys. Chem.* **1995**, 99, 10694-10697.
151. Endo, M.; Takeuchi, K.; Igarashi, S.; Kobori, K.; Shiraishi, M.; Kroto, H. W. The production and structure of pyrolytic carbon nanotubes (PCNTs). *Phys. Chem. Solids* **1993**, 54, 1841-1848.
152. Bhauriyal, P.; Mahata, A.; Pathak, B. A computational study of single-walled carbon nanotube based ultrafast high capacity Al battery. *Chem.-Asian J.* **2017**, 12, 1944-1951.
153. Chavan, R.; Desai, U.; Mhatre, P.; Chinchole, R. A Review: Carbon nanotubes. *Int. J. Pharm. Sci. Rev. Res.* **2012**, 13, 125-134.
154. De Volder, M. F.; Tawfick, S. H.; Baughman, R. H.; Hart, A. J. Carbon nanotubes: present and future commercial applications. *Science* **2013**, 339, 535-539.
155. Abdalla, S.; Al-Marzouki, F.; Al-Ghamdi, A. A.; Abdel-Daiem, A. Different technical applications of carbon nanotubes. *Nanoscale Res. Lett.* **2015**, 10, 358.
156. Alshehri, R.; Ilyas, A. M.; Hasan, A.; Arnaout, A.; Ahmed, F.; Memic, A. Carbon nanotubes in biomedical applications: factors, mechanisms, and remedies of toxicity. *J. Med. Chem.* **2016**, 59, 8149-8167.
157. Schnorr, J. M.; Swager, T. M. Emerging applications of carbon nanotubes. *Chem. Mater.* **2011**, 23, 646-657.
158. Bekyarova, E.; Ni, Y.; Malarkey, E. B.; Montana, V.; McWilliams, J. L.; Haddon, R. C.; Parpura, V. Applications of carbon nanotubes in biotechnology and biomedicine. *J. Biomed. Nanotechnol.* **2005**, 1, 3-17.
159. Khanna, S.; Islam, N. Carbon nanotubes-properties and applications. *Organic and Medicinal Chem. Int. J.* **2018**, 7, 555705.

160. Alshehri, M. H.; Cox, B. J.; Hill, J. M. Interaction of double-stranded DNA inside single-walled carbon nanotubes. *J. Math. Chem.* **2012**, *50*, 2512-2526.
161. Su, Z.; Zhu, S.; Donkor, A. D.; Tzoganakis, C.; Honek, J. F. Controllable delivery of small-molecule compounds to targeted cells utilizing carbon nanotubes. *J. Am. Chem. Soc.* **2011**, *133*, 6874-6877.
162. Dappe, Y. J. Encapsulation of organic molecules in carbon nanotubes: role of the van der Waals interactions. *J. Phys. D: Appl. Phys.* **2014**, *47*, 083001.
163. Miners, S. A.; Rance, G. A.; Khlobystov, A. N. Chemical reactions confined within carbon nanotubes. *Chem. Soc. Rev.* **2016**, *45*, 4727-4746.
164. Manzetti, S. Molecular and crystal assembly inside the carbon nanotube: encapsulation and manufacturing approaches. *Adv. Manuf.* **2013**, *1*, 198-210.
165. Kou, L.; Tang, C.; Wehling, T.; Frauenheim, T.; Chen, C. F. Emergent properties and trends of a new class of carbon nanocomposites: graphene nanoribbons encapsulated in a carbon nanotube. *Nanoscale* **2013**, *5*, 3306-3314.
166. Lee, J.; Lee, W.; Sim, K.; Han, S.-H.; Yi, W. Field emission properties of single-walled carbon nanotube with amphoteric doping by encapsulation of TTF and TCNQ. *J. Vac. Sci. Technol. B* **2008**, *26*, 847-850.
167. Shiraishi, M.; Nakamura, S.; Fukao, T.; Takenobu, T.; Kataura, H.; Iwasa, Y. Control of injected carriers in tetracyano-p-quinodimethane encapsulated carbon nanotube transistors. *Appl. Phys. Lett.* **2005**, *87*, 093107.
168. Nieto-Ortega, B.; Villalva, J.; Vera-Hidalgo, M.; Ruiz-González, L.; Burzurí, E.; Pérez, E. M. Band-gap opening in metallic single-walled carbon nanotubes by encapsulation of an organic salt. *Angew. Chem., Int. Ed.*, **2017**, *56*, 12240-12244.
169. Gao, C.; Guo, Z.; Liu, J. H.; Huang, X. J. The new age of carbon nanotubes: An updated review of functionalized carbon nanotubes in electrochemical sensors. *Nanoscale* **2012**, *4*, 1948-1963.
170. Setaro, A. Advanced carbon nanotubes functionalization. *J. Phys.: Condens. Matter* **2017**, *29*, 423003.
171. Xu, J.; Cao, Z.; Zhang, Y.; Yuan, Z.; Lou, Z.; Xu, X.; Wang, X. A review of functionalized carbon nanotubes and graphene for heavy metal adsorption from water: preparation, application, and mechanism. *Chemosphere* **2018**, *195*, 351-364.

172. Sun, Y.-P.; Fu, K.; Lin, Y.; Huang, W. Functionalized carbon nanotubes: properties and applications. *Acc. Chem. Res.* **2002**, *35*, 1096-1104.
173. Alshehri, M. H.; Cox, B. J.; Hill, J. M. Interaction of double-stranded DNA inside single-walled carbon nanotubes. *J. Math. Chem.* **2012**, *50*, 2512-2526.
174. Lulevich, V.; Kim, S.; Grigoropoulos, C. P.; Noy, A. Frictionless sliding of single-stranded DNA in a carbon nanotube pore observed by single molecule force spectroscopy. *Nano Lett.* **2011**, *11*, 1171-1176.
175. Salvador-Morales, C.; Flahaut, E.; Sim, E.; Sloan, J.; Green, M. L. H.; Sim, R. B. Complement activation and protein adsorption by carbon nanotubes. *Mol. Immunol.* **2006**, *43*, 193-201.
176. Mandal, B.; Sarkar, S.; Sarkar, P. Energetics and electronic structure of encapsulated graphene nanoribbons in carbon nanotube. *J. Phys. Chem. A* **2013**, *117*, 8568-8575.
177. Kou, L.; Tang, C.; Wehling, T.; Frauenheim, T.; Chen, C. F. Emergent properties and trends of a new class of carbon nanocomposites: graphene nanoribbons encapsulated in a carbon nanotube. *Nanoscale* **2013**, *5*, 3306-3314.
178. Nieto-Ortega, B.; Villalva, J.; Vera-Hidalgo, M.; Ruiz-González, L.; Burzurí, E.; Pérez, E. M. Band-gap opening in metallic single-walled carbon nanotubes by encapsulation of an organic salt. *Angew. Chem., Int. Ed.* **2017**, *56*, 12240-12244.
179. Li, K.; He, H. Y.; Xu, B.; Pan, B. C. The stabilities of gallium nanowires with different phases encapsulated in a carbon nanotube. *J. Appl. Phys.* **2009**, *105*, 054308.
180. Parq, J. H.; Yu, J.; Kim, G. First-principles study of ultrathin (2×2) Gd nanowires encapsulated in carbon nanotubes. *J. Chem. Phys.* **2010**, *132*, 054701.
181. Zhou, J.; Yan, X.; Luo, G.; Qin, R.; Li, H.; Lu, J.; Mei, W. N.; Gao, Z. Structural, electronic, and transport properties of Gd/Eu atomic chains encapsulated in single-walled carbon nanotubes. *J. Phys. Chem. C* **2010**, *114*, 15347-15353.
182. Paduani, C. Structure and electronic properties of a Mn nanowire encapsulated in carbon nanotubes. *J. Solid State Chem.* **2013**, *201*, 201, 204-207.
183. Wang, H.; Li, B.; Yang, J. Electronic, optical, and mechanical properties of diamond nanowires encapsulated in carbon nanotubes: A first-principles view. *J. Phys. Chem. C* **2017**, *121*, 3661-3672.

184. Li, Y.; Bai, H.; Li, L.; Huang, Y. Stabilities and electronic properties of nanowires made of single atomic sulfur chains encapsulated in zigzag carbon nanotubes. *Nanotechnology* **2018**, *29*, 415703.
185. Li, Y.; Bai, H.; Lin, F.; Huang, Y. Energetics and electronic structures of nitrogen chains encapsulated in zigzag carbon nanotube. *Physica E* **2018**, *103*, 444-451.
186. Kuwahara, R.; Kudo, Y.; Morisato, T.; Ohno, K. Encapsulation of carbon chain molecules; in single-walled carbon nanotubes. *J. Phys. Chem. A* **2011**, *115*, 5147-5156.
187. Khorsand, A.; Jamehbozorgi, S.; Ghiasi, R.; Rezvani, M. Structural, energetic and electrical properties of encapsulation of penicillamine drug into the CNTs based on vdW-DF perspective. *Physica E* **2015**, *72*, 120-127.
188. Yumura, T.; Yamashita, H. Key factors in determining the arrangement of π -conjugated oligomers inside carbon nanotubes. *Phys. Chem. Chem. Phys.* **2015**, *17*, 22668-22677.
189. Wang, Y.; Xu, Z. Interaction mechanism of doxorubicin and SWCNT: protonation and diameter effects on drug loading and releasing. *RSC Adv.* **2016**, *6*, 314-322.
190. García, G.; Ciofini, I.; Fernández-Gómez, M.; Adamo, C. Confinement effects on UV-visible absorption spectra: β -carotene inside carbon nanotube as a test case. *J. Phys. Chem. Lett.* **2013**, *4*, 1239-1243.
191. Orellana, W.; Vasquez, S. O. Endohedral terthiophene in zigzag carbon nanotubes: density functional calculations. *Phys. Rev. B* **2006**, *74*, 125419.
192. Debbichi, L.; Dappe, Y. J.; Alouani, M. Effect of van der Waals interaction on energetics and transport properties of a single anthracene molecule adsorbed or confined inside a carbon nanotube. *Phys. Rev. B* **2012**, *85*, 045437.
193. Chernov, A. I.; Fedotov, P. V.; Talyzin, A. V.; Suarez Lopez, I.; Anoshkin, I. V.; Nasibulin, A. G.; Kauppinen, E. I.; Obratsova, E. D. Optical properties of graphene nanoribbons encapsulated in single-walled carbon nanotubes. *ACS Nano* **2013**, *7*, 6346- 6353.
194. Tripathy, M. K.; Jena, N. K.; Samanta, A. K.; Ghosh, S. K.; Chandrakumar, K.R.S. Effect of confinement on the structure and energetics of Zundel cation present inside the hydrophobic carbon nanotubes: an *ab initio* study. *Theor. Chem. Acc.* **2014**, *133*, 1576.
195. Tripathy, M. K.; Jena, N. K.; Samanta, A. K.; Ghosh, S. K.; Chandrakumar, K.R.S. Theoretical investigations on Zundel cation present inside boron-nitride nanotubes: Effect of confinement and hydrogen bonding. *Chem. Phys.* **2015**, *446*, 127-133.

196. Sozykin, S. A.; Beskachko, V. P. Structure of endohedral complexes of carbon nanotubes encapsulated with lithium and sodium. *Mol. Phys.* **2013**, 111, 930-938.
197. Li, Y.; Kaneko, T.; Ogawa, T.; Takahashi, M.; Hatakeyama, R. Novel properties of single-walled carbon nanotubes with encapsulated magnetic atoms. *Jpn. J. Appl. Phys.* **2008**, 47, 2048-2055.
198. del Carmen Giménez-López, M.; Moro, F.; La Torre, A.; Gómez-García, C. J.; Brown, P. D.; van Slageren, J.; Khlobystov, A. N. Encapsulation of single-molecule magnets in carbon nanotubes. *Nat. Commun.* **2011**, 2, 407.
199. Kumar, P.; Ramachandran, C. N.; Mishra, B. K.; Sathyamurthy, N. Interaction of rare gas dimers in the confines of a carbon nanotube. *Chem. Phys. Lett.* **2015**, 618, 42-45.
200. Balasubramani, S. G.; Singh, D.; Swathi, R. S. Noble gas encapsulation into carbon nanotubes: Predictions from analytical model and DFT studies. *J. Chem. Phys.* **2014**, 141, 184304.
201. Clark, T. *A Handbook of Computational Chemistry*, Wiley, **1985**.
202. Jensen, F. *Introduction to Computational Chemistry*, John Wiley & Sons, Chichester, **2013**.
203. Leach, A. R. *Molecular Modelling: Principles and Applications*, Pearson Education Limited, Harlow, **2001**.
204. Szabo, A.; Ostlund, N. S. *Modern Quantum Chemistry: Introduction to Advanced Electronic Structure Theory*, Dover Publications Inc., Mineola, **1989**.
205. Atkins, P. W.; Friedman, R. S. *Molecular quantum mechanics*, Oxford University Press, Oxford, **2011**.
206. Levine, I. N. *Quantum Chemistry*. 7th Edition, Pearson, **2014**.
207. Griffiths, D. *Introduction to Quantum Mechanics. 2nd Edition*, Pearson, **2005**.
208. Cramer, C. *Essentials of Computational Chemistry: Theories and Models*, Wiley, **2005**.
209. Parr, R. G.; Yang, W. *Density Functional Theory of Atoms and Molecules*, Oxford University Press, Oxford, **1989**.
210. Koch, W.; Holthausen, M. C. *A Chemist's Guide to Density Functional Theory*, Wiley-VCH, Weinheim, **2012**.
211. Thomas, L. H. In *Mathematical Proceedings of the Cambridge Philosophical Society*, Vol. 23, Cambridge Univ Press, **1927**, 542.
212. Fermi, E. Statistical method to determine some properties of atoms. *Rend. Accad. Naz. Lincei* **1927**, 6, 602.

213. Dirac, P. A. M. On the annihilation of electrons and protons. Mathematical proceedings of the Cambridge philosophical society. *Proc. Cambridge Phil. Roy. Soc.* **1930**, 26, 361-365.
214. Hohenberg, P.; Kohn, W. Inhomogeneous electron gas. *Phys. Rev. B* **1964**, 136, 864-871.
215. Kohn, W.; Sham, L. J. Self-consistent equations including exchange and correlation effects. *Phys. Rev.* **1965**, 140, 1133-1138.
216. Perdew, J. P.; Zunger, A. Self-interaction correction to density-functional approximations for many-electron systems. *Phys. Rev. B* **1981**, 23, 5048-5079.
217. Perdew, J. P.; Wang, Y. Accurate and simple analytic representation of the electron-gas correlation energy. *Phys. Rev. B* **1992**, 45, 13244-13249.
218. Vosko, S. J.; Milk, L.; Nusair, M. Accurate spin-dependent electron liquid correlation energies for local spin density calculations: a critical analysis. *Can. J. Phys.* **1980**, 58, 1200-1211.
219. Perdew, J. P.; Burke, K.; Wang, Y. Generalized gradient approximation for the exchange-correlation hole of a many-electron system. *Phys. Rev. B*, **1996**, 54, 16533-16539.
220. Becke, A. D. Density-functional exchange-energy approximation with correct asymptotic behavior. *Phys. Rev. A* **1988**, 38, 3098-3100.
221. Lee, C.; Yang, W.; Parr, R. G. Development of the Colle-Salvetti correlation-energy formula into a functional of the electron density. *Phys. Rev. B* **1988**, 37, 785-789.
222. Perdew, J. P. Density-functional approximation for the correlation energy of the inhomogeneous electron gas. *Phys. Rev. B* **1986**, 33, 8822-8824.
223. Perdew, J. P.; Burke, K.; Ernzerhof, M. Generalized gradient approximation made simple. *Phys. Rev. Lett.* **1996**, 77, 3865-3868.
224. Becke, A. D. Density-functional thermochemistry. III. The role of exact exchange. *J. Chem. Phys.* **1993**, 98, 5648-5652.
225. Stephens, P. J.; Devlin, F. J.; Chabalowski, C. F.; Frisch, M. J. *Ab initio* calculation of vibrational absorption and circular dichroism spectra using density functional force fields. *J. Phys. Chem.* **1994**, 98, 11623-11627.
226. Adamo, C.; Barone, V. Toward reliable density functional methods without adjustable parameters: The PBE0 model. *J. Chem. Phys.* **1999**, 110, 6158-6170.
227. Heyd, J.; Scuseria, G. E.; Ernzerhof, M. Hybrid functional based on a screened coulomb potential. *J. Chem. Phys.* **2003**, 118, 8207-8215.

228. Zhao, Y.; Truhlar, D. G. The M06 suite of density functionals for main group thermochemistry, thermochemical kinetics, noncovalent interactions, excited states, and transition elements: two new functionals and systematic testing of four M06-class functionals and 12 other functionals. *Theor. Chem. Account* **2008**, *120*, 215-241.
229. Becke, A. D. A new mixing of Hartree-Fock and local density-functional theories. *J. Chem. Phys.* **1993**, *98*, 1372-1377.
230. Zhao, Y.; Schultz, N. E.; Truhlar, D. G. Exchange-correlation functional with broad accuracy for metallic and nonmetallic compounds, kinetics, and noncovalent interactions *J. Chem. Phys.* **2005**, *123*, 161103.
231. Zhao, Y.; Truhlar, D. G. Exploring the limit of accuracy of the global hybrid meta density functional for main-group thermochemistry, kinetics, and noncovalent interactions. *J. Chem. Theor. Comput.* **2008**, *4*, 1849-1868.
232. Peverati, R.; Truhlar, D. G. M11-L: A local density functional that provides improved accuracy for electronic structure calculations in chemistry and physics. *J. Phys. Chem. Lett.* **2012**, *3*, 117-124.
233. Peverati, R.; Truhlar, D. G. Improving the accuracy of hybrid Meta-GGA density functionals by range separation. *J. Phys. Chem. Lett.* **2011**, *2*, 2810-2817.
234. Peverati, R.; Truhlar, D.G. Exchange–correlation functional with good accuracy for both structural and energetic properties while depending only on the density and its gradient. *J. Chem. Theor. Comput.* **2012**, *8*, 2310-2319.
235. Sathe, R. Y.; Kumar, T. J. D. Paracyclophane functionalized with Sc and Li for hydrogen storage. *Chem. Phys. Lett.* **2018**, *692*, 253-257.
236. Kumar, S.; Sathe, R. Y.; Kumar, T. J. D. Sc and Ti-functionalized 4-tert-butylcalix[4]arene as reversible hydrogen storage material. *Int. J. Hydrogen Energy* **2019**, *44*, 12724-12732.
237. Hobza, P.; Šponer, J.; Reschel, T. Density functional theory and molecular clusters. *J. Comput. Chem.* **1995**, *16*, 1315-1325.
238. Allen, M.; Tozer, D. J. Helium dimer dispersion forces and correlation potentials in density functional theory. *J. Chem. Phys.* **2002**, *117*, 11113-11120.
239. Kristyán, S.; Pulay, P. Can (semi)local density functional theory account for the London dispersion forces? *Chem. Phys. Lett.* **1994**, *229*, 175-180.
240. Grimme, S. Semiempirical GGA-type density functional constructed with a long-range dispersion correction. *J. Comput. Chem.* **2006**, *27*, 1787– 1799.

241. Grimme, S.; Antony, J.; Ehrlich, S.; Krieg, H. A consistent and accurate ab initio parameterization of density functional dispersion correction (DFT-D) for the 94 elements H-Pu. *J. Chem. Phys.* **2010**, *132* 154104.
242. Grimme, S. Semiempirical GGA-type density functional constructed with a long-range dispersion correction. *J. Comp. Chem.* **2006**, *27*, 1787-1799.
243. Goerigk, L.; Grimme, S. Efficient and accurate double-hybrid-Meta-GGA density functionals-evaluation with the extended GMTKN30 database for general main group thermochemistry, kinetics, and noncovalent interactions. *J. Chem. Theor. Comput.* **2011**, *7*, 291-309.
244. Chai, J.-D.; Gordon, M.-H. Long-range corrected hybrid density functionals with damped atom-atom dispersion corrections. *Phys. Chem. Chem. Phys.* **2008**, *10*, 6615-6620.
245. De Oliveira, O. V.; Gonçalves, A. da S. Quantum chemical studies of endofullerenes (M@C₆₀) where M = H₂O, Li⁺, Na⁺, K⁺, Be²⁺, Mg²⁺, and Ca²⁺. *Comp. Chem.* **2014**, *2*, 51-58.
246. Schiller, F.; Ruiz-Osés, M.; Ortega, G. E.; Segovia, P.; Martínez-Blanco, J.; Doyle, B. P.; Pérez-Dieste, V.; Lobo, J.; Néel, N.; Berndt, R.; Kröger, J. Electronic structure of C₆₀ on Au(887). *J. Chem. Phys.* **2006**, *125*, 144719.
247. Scheier, P.; Dünser, B.; Wörgötter, R.; Lezius, M.; Robl, R.; Märk, T. D. Appearance and ionization energies of singly, doubly, and triply charged C₆₀ and its fragment ions produced by electron impact ionization. *Int. J. Mass Spectrom. Ion Processes* **1994**, *138*, 77-93.
248. Palpant, B.; Otake, A.; Hayakawa, F.; Negishi, Y.; Lee, G. H.; Nakajima, A.; Kaya, K.; Photoelectron spectroscopy of sodium-coated C₆₀ and cluster anions. *Phys. Rev. B. Condens. Matter. Mater. Phys.* **1999**, *60*, 4509-4512.
249. Slater, J. C. Atomic shielding constants. *Phys. Rev.* **1930**, *36*, 57-64.
250. Boys, S. F. Electronic wave functions - I. A general method of calculation for the stationary states of any molecular system. *Proc. R. Soc. London Ser. A.* **1950**, *200*, 542.
251. Krishnan, R.; Binkley, J. S.; Seeger, R.; Pople, J. A. Self-consistent molecular orbital methods. XX. A basis set for correlated wave functions. *J. Chem. Phys.* **1980**, *72*, 650- 654.
252. Dunning, T. H. Gaussian basis sets for use in correlated molecular calculations. I. The atoms boron through neon and hydrogen *J. Chem. Phys.* **1989**, *90*, 1007-1023.
253. Runge, E.; Gross, E. K. U. Density-functional theory for time-dependent systems. *Phys. Rev. Lett.* **1984**, *52*, 997-1000.

254. Casida, M. E. Time-dependent density-functional theory for molecules and molecular solids. *J. Mol. Struct.:(THEOCHEM)* **2009**, 914, 3–18.
255. Marques, M. A. L.; Maitra, N. T.; Nogueira, F. M. S.; Gross, E. K. U.; Rubio, A. *Fundamentals of Time-Dependent Density Functional Theory*; Springer Berlin Heidelberg: Germany, **2012**.
256. Borden, W. T.; Davidson, E. R.; Feller, D. RHF and two-configuration SCF calculations are inappropriate for conjugated diradicals. *Tetrahedron* **1982**, 38, 737-739.
257. Noodleman, L. Valence bond description of antiferromagnetic coupling in transition metal dimers. *J. Chem. Phys.* **1981**, 74, 5737-5743.
258. Noodleman, L.; Baerends, E. J. Electronic structure, magnetic properties, ESR, and optical spectra for 2-iron ferredoxin models by LCAO-X.alpha. valence bond theory. *J. Am. Chem. Soc.* **1984**, 106, 2316-2327.
259. Noodleman, L.; Case, D. A.; Aizman, A. Broken symmetry analysis of spin coupling in iron-sulfur clusters. *J. Am. Chem. Soc.* **1988**, 110, 1001-1005.
260. Renard, V.T.; Piot, B. A.; Waintal, X.; Fleury, G.; Cooper, D.; Niida, Y.; Tregurtha, D.; Fujiwara, A.; Hirayama, Y.; Takashina, K. Valley polarization assisted spin polarization in two dimensions. *Nat. Commun.* **2015**, 6, 7230.
261. Frisch, M. J.; Trucks, G. W.; Schlegel, H. B.; Scuseria, G. E.; Robb, M. A.; Cheeseman, J. R.; Scalmani, G.; Barone, V.; Mennucci, B.; Petersson, G. A.; et al. Gaussian 09, Revision D.01; Gaussian, Inc: Wallingfoed, CT, **2013**.
262. Boys, S. F.; Bernardi, F. The calculation of small molecular interactions by the differences of separate total energies. Some procedures with reduced errors. *Mol. Phys.* **1970**, 19, 553-566.
263. Roy, D. Todd, K.; John, M. GaussView, Version 5; Semichem Inc: Shawnee Mission, KS, **2009**.
264. Lee, K. H.; Park, S. S.; Suh, Y.; Yamabe, T.; Osawa, E.; Lüthi, H. P.; Gutta, P.; Lee, C.; Similarities and difference between $(C_{60})_2^{2-}$ and $(C_{59}N)_2$ conformers. *J. Am. Chem. Soc.* **2001**, 123, 11085-11086.
265. Sadjadi, M. S.; Farhadyar, N.; Azarakhshi, F.; Najafi zadeh, F.; Sahba, R. NBO analysis and theoretical thermodynamic study of (5,5) & (6,6) armchair carbon nanotubes *via* DFT method. *Int. J. Bio-Inorg. Hybr. Nanomater.* **2016**, 5, 53-60.

266. Sinnokrot, M. O.; Sherrill, C. D. Highly accurate coupled cluster potential energy curves for the benzene dimer: sandwich, T-shaped, and parallel-displaced configurations. *J. Phys. Chem. A* **2004**, 108, 10200-10207.
267. Kawahara, S.; Tsuzuki, S.; Uchimaru, T. Ab initio calculation of interaction nature of borazine B₃N₃H₆ dimer. *J. Chem. Phys.* **2003**, 119, 10081.
268. Verma, K.; Viswanathan, K. S. The borazine dimer: the case of a dihydrogen bond competing with a classical hydrogen bond. *Phys. Chem. Chem. Phys.* **2017**, 19, 19067-19074.

